

University of Wollongong - Research Online

Thesis Collection

Title: A study on wear and surface roughness of work roll in cold rolling

Author: Hongchun Li

Year: 2008

Repository DOI:

Copyright Warning

You may print or download ONE copy of this document for the purpose of your own research or study. The University does not authorise you to copy, communicate or otherwise make available electronically to any other person any copyright material contained on this site.

You are reminded of the following: This work is copyright. Apart from any use permitted under the Copyright Act 1968, no part of this work may be reproduced by any process, nor may any other exclusive right be exercised, without the permission of the author. Copyright owners are entitled to take legal action against persons who infringe their copyright. A reproduction of material that is protected by copyright may be a copyright infringement. A court may impose penalties and award damages in relation to offences and infringements relating to copyright material.

Higher penalties may apply, and higher damages may be awarded, for offences and infringements involving the conversion of material into digital or electronic form.

Unless otherwise indicated, the views expressed in this thesis are those of the author and do not necessarily represent the views of the University of Wollongong.

Research Online is the open access repository for the University of Wollongong. For further information contact the UOW Library: research-pubs@uow.edu.au

University of Wollongong Theses Collection

University of Wollongong Theses Collection

University of Wollongong

Year 2008

A study on wear and surface roughness
of work roll in cold rolling

Hongchun Li
University of Wollongong

Li, Hongchun, A study on wear and surface roughness of work roll in cold rolling, PhD thesis, School of Mechanical, Materials and Mechatronic Engineering, University of Wollongong, 2008. <http://ro.uow.edu.au/theses/125>

This paper is posted at Research Online.
<http://ro.uow.edu.au/theses/125>

NOTE

This online version of the thesis may have different page formatting and pagination from the paper copy held in the University of Wollongong Library.

UNIVERSITY OF WOLLONGONG

COPYRIGHT WARNING

You may print or download ONE copy of this document for the purpose of your own research or study. The University does not authorise you to copy, communicate or otherwise make available electronically to any other person any copyright material contained on this site. You are reminded of the following:

Copyright owners are entitled to take legal action against persons who infringe their copyright. A reproduction of material that is protected by copyright may be a copyright infringement. A court may impose penalties and award damages in relation to offences and infringements relating to copyright material. Higher penalties may apply, and higher damages may be awarded, for offences and infringements involving the conversion of material into digital or electronic form.

A Study on Wear and Surface Roughness of Work Roll in Cold Rolling

A thesis submitted to fulfill the requirements
for the award of the degree

Doctor of Philosophy

from

University of Wollongong

by

Hongchun Li

BEng

School of Mechanical, Materials and Mechatronic Engineering

Faculty of Engineering

2008

DECLARATION

This is to certify that the work presented in this thesis was carried out by the author in the school of Mechanical, Materials and Mechatronic Engineering, University of Wollongong, Australia, and has not been submitted for a degree to any other university or institute.

HONGCHUN LI

ACKNOWLEDGMENTS

I am deeply grateful and give thanks to Professor A. K. Tieu and Associate Professor Zhengyi Jiang for their guidance, close supervision, and continuous encouragement during the course of this thesis.

I would also thank the following staff members:

- Mr Bob de Jong and Mr. Jose Gonzalez on the GLEEBLE-3500
- Mr. Ron Marshall and Mr. Martin Morillas in the University workshop for helping to set the Lateral-setting Test (LST) mini-mill onto the Gleeble 3500 and completing the LST experiments
- Mr. Greg Tillman and Mr. Nick Mackie in the Metrology Lab area and Dr Phil Whitten on AFM for their training and guidance when preparing and analysing the LST samples
- Dr Hongtao Zhu and Mr Hejie Li who assist me to correct my thesis.

I further thank Mr. Chunguang Meng and Dr Weihua Sun, in the Jinan Iron and Steel Ltd. Co., P. R. China for their assistance in the design and manufacture of the LST mini-mill. Without their help it would have been impossible to obtain the LST mini-mill and the test results on time.

I am also very grateful to the University of Wollongong for providing the UPA scholarships.

Finally, I give my heartfelt thanks to my daughter Christina Q. Sun and my husband, Dr Weihua Sun for their love and help during my PhD study.

ABSTRACT

The objective of this study is to improve our understanding of the evolution and tribological behaviour of work roll surfaces in cold rolling because surface deterioration affects the quality of products and the efficiency of production. The cost of rolls is almost 25% of the cost of cold steel production. An experimental Lateral Set-testing (LST) mini-mill was developed to make use of the Gleeble 3500 thermo-mechanical simulator functions to evaluate, for the first time, the roll material surface features, surface roughness, fast Fourier transform (FFT) and Power Spectral Density (PSD) of frequency distribution, after single and multi-pass rolling.

A low carbon-steel was prepared for the paired disc and then experiments on disc-to-disc wear were carried out to test surface deterioration and friction.

In the laboratory, material imitating an industrial roll was manufactured. One batch contained 4%Cr and another contained 4%Cr plus approximately 0.1% Ti. These materials were compared against each other in the LST and disc-to-disc experiments.

Experiments considered a series of parameters, including strip reduction, speed, and lubrication, while the disc-to-disc experiments considered duration of wear, forward and backward slip and load amplitude. The surfaces of the LST roller and disc were evaluated by surface technologies such as Atomic Force Microscope (AFM), Scanning Electron Microscope (SEM), and surface profile-meters. Transmission Electron Microscope (TEM) and X-ray diffraction

were helpful when analysing features of the roll microstructure that affects the wear properties.

Test results from the mini-mill reveal that dominant waviness of the surface roughness still exists on the surface after a single pass of rolling and a 30.5% reduction is a critical reduction level that has a significant influence on the density of power spectrum. A rougher work piece results in a larger power spectrum of the surface profile. It has found that the PSD altitude of the roller surface is significantly affected axially but is more sensitive to its original surface roughness circumferentially. It is distributed in an inverse order to the surface roughness in a high frequency domain. The addition of Ti alters surface deterioration. Lubrication has a significant effect on surfaces containing either 4%Cr or 4%Cr+Ti, affecting surface roughness of rollers containing 4%Cr more significantly.

In the disc-to-disc tests, more material was removed in the first 60 minutes from the disc containing Ti than the disc containing only 4%Cr. In general, roll material with 4%Cr+Ti reveals to have better anti-abrasive properties than the roll with only 4%Cr, while lubrication significantly reduced the wear rate and amount of material removed from both materials. The speed of the disc influences the weight loss, ie, the higher the speed the greater the amount of material removed. The slip rate also affects roll wear and weight loss because as the speed increases, so do the slip and loss of weight.

The coefficients of friction are between 0.35~0.75 when the contact was dry and 0.06~0.11 when lubrication was applied. Adhesive friction dominated the dry

contact while a mixed lubrication regime features friction behaviour when emulsion lubrication was applied. A backward slip of 2% and a forward slip of 1.5% resulted in a different coefficient of friction in dry contact mode although the corresponding torques were similar.

The torque and coefficient of friction are found to increase with disc speed in dry contact condition.

Lubrication alters the friction of both materials. The coefficient of friction decreases with speed on the disc with added Ti but the effect of load is in the opposite trend, while the disc with 4%Cr was less influenced by speed. The coefficient of friction is more sensitive to load at higher speeds on the disc with 4%Cr than at slower speeds on the disc with Ti added.

This indicates that the addition of Ti enhances the tribological behaviour of rollers because the disc with Ti additive is characterised by carbonitrides precipitated in a refined tempered martensitic matrix. Coarse carbides characterise the 4%Cr disc materials.

Surface defects of the work rolls, including banding, spalling, marking and welding in a cold strip plant, were investigated. It was found that early failures principally resulted from operational factors and roll material off-specification micro-structure defects rather than wear.

It is recommended that different grades materials of the roll and strip with different roughness and hardness to be tested and studied on the evolution and tribological behaviour of roll surfaces in the future.

LIST OF CONTENT

DECLARATION	
ACKNOWLEDGMENTS	i
ABSTRACT	ii
LIST OF CONTENT	v
LIST OF FIGURES	xii
LIST OF TABLES	xviii
NOMENCLATURE	xix
LIST OF PUBLICATIONS DURING THE PhD COURSE	xxi
Chapter 1 Literature Review and Scope of Work in the Present Study	1
1.1 Introduction	1
1.2 Wear mechanisms	2
1.2.1 Adhesive wear	2
1.2.2 Abrasive wear	2
1.2.3 Fatigue wear	2
1.2.4 Chemical wear	3
1.2.5 Roll wear	3

LIST OF CONTENT

1.3 Metallurgical factors affecting roll wear	4
1.3.1 Basic requirement of work rolls	4
1.3.2 Conventional cold work roll material	5
1.3.3 Forged steel roll with added Ti	7
1.4 Studies carried out on roll wear	8
1.4.1 Lubrication in cold rolling and its effect on roll wear	8
1.4.2 Investigation on the evolution of surface topography in cold rolling	10
1.4.3 Experiments for cold work roll wear	12
1.4.4 Modelling of roll wear	16
1.5 Problems and findings from the literature review	21
1.6 Scope of work in the present study	21
Chapter 2 LST design of the Mini-mill Driven by the Gleeble 3500 System	24
2.1 Introduction	24
2.2 Description of the LST mill	25
2.2.1 Design considerations	25
2.2.2 Experimental principle	26
2.2.3 Configurations of the LST-mill	27
2.3 Design of the mill	32
2.3.1 Basic parameters	32
2.3.2 Designs	37

2.4 Assembly	37
2.5 Application of the LST facility	38
2.5.1 Samples of deformed strip	38
2.5.2 Appearance of a worked roller surface	39
2.5.3 Force with the Gleeble system	40
2.6 Findings	41
2.7 Summary	41
Chapter 3 Experimental Instruments and Methodology	43
3.1 Introduction	43
3.2 Test materials	43
3.3 Single and multi-pass rolling tests by the LST	45
3.3.1 Gleeble 3500 Thermo-Mechanical Simulator	46
3.3.2 Lateral Setting Test procedure	46
3.4 Disc-to-disc wearing tests	47
3.4.1 Equipment	47
3.4.2 Wearing test procedure	49
3.5 Facilities and approaches to evaluate the experimental samples	51
3.5.1 Atomic Force Microscopy (AFM)	51
3.5.2 Hommel Tester T1000 for roughness measurement	53
3.5.3 Phillips XL30 Scanning Electron Microscope (SEM)	54
3.6 Summary	55

Chapter4 Study on Roll Surface Profile Changes by Single and Multi-pass Stalled Rolling	56
4.1 Introduction	56
4.2 Changes in surface morphology after single pass rolling	57
4.2.1 Surface roughness	57
4.2.2 3-D roller surface topography after a single-pass of rolling	62
4.3 Enhanced surface features analysis using Fast Fourier Transform (FFT) and Power Spectrum Density (PSD)	65
4.3.1 Definitions of FFT and PSD	65
4.3.2 Surface profile after different reductions of the work piece	65
4.3.3 Surface profile of different initial roller surface roughness after rolling	69
4.3.4 Surface profile with different work pieces roughness	73
4.4 Surface profiles of the roll after multi-pass rolling	75
4.4.1 Effect of lubrication on the evolution of surface roughness	75
4.4.2 Effect of Ti-enhancement on the roller surface after multi-pass rolling	83
4.5 Findings	88
4.6 Summary	89
Chapter 5 Tribological Behaviour of Roll Materials by Disc-to-Disc experiments	91
5.1 Introduction	91
5.2 Effect of wear duration	92

LIST OF CONTENT

5.2.1 Weight loss	93
5.2.2 Changes in surface roughness	94
5.3 Effect of load on roll wear	97
5.3.1 Weight loss to experiment loads	97
5.3.2 Surface roughness to loads	102
5.4 Surface profile as function of disk speed	105
5.5 Differences in speed between the sample and material	109
5.6 Test conditions on the coefficient of friction and torque	111
5.6.1 Disc slip	112
5.6.2 Result of speed on torque and the coefficient of friction	114
5.6.3 Result of load on torque and the coefficient of friction with lubrication	117
5.7 Findings	120
5.8 Summary	120
Chapter 6 Micro-structure and Tribological Behaviour of Roll	123
Material with Ti-additive	
6.1 Introduction	123
6.2 Micro-structure and mechanical properties of the roll material	124
6.2.1 Experimental	124
6.2.2 Microstructure and phase characteristics	124
6.2.3 Carbonitrides in the material with 4%Cr+Ti	128
6.3 Wear pattern of material with 4%Cr+Ti	130

LIST OF CONTENT

6.3.1 Heave deformation, flattening, and abrasive wear	131
6.3.2 Ploughing and delamination wear	133
6.3.3 Wear and micro-structure	136
6.4 Friction	140
6.5 Findings	142
6.6 Summary	142
Chapter 7 Case Studies on Premature Failure of Work Rolls in a Cold Mill Plant	144
7.1 Introduction	144
7.2 Rolling process and parameters	145
7.3 Results and discussion	147
7.3.1 Samples of work rolls	147
7.3.2 Spalling	148
7.3.3 Strip welding	152
7.3.4 Mechanical marking and banding	154
7.4 Conclusion	157
Chapter 8 Conclusion and Future Work	159
8.1 Introduction	159
8.2 General conclusion	159
8.2.1 Innovation of the LST facility	159
8.2.2 Roll surface features after single pass and multi-pass stalled rolling	160

LIST OF CONTENT

8.2.3 Tribological properties of 4%Cr and 4Cr+Ti materials	161
8.2.4 Case studies of the premature failure of a cold work roll	163
8.3 Suggestions for future work	163
8.3.1 LST equipment	164
8.3.2 Disc-to-disc wear tests	164
Reference	166
APPENDIX I Details of design of the mini mill	181
APPENDIX II Power Spectrum Density	188
APPENDIX III Skewness, Root Mean Square and Kurtosis of Surface Roughness	191

LIST OF FIGURES

Figure 1.1	Comparison of change in surface roughness between a conventional 5%Cr type work roll and a 0.1%Ti-enhanced	7
Figure 1.2.	Schemetic diagram of tribological testers	14
Figure 1.3	Mixed-film lubrication in cold rolling	18
Figure 2.1.	Schematic view of the LST mini-mill system	26
Figure 2.2	Overall view of the LST-mill	28
Figure 2.3	Configuration of the LST-mill stands	29
Figure 2.4	Configuration of the coupling mount on the LST-mill stands	30
Figure 2.5	Structure of the strip clamp	31
Figure 2.6.	Gleeble system chamber (elevated view)	33
Figure 2.7	Half fixed mini-mill into the Gleeble chamber	33
Figure 2.8	Strip undertakes lateral pressure on the left side	34
Figure 2.9	Assembly of the mill	36
Figure 2.10	Assembling of the LST-mill	38
Figure 2.11	Photos of the deformed LCS strip	39
Figure 2.12	Surface of the roller after rolling	40
Figure 2.13	LST mini-mill forces acquired by the Gleeble system	41
Figure 3.1	A schematic diagram of roll and disc manufacturing	45
Figure 3.2	MMS-2B disc-to-disc test system	48
Figure 3.3	Schematic view of the disc-to-disc setting	48

LIST OF FIGURES

Figure 3.4	Schematic view of the disc-to-disc test system	49
Figure 3.5	Design of the probe and its four silicon nitride cantilevers showing spring constants (N/m)	51
Figure 3.6	AFM scanning positions on each roller surface after the LST tests	52
Figure 3.7	Hommel Tester T1000 instrument	53
Figure 4.1	Effect of reduction on the roll surface roughness	58
Figure 4.2	Influence of the strip sample roughness on roll surface roughness	59
Figure 4.3	Roll surface roughness compared to its initial surface profile	60
Figure 4.4	Surface topographies of the 4%Cr roller before test and after one pass of rolling at 26.6% reduction	63
Figure 4.5	Surface topographies of the 4%Cr+Ti rollers before test and after one pass of rolling at 26.6% reduction.	64
Figure 4.6	PSD analysis of roller surface at different reductions in the work piece	66
Figure 4.7	Comparison of section analysis of the 4%Cr roller surface at reductions of 26.6% and 30.5%	68
Figure 4.8	PSD analysis of roller surface after rolling with different initial surface roughness	70
Figure 4.9	Cross section analysis of surface after rolling	72
Figure 4.10	PSD analysis of the surface with different work piece roughness	74
Figure 4.11	Evolution of surface roughness of the roller with 4%Cr	76

LIST OF FIGURES

Figure 4.12	Evolution of Surface roughness for the 4%Cr+Ti roller	76
Figure 4.13	Skewness and kurtosis before and after rolling (4%Cr)	78
Figure 4.14	Skewness and kurtosis before and after rolling (4%Cr+Ti)	78
Figure 4.15	Surface morphologies of the 4%Cr rollers before and after 5, 10 and 20 passes of rolling tests	80
Figure 4.16	Surface morphologies of the 4%Cr+Ti rollers before and after 5, 10 and 20 passes of rolling at dry-contacting	81
Figure 4.17	Surface morphologies of the 4%Cr+Ti rollers at oil-lubricating before (a) and after (b) 5, (c) 10 and (d) 20 passes of rolling tests	82
Figure 4.18	Roll surface PSD analysis	84
Figure 4.19	4% Cr roll surface section analysis	85
Figure 4.20	4% Cr+Ti roll surface section analysis	86
Figure 5.1	weight loss versus test duration under dry contact conditions	94
Figure 5.2	Weight loss versus test duration with lubrication	94
Figure 5.3	Surface roughness versus test duration under dry contact conditions	95
Figure 5.4	Surface roughness versus test duration with lubrication conditions	95
Figure 5.5	Initial surface of the 4%Cr disc ($R_a=0.66\mu\text{m}$)	96
Figure 5.6	Initial surface of the 4%Cr+Ti disc ($R_a=1.0\mu\text{m}$)	96
Figure 5.7	Surface morphology of discs in dry contact after a series of wear intervals	98
Figure 5.8	Surface morphology of discs with lubrication after a series	99

LIST OF FIGURES

	of wear intervals	
Figure 5.9	Weight loss to loads under dry contact conditions	100
Figure 5.10	Weight loss to load under lubrication conditions	100
Figure 5.11	Comparison between dry and lubricating contacts of 4%Cr discs under different loads.	101
Figure 5.12	Roll surface after 30min under 1000N under dry contact and slip =1.5%	102
Figure 5.13	Changes in surface roughness to load in dry contact	103
Figure 5.14	Changes in surface roughness to load in lubricating contact	104
Figure 5.15	Weight loss to speed at dry mode	106
Figure 5.16	Weight loss to speed at lubricating mode	106
Figure 5.17	Surface of discs after testing at each speed	108
Figure 5.18	Surface roughness to disc speed with lubricating	109
Figure 5.19	Weight loss to speed differences under dry contact	110
Figure 5.20	Surface roughness to speed differences under dry contact	111
Figure 5.21	Result of slip on torque and coefficient of friction at dry contact	112
Figure 5.22	SEM photography of the surface after 30 minutes wear at 1000N at dry contact	113
Figure 5.23	Result of disc speed on torque and friction under dry contact.	115
Figure 5.24	Result of speed on torque and friction under lubrication	116
Figure 5.25	Result of disc load on torque and coefficient of friction with lubrication	118

LIST OF FIGURES

Figure 5.26	Surface comparisons between the two materials at lubricated contact under different loads	119
Figure 6.1	Optical micrographs of the test rolls	125
Figure 6.2	TEM image of replicas taken from 4%Cr roll	126
Figure 6.3	TEM image of replicas taken from 4%Cr+Ti roll	126
Figure 6.4	XRD pattern for the surface of 4%Cr+Ti roll	127
Figure 6.5	TEM image of thin foil taken from 4%Cr+Ti roll	128
Figure 6.6	Chemical composition of titanium carbon nitride in the material with 4%Cr+Ti	129
Figure 6.7	TEM image of thin foil taken from 4%Cr+Ti roll showing the presence of Ti(C, N)	130
Figure 6.8	Disc surface flattening	132
Figure 6.9	Disc surface flaking and further flattening	134
Figure 6.10	Disc surface flaking and further flattening	135
Figure 6.11	Microstructure 0.1mm underneath the disc surface of both disc materials before wearing	137
Figure 6.12	TEM micrograph of the worn disc surface after 480 minutes	138
Figure 6.13	Electro Probe tests of the flakes collected after disc-to-disc wear	139
Figure 6.14	Change in coefficient of friction coefficient changing during 480 minutes of wear	140
Figure 6.15	Grooved surface in dry contact after 120 minutes wear at 1000N and 597rpm, in the disc-to-disc tests	142
Figure 7.1	2-stand tandem cold strip mill	146

LIST OF FIGURES

Figure 7.2	Spalling of work rolls	148
Figure 7.3	Microstructure of the material of work roll	149
Figure 7.4	Crack on roll A	150
Figure 7.5	Normal stress gradients developed as a result of contact with the rolled strip	151
Figure 7.6	Shear stress gradients developed as a result of contact with the rolled strip	151
Figure 7.7	Relationship between the length of rolled strip and surface roughness	152
Figure 7.8	4%Cr disc surface welding in the disc-to-disc dry-contact wearing tests	153
Figure 7.9	Strip welding	154
Figure 7.10	Mechanical marks and banding	155
Figure 7.11	Surface crack and banding on the disc with 4% Cr in the dry contact wear tests	156
Figure A.1	Assembly of the mill	182
Figure A.2	Roller shaft	182
Figure A.3	Roller-ring	183
Figure A.4	Bushings	184
Figure A.5	Rods	185
Figure A.6	Covers	186
Figure A.7	Coupling mount	187
Figure A.8	Block for roll gap adjusting	188

LIST OF TABLES

Table 1.1	Evolution of chemical compositions for cold work roll	6
Table 3.1	Chemical composition of low-carbon steel	44
Table 3.2	Chemical composition of roll materials	44
Table 4.1	Rolling parameters of the mini-mill tests	57
Table 4.2	The 4%Cr roll surface FFT features before and after rolling at 26.6% and 30.5% reductions	69
Table 4.3	The 4%Cr roll surface FFT features before and after rolling at 26.6% and 30.5% reductions	73
Table 4.4	Rmax by Hommel Tester T1000	77
Table 4.5	PSD features by Hommel Tester T1000	83
Table 5.1	Chemical composition of the partnered disc	91
Table 5.2	Emulsion used in the experiments	92
Table 5.3	Ratios of friction between dry and lubrication contact	117
Table 6.1	Vickers of different carbides	139
Table 7.1	Rolling parameters	147
Table 7.2	Work roll parameters	147

NOMENCLATURE

ACF	auto-correlation function
AFM	Atomic Force Microscope
f	frequency
FEM	Finite Element Method
LST	Lateral-setting test
L	length
l_{x0} and l_{y0}	integrated width and depth
N	number of data points
P	power
PSD	Power Spectrum Density
LCS	low carbon steel
R	roll radius
EAB	Electronic Analytical Balance
Ra	Roughness Average
R_{ku}	kurtosis
R_{max}	maximum roughness
R_q	root mean square roughness
R_{sk}	skewness
Rz	average maximum height
SEM	Scanning Electron Microscopy

NOMENCLATURE

W	Roll speed in rpm
SPM	Scanning Probe Microscopy
FFT	Fast Fourier Transform
τ	shear strength
ε	percentage reduction, %
ε and $\dot{\varepsilon}$	strain and strain rate
μ	coefficient of friction
v	rolling velocity
σ	Strength (MPa)
TEM	transmission electron microscopy
EDX	energy-dispersive X-ray

LIST OF PUBLICATIONS DURING THE PHD COURSE

1. **Hongchun Li**, Zhengyi Jiang, Kiet A. Tieu, Weihua Sun, Analysis of premature failure of work rolls in a cold strip plant, *Wear* 263 (2007) 1442–1446.
2. **Hongchun Li**, Zhengyi Jiang, Kiet A. Tieu, Weihua Sun, Surface Roughness and Wear of Work Roll Containing Ti in Cold Strip Rolling. *Advanced Materials Research*, Vol. 32 (2008), pp 157-160.
3. **Hongchun Li**, Weihua Sun, A. K. Tieu, Z. Y. Jiang, A Study on Roll Surface Profile Changes by Multi-pass Stalled Cold Rolling of Steel, in M. Pietrzyk et al: *Proceedings of Metal Forming 2008*, Krakow, Sept 24-28, 2008.
4. **Hongchun Li**, Weihua Sun, A. K. Tieu, Z. Y. Jiang, A Microscopic Examination on Work Roll Wearing Behaviour by Disc-to-Disc experiments in Cold Rolling of Steel, in M. Pietrzyk et al: *Proceedings of Metal Forming 2008*, Krakow, Sept 24-28, 2008.
5. Weihua Sun, **Hongchun Li**, A. K. Tieu, Z. Y. Jiang, Experimental study on deformation behavior of oxide scale during hot rolling of steel, in M. Pietrzyk et al: *Proceedings of Metal Forming 2008*, Krakow, Sept 24-28, 2008.
6. **Hongchun Li**, Chunguang Meng, Weihua Sun, Bob de Jong, A Mill Configured for a Thermo-mechanical Simulating Test system. US Patent, Application Number: 12017998. Receipt Date: 22-JAN-2008

Chapter 1 Literature Review and Scope of Work in the Present Study

1.1 Introduction

In practical cold rolling the roll surface roughness is essential for product quality, production efficiency, and cost. It is estimated that roll consumption accounts for approximately 25% of operational costs in cold rolling which means that a productive operation is vital to low cost and high quality cold rolling production and surface roughness deterioration is always an important topic for cold rolling operators. Lubrication is an important application in cold rolling of steel and it plays a significant role in determining the strip surface quality, power consumption, and roll wear rate. Chang and Wilson [1] explored the mixed lubrication of rolling under low speed conditions. Kosasih and Tieu [2] pointed out in their study that cold rolling is normally operated in mixed lubrication regime where the load is “generated by the hydrodynamic pressure of the lubricant in between the valley of the roughness asperity and the pressure at the contacting asperity surfaces.” However, wear is always an important issue in roll operations. In fact, the material specification, manufacturing process and operational life may play a key role in the roll wear pattern.

In this chapter the wear mechanism of a cold rolling work roll, the metallurgical factors and studies brought about by researchers will be reviewed. The scope of work in this thesis will also be introduced at the end of the chapter.

1.2 Wear mechanisms

It is well accepted that adhesive, abrasive, fatigue, and corrosive wear may each play a role in cold rolling wear [3, 53, 137-138, 66, 165, 167-168]. The wear patterns may exist separately or in a mixed regime.

1.2.1 Adhesive wear

When the workpiece and the roll plow through the interface lubricant film, the asperities can weld together over some parts of the true contact area to form friction junctions which must be broken for sliding to continue. The amount of wear then depends on where the junction is broken. If the break occurs at the original interface there is no wear but if it occurs at a distance away from the interface a fragment of material is transferred from one surface to the other [3, 53, 137-138, 168].

1.2.2 Abrasive wear

In cold rolling, the work piece and the work roll usually operate in an environment containing significant amounts of dirt and metallic wear particles that are often fully work-hardened. When the workpiece and the cold rolling roll are in contact, abrasion occurs between the twobodies and these hard, rough abrasive particles are trapped between the two sliding surfaces [3, 138, 167-168].

1.2.3 Fatigue wear

A cold work roll contains many defects from the manufacturing processes of the

roll such as microstructural defects, non-metallic inclusions, and micro-cracks. These defects usually cause a collection of internal stresses in a work roll. In addition, there are internal stresses resulting from heat treatment. The contact load produces the maximum compressive stress at the surface and maximum shear stress some distance below the surface. As rolling proceeds, sub-surface elements are subjected to a stress cycle for each passage of a roller which is almost entirely responsible for dissipating energy in rolling contact [3, 137].

1.2.4 Chemical wear

Chemical wear is defined as a material loss due to tribo-chemical reactions between the lubricant, tool, workpiece, and environment [3, 168].

1.2.5 Roll wear

Roll wear may be classified into two categories, reduction in diameter due to macroscopic wear and reduction in roughness [137-138]. The fact is that when a ‘softer’ material is rolled by a ‘harder’ work roll the abrasive action of the debris is a prime cause of wear. This wear is accelerated in the presence of hard oxide generated by de-oxidation operation and/or hard precipitates in steel making and/or processing, supported by a strong substrate. The former type of abrasion is named as two-body abrasion, while the latter will result in three-body abrasion when the embedded hard grit is drawn by load [137-138]. When ‘harder’ materials are rolled then adhesive wear can be expected. When rolls with a film of lubricant between them are stopped for a long period of time then localised

chemical wear may occur. Wear from fatigue occurs with cyclic stress and uneven distribution of stress due to localised wear, grinding cracks, residual stress in the roll and hydrogen pick up in contact with emulsion [138]. Some examples of roll wear are [3-7, 66]:

- Aluminum oxide abrasives in the Al-killed steel strip [3];
- Wear particles are flattened by an increasing rolling load and the associated high temperature turns them into oxides that cause a grinding action [4];
- The aluminum oxides generated in hot rolling appear on the surface of the steel strip when cold rolled produce a grinding action [5];
- Iron soap generated by metal and the free fatty acids contained in the rolling oil, promote lubricity and prevent metallic contact and thus minimises the changes of roughness [6];
- Surface roughness deteriorates when the strip enters the roll bite during high speed rolling. The work roll campaign is determined by the amount of surface roughness modification [7, 66].

1.3 Metallurgical factors affecting roll wear

1.3.1 Basic requirement of work rolls

Work rolls play a dominant role in steel rolling. They operate under extremely arduous conditions and are subjected to high cyclic loading and high levels of abrasion. In cold rolling, the major roll problem lies in the surface that is

subjected to high pressure, friction, and the thermal stress resulting from change of temperature. In fact, the deformation resistance of the workpiece is much higher compared to that of hot rolling. The roll surface at the bite can be subjected to pressure greater than 1000 MPa and an interfacial shear stress generated by friction [66]. The life of a cold work roll is limited by the deterioration of the surface finish due to wear through fatigue-based mechanisms. This means that the material must be hardened correctly and have good ductility and wear resistance. To fulfill these requirements the materials must have a tensile strength of approximately 2000 MPa, a high degree of internal cleanliness and homogeneous structure [66].

A homogenous hardened layer with good anti-abrasive properties at the surface are critical criteria. To achieve this goal various types of chemical designs and processing methods have been introduced into their manufacture.

1.3.2 Conventional cold work roll material

Cold work rolls are conventionally manufactured by the casting and forging route followed by heat treatment through quenching and tempering. The aim of a chemical design is to improve the mechanical properties of the material, especially its anti-wear properties. Carbon is the most effective element for increasing hardness. With the development of metallurgical technology, the size, type, and amount of carbide can affect the wear rate of high carbon steels [66]. It was believed that an increase in the amount of carbide can increase wear resistance

[8-9], especially where there is a strong abrasive component [10]. Chromium is a very strong carbide forming element which readily precipitates as an M_7C_3 type carbide, and therefore measures of raising the chromium content were adopted to improve roll life [66]. In the meantime molybdenum, manganese, and nickel are often added to improve the quench hardening ability and anti-wear properties [8-14]. A high chromium roll with 0.8% carbon and 7% Cr was developed and put into practice with an expectation of improved anti-wear properties from the dispersed carbides in the tempered martensite of the surface layer [15]. However, excessive addition of alloys imperiled the microstructure due to segregation of alloy elements. Furthermore, manganese and nickel may increase the superabundant retained-austenite from which local stress and micro-cracks will occur when the retained-austenite transforms into martensite under high stress. Therefore, the risk of surface flaking underlies the cycled stress during rolling. Table 1.1 illustrates the evolution of chemical compositions for cold work rolls [15].

Table 1.1 Evolution of the chemical composition of cold work rolls [15]

<div>Please see print copy for table 1.1</div>
--

1.3.3 Forged steel roll with added Ti

The microstructure of a cold work roll is characterised as tempered martensite with dispersed carbides. An increased volume of carbide dispersion improves the anti-wear properties and it is believed that a finer and more even distribution of carbides increases its ductility and wear properties. Titanium is known as its strong affinity with carbon and nitrogen. Fine carbon-nitrides precipitate even during solidification of Ti steels and therefore titanium becomes one of the most effective elements for improving wear [16].

According to the work published by Shimizu et al [17], a comparison of rolling practices was carried out between a conventional 5% Cr forged steel roll and a 5% Cr +0.1% Ti type. As shown in Figure 1.1, the conventional 5% Cr type roll initially wears quickly and its roughness decreases twice as much as a roll

'Please see print copy for figure 1.1'

Figure 1.1 Comparison of changes in surface roughness between a conventional 5%Cr type work roll and a 0.1%Ti-enhanced [17]

with 0.1% Ti added. As the rolling length increased further there was very small change in surface roughness change for the Ti enhanced work roll, which validated the steady roughness changing characteristics. This industrial practice demonstrates the ability of Ti enhanced work roll to regenerate its surface roughness for cold rolling. It is expected that cold rolling mills profit from a higher rolling speed and roll sliding as well as prolonged roll life when Ti enhanced rolls are used [15].

1.4 Studies carried out on roll wear

1.4.1 Lubrication in cold rolling and its effect on roll wear

Wear and friction are important issues that arouse the interest of many researchers in the field of contact mechanics and metal processing [46-54]. Contact between roll and work piece inevitably creates friction and roll wear which not only damages the rolls, but also reduces production and causes quality problems. As a result, lubrication must be used.

The property of a lubricant is often evaluated by its frictional characteristics in the roll bite [46-47, 56-60]. The effectiveness of lubrication in cold rolling lies in the fact that the interface between the roll and the strip is separated by an oil film trapped by the asperities on the surface of both roll and strip [46, 51, 61], which leads to a reduction in the coefficient of friction. In the meantime, lubrication is used to avoid roll-strip sticking due to extreme frictional heat and deformation energy. Furthermore, the surface of the roll is protected from oxidation by the

lubricant [15, 47, 49].

Configuration of a critical oil film is important for making the lubrication effective. Hydrodynamic lubrication, mixed regime, and boundary lubrication mechanisms are often used [15, 46, 49, 51, 56, 58, 62-63]. Under the milled film regime lubrication regime the oil film between the roll and the work piece should be capable of resisting extremely high pressure. If this film of oil is too thin however, it may break down and cause damage the roll and strip and cause a breakdown in production [15].

In practice, lubricants are often made by mixing oil in water emulsion so the oil lubricates while the water cools the work roll. The oil may be mineral, animal, plant, or synthetic fat, but whichever is used, anti-oxidation and anti-corrosion additives must be mixed into the emulsion. According to Lenard [58], appropriate boundary additives may be added to this emulsion to control friction. The effect of additives on lubrication is examined in the references [18-21, 51, 58].

Viscosity is one of the most important parameters for evaluating the tribological characteristics of oil. Wilson [22] pointed out that the thickness of oil film depends on the viscosity of oil, the viscosity-pressure parameter and rolling velocity. Sutcliffe's work [51] on the plane strain compression of aluminium strip indicated that a reduced viscosity of oil directly causes less effective oil entrapment. Lenard [24, 46, 58, 61] investigated the viscosity of lubricants on

mill load in cold rolling by considering viscosity, roll roughness, rolling speed, and reduction as independent parameters. It was found in Lenard's study that the effect of viscosity on decreasing the magnitude of forward slip was "apparent at higher velocities and reductions but not observable at lower speeds and lower reductions" [61]. In fact, the interface between the roll and the workpiece influences the lubricating regime to a great extent [24, 58]. It is known that the surface roughness and even the material processed may play important roles in this tribological phenomenon when the viscosity is considered in lubricating regimes [24, 46, 58].

Although a great deal of work has been carried out to characterise lubricating matters in cold rolling, its effect on roll wear, especially on the evolution of surface roughness, was seldom found as a research topic [46]. Due to the complexity of additives and concentrations of oil-in-water emulsion, only two extreme conditions, dry and oil lubrication, are considered to simplify the present study because when "the dynamic concentration theory of emulsion lubrication is valid, ..., the amount of the oil is not as significant as its presence or absence." [58]

1.4.2 Investigation on the evolution of surface topography in cold rolling

The resistance to surface roughness change determines the performance of a work roll. Surface deterioration and wear may be affected by normal and localised loading, interface frictional shear stress, friction hill, thermal cycling of

the surface, material flow stress, and the lubricant [25, 64]. It is known that surface deterioration mechanisms are principally abrasive wear, low cycle fatigue, cracking and spalling.

Cracking and spalling stem from fatigue fracture at the barrel surface or just below the surface where localised thermal shock, combined tensile and shear stress, operational factors, and metallurgical features originate [65-69].

Abrasive wear has been demonstrated by abrasion scratches of a roll after a campaign while roll mark is believed to be associated with hardness and microstructure of the roll material [65]. However, due to the large hardness difference between the work roll and work piece, substantial amounts of material from the workpiece will be transferred to the surface of a roll under high friction [46]. The effect that layers of material transferring onto the work roll has on the surface roughness of cold rolled strip has been thoroughly investigated [70-73], where the surface finish of the workpiece were accounted for. In fact, the transfer layer helps to eliminate surface pits on the strip surface on one hand while introduce scoring marks on the other [74]. The material deposited on the roll surface will certainly contaminate the roll surface, leading to roll surface deterioration, and produce a rough surface on the work piece [26, 73, 75, 100].

Fatigue damage to the surface is another source of wear. Results from several experiments focusing on contact of surface [60, 76-79, 81] indicate that the wear rate depends on the number of contact cycles and originates from “initial

hardening, crack initiation, and its growth typical of pure fatigue” [82]. It was found that a higher cyclic load increases the wear rate and deteriorates the surface rapidly. Meanwhile, the microstructure feature and inclusions are also responsible for crack initiation [81, 83-84]. It was also found that residual stress from a cyclic load will induce decomposition of some retained austenite in a surface that is not properly heat treated. The phase transformation will again bring about inner stress which in turn affects the fatigue properties of the tool material [79].

Roll surface morphology in cold rolling strips is a really interesting topic because of its importance in practice but there is, however, a lack of extensive study [46, 66, 85-87]. As mentioned above, a huge amount of work investigating the surface roughness of a work piece has already been done. The effect of roll surface roughness on rolling loads and friction has also been carried out sufficiently by many researchers [58-61, 71, 89], although a detailed investigation of the evolution of roll surface morphology is seldom found in published works [46, 90]. This evolution will be considered in this thesis.

1.4.3 Experiments for cold work roll wear

Wear is an important engineering issue that interests many researchers [49, 64, 80-81, 90-93]. To make a clear assessment of the characteristics of worn surfaces, different experimental facilities have been introduced into the study of work roll wear.

Method of surface evaluation

The evaluation of the characteristics of a roll surface is the basic technique in surface science. This is normally done using a surface profiler, optical microscope analysis, and SEM or scanning laser microscope. In recent years the nano-tribology method has been introduced to characterise the surface properties in steel rolling using AFMs [27-29], which give a comprehensive understanding of the surface spectrum of both the roll and the workpiece. In order to evaluate the surface texture, replicas are often used to replicate the roll surface [29-30, 71, 94-96]. A Hommel Tester T1000 makes it possible to measure roughness on the periphery with a resolution of 0.01 microns [29]. Among these techniques to estimate surface features, Sutcliffe [96, 97] introduced computational analysis using Matlab on a two-dimensional grid exported from a Zygo, non-contacting three-dimensional interferometric profilometer.

It is assumed that in practice the surface roughness of a cold rolled strip is generated by contact with the roll surfaces and hence any change in the surface of the product is a result of roll wear during service. It was demonstrated that decays of shot blast textured (SBT) and electro-discharge textured (EDT) surfaces were reflected by changes to the properties of sheet texture on average surface roughness from coil to coil over rolling campaigns [31-32]. In Ref. [33], it was further indicated that Lasertex can scan three dimensional sheet textures and assess changes in the roll textures, although this has been contradicted by Ref. [34], which asserts that the strip produced cannot be used to measure the

gradual wear of a pair of rolls in the mill.

Equipment for experiments on wear

Experiments on the wear of work roll materials are usually carried out by pin-on-disc, ball-on-disc, or disc-on-disc tests [35-37, 62, 73, 79, 90, 98-100], as shown in Figure 2.

(a) (b) (c)

'Please see print copy for figure 1.2 (a) (b) (c)

**Figure 1.2 Schematic diagram of tribological testers [After Ref. 62 and 64]
(a) pin on disc; (b) ball on disc and (3) disc on disc**

There are advantages and disadvantages with each of these three methods. With the pin on disc tests, the instrument simplifies the procedure to deal with the pin samples and the rated disc materials but the friction pattern between pin and disc seems to be limited to slide friction and the contact interface between the work roll and workpiece in the roll bite is different. Ball-on-disc experiments can be used to determine fatigue wear properties and roll material scuffing [62, 79]. The

disc-on-disc wear test has been widely used by a large number of authors to simulate roll wear [90, 98]. This device allows for a large range of working pressures and long sliding distance to simulate cyclic wear. However, it is quite different from realistic cold rolling conditions due to the large ratio of elastic to plastic deformation.

Of all the methodologies applied to examine wear, experimental cold rolling may be the most realistic measure to simulate the contact conditions in the roll bite and evaluate the influence of rolling parameters on the wear properties of a work roll. Lenard and his co-workers have carried out many experiments to investigate the tribological features in the roll bite during cold rolling [46, 48, 58, 61, 63, 88, 101], by taking roll surface roughness and lubricating conditions into account. Lenard et al also considered the friction, focusing on rolling loads, forward slip, performance of lubricant, and the surface finish of the workpiece. As it is not feasible in practice to carry out a detailed inspection of the evolving roll surface because the rolls are very expensive, a new approach, an upsetting rolling test (URT) [102-103], has recently been introduced to measure the impact of the rolling parameters on the quality of the final surface of the work piece. The advantage of URT lies in the fact that a large range of rolling forces and torques, a front tension on the strip and a reasonable reduction of the work piece can be used to simulate contact conditions in cold rolling. However, using URT to characterise the roll surface is still being explored by Dubar and his co-workers [102-103].

Because the difference in hardness between the roll and the workpiece is large, any gradual change in surface asperity is seldom considered. As mentioned previously, much research work has been carried out to study the surface features on the strip side [72, 95-97, 96, 102, 104-105], but a comprehensive understanding of change in work roll surface roughness still needs observation under simulated heavy reduction contact conditions.

1.4.4 Modelling roll wear

Modelling the contact mechanics has become a powerful method for understanding the tribological phenomena of the interface between the tool and the work piece while forming cold metal. A wide variety of methods have been applied using numerical analysis [111], computational simulation [112-115] and empirical formulations [94, 101, 106]. A huge amount of research works have focused on contact mechanics and lubricating regimes [62, 71], frictions [110] and the surface properties of the work piece [109], but roll wear is seldom considered.

Simulating a rough surface

In many research works on roll and work piece tribological issues, asperity contact is assumed to be on the work piece side while the surface geometry of the tool is often assumed to be a smooth surface [97, 108, 116]. In fact both the tool and the work piece have asperities on their interfaces and therefore modelling and simulating a rough surface is necessary to accurately simulate the roll wear mechanism in cold rolling.

To build up a rough surface digitally it is essential to create reference data with defined logic, expected values of geometric and statistical quantity, and importantly, variable and randomness [40, 104]. Karpenko and Akay [117] presented a detailed review of progressive computational models on the asperity geometry of a contact surface. Many researchers suggest that a three dimensional random surface topography be generated [38-39, 104, 118], although in practice the requirement of accuracy against an expected geometric and statistic quantity is seldom fulfilled [104].

According to the examination of a rough surface [29], an isotropic ‘bell-shaped’ Gaussian height distribution is a feature of the ground surface. Meanwhile, the amplitude of surface roughness is also represented by the power spectrum which is defined as a plot of power as a function of the spatial wavelength, or frequency. The power spectrum density (PSD) function reveals periodic surface features that appear to be “random” and provide a graphic representation of how such features are distributed. It is assumed that a relatively small set of spectral frequencies is sufficient to describe all the surface features of the sinusoidal nature of a composite wave. In order to characterise the morphology of a rough surface, an auto-correlation function (ACF) [39, 104, 117] is introduced to define the isotropic features of asperity height distribution of a digitally generated surface roughness.

A discrete form of the ACF is expressed by

$$R_{zz}(k, m) = \sigma^2 e^{-2.3[(k/l_x)^2 + (m/l_y)^2]} \quad (1.1)$$

where $k=0, 1, 2, \dots, l_x$, $m=0, 1, 2, \dots, l_y$, and l_x and l_y represent the non-dimensional correlation lengths in x and y directions [39]. For the isotropic surfaces considered, $l_x=l_y=l=33$. σ is the desired value of multiplied standard deviation value.

Lubrication regime

Lubrication and friction have become key concerns when studying surface wear. It is suggested that valleys among the asperities on the roll and work piece interface trap the lubricant into the roll bite and generate mixed-film lubrication in strip rolling [116], as shown in Figure 1.3. Contact mechanics is also an interesting issue when modeling lubrication in cold rolling.

'Please see print copy for figure 1.3'

Figure 1.3 Mixed-film lubrication in cold rolling [116].

A full film regime was assumed in many works [42-44], although in practice a mixed film lubrication regime prevails in the contact zone between the roll and the work-piece interface [45-47, 71, 108, 116, 120-121]. In Ref [121], Sutcliffe et al divided the contact zone of the roll and work piece into three zones when

modelling friction in a roll bite with mixed lubrication, an inlet zone, a transition zone, and a work zone. In this work he assumed that the work piece is rigid plastic and there is no bulk deformation in the inlet zone, and neglected elastic deformation. Lu and Tieu [108] incorporated elastic deformation of the rolled material when they developed a mixed film lubrication model in the inlet zone. It has been found in Ref [108] that elastic deformation of the strip enlarges the length of the inlet zone and the results of mixed film model are quite different from those of the full film model.

Roughness transfer

A large number of researches on surface transfer have been carried out on the cold forming of metal by computational modelling coupled with experimental simulation [70, 97, 102-103, 122-123]. However, most of these work examined the work piece surface roughness transfer but in published papers not much was found on the roll surface. There is an enormous difference in hardness between the roll and the work piece and hence the rolls are always taken as rigid bodies, as has already been mentioned in Ref [46]. Nevertheless, the methodologies for investigating the surface transfer of a work piece may reveal some guides when studying the roll surface.

In these studies Sutcliffe et al [70], carried out a theoretical investigation on drawing tests of artificially indented stainless steel strips, and confirmed the usefulness of a strip drawing rig as a tool to model change in the surface

topography during rolling by matching the lubrication regimes. The results indicate an agreement with experimental verification when extending a “micro-plasto-hydrodynamic lubrication” and “mixed lubrication” model to predict change in the pit area of indented and shot blasted surfaces while taking account of variations in sliding speed and strain rate during rolling and drawing [111, 112]. In their study on wire surface drawn with rougher dies, Le and Sutcliffe [124] found that “the lubrication has broken down, leading to ploughing or smearing of material picked up onto the tool surface.”

Ma and Tieu [45, 116-123] developed a finite-element model to simulate asperity flattening by simplifying the asperities as having one, two, and three wavelength profiles established from roughness measurement of a steel sheet. In their studies the evolution of real contact area, surface roughness, distribution of contact pressure, and variation of friction force were examined at the interface between the work roll and work piece under various degrees of friction. Less contact area and more concentrated local pressure were acknowledged in the three-wavelength model than the other two models [116].

Büntgen and his co-worker [122] also developed an FEM model to simulate the roughness transfer characteristics of a surface textured by an electron beam after temper rolling where they observed penetration and reverse extrusion phenomena. This led to a substitute profile model. When Dubar and his co-workers [103, 102] predicted the local behaviour of surface asperities with

FEM during cold rolling, they found that the plastic strain behaviour was modified by forward slip and the reduction ratio through pressure and shear force. They concluded that a quantity of iron residues could be defined as “a function of the local plastic strain and the plastic energy solution” [102].

1.5 Problems and findings from the literature review

Due to the hardness, strength, and expense of roll materials, researchers have to study wear by investigating strip in an experimental mill or by replicas from a worn work roll. Not many papers were found which studied the roll surface asperities pass by pass. Meanwhile, wear experiments were limited to dry contact sliding or by lubricating emulsions which are mixture of water and oil. Furthermore it is hard to find any duplicated roll materials from a cold mill plant to investigate roll material microstructure and its failure cases.

Therefore, an innovative experimental facility to fulfill the requirements of analysing the surface by stalled rolling will be a valuable contribution to this field of research. It will be more practical if an industrial emulsion is introduced into experiments on roll wear. Further, it is interesting to correlate the results of laboratory experiments to analysis of industrial roll failures.

1.6 Scope of the present study

According to the above literature review, a study on roll wear may involve roll materials, tribology phenomena in the roll bite, and surface deterioration.

Further, it should be understood that roll wear is also affected by the chemical composition of a work piece, rolling speed, reduction, work roll diameter, temperature of a work piece, surface roughness, and viscosity of lubricant. The aim of the present work is focusing on the roll wear and its surface roughness to study roll material wear.

The objective of the present study is to emphasise how the surface of a cold work roll deteriorates. To achieve this goal the following investigations are expected to increase our understanding of the mechanisms of roughness changes.

- i) A 4%Cr roll material is introduced to investigate its wear characteristics. The chemical composition and mechanical properties of the test material will be modelled for practical service in a cold rolling mill. A 4%Cr+Ti forged roll material is also tested to make a comparison of wear properties so that a better understanding on roll surface profile evolution can be obtained.
- ii) To identify the evolving roll surface pass by pass, a Lateral-setting test (LST) mini-mill is fitted into a Gleeble 3500 Thermal Mechanical simulation system and a disc-to-disc test machine is also used to examine surface deterioration after different load cycles of experiments.
- iii) Experiments are carried out on the LST at a series of reduction, deformation speeds with dry and oil lubrication. The driving forces for deformation will be collected from each test. A low-carbon steel strip is

used in the tests. The LST samples of the roll material will be analysed on an Atomic Forced Microscope (AFM) to characterise the surface features. Asperities flattening or breaking will be investigated from the data collected.

- iv) On the disc-to-disc test, variable load weights, forward slips, rotating speeds, various cycles, and two lubricating conditions are to be investigated for different roll materials vs a carbon steel disc. The surfaces of each disc will be examined under SEM and any deterioration is expected to be evaluated.
- v) Friction patterns will be analysed for the disc-to-disc test.
- vi) The microstructure of the Ti-additive material is studied to better understand its tribological properties.
- vii) Cases where forged alloy work rolls in a two-stand compact cold mill failed prematurely will be studied by taking the tribological properties of similar roll material into account.

Chapter 2 LST design of the Mini-mill Driven by the Gleeble 3500 System

2.1 Introduction

The sliding contact and high pressure between the strip and the work roll in cold rolling results in roll wear that affects the precision of the strip surface quality. An in-depth investigation on roll wear has practical significance [1]. The aim of this investigation on work roll wear is to develop a better understanding of the evolution of tribological behaviour of work rolls in cold rolling with the longer term aim of providing strategies for improving the quality of rolled strip.

Roll materials are difficult to machine and are expensive, therefore studies on surface wear are usually carried out experimentally or semi-experimentally in the laboratory [2]. This is why many researchers have carried out wear experiments to study the surface characteristics of a work piece. In this thesis, an innovative mini-mill[†] conveniently attached to the Gleeble 3500 Simulation System has been used to investigate surface deterioration under simulated rolling conditions that involve reduction, rolling speed (strain rate), surface roughness of rolls and work pieces. Experimental data obtained by the test will be helpful for investigating the wear mechanism.

In this chapter the design of the mini-mill is described. The mill is the first of its

[†] The author has applied a US patent on the embodiment of the mini-mill attached to the Gleeble, No. 6 on publication list, page xxi.

kind and the innovation that is introduced to the wear study of rolls and rolling process will help open a new field of simulation tests on the thermo-mechanical simulator Gleeble system.

2.2 Description of the LST mill

2.2.1 Design considerations

The rolling simulation is provided by the moving work piece driven by the Gleeble Digital Control System. The sample is clamped by a jaw of the Gleeble and driven into the roll gap. Thus the mini-mill is called a Lateral-setting Test system (LST) when compared with an upsetting rolling test (URT) [102]. To accomplish the proposed experiments the mini-mill should satisfy some basic functions. The most important issue in designing and manufacturing the mill is its dimensions because it must fit into the space within the Gleeble chamber. Because of the space limitation, the mill itself must be easy to assemble and disassemble, and so too the samples. In addition, each part of the mill must be strong enough to withstand the rolling process. The detailed requirements are as follows.

- a) The structure and its components must fit in the chamber but do not affect the Gleeble basic function.
- b) When the mill is working it must be suspended in the Gleeble chamber and held by the Gleeble fixture. A specially devised jig aligns the traversing test piece to enter the roll gap and transfers the driving forces.
- c) The experiments focus on the surface area of the roll that contacts the work

- piece, so as to simplify the sampling of the roll material, each work roll is designed as a roller ring fitted on a shaft. The roller ring is made of specific roll materials while the shaft is made from conventional bearing material.
- d) The roll gaps can be adjusted by spacers of varying thicknesses so that different reduction can be applied.
- e) There are more than 134 experiments planned for the test program which means it is inevitable that the roll (the sample) and the work piece (the strip) will be replaced frequently.

2.2.2 Experimental principle

Figure 2.1 is a schematic diagram showing the basic elements of the LST mini-mill system.

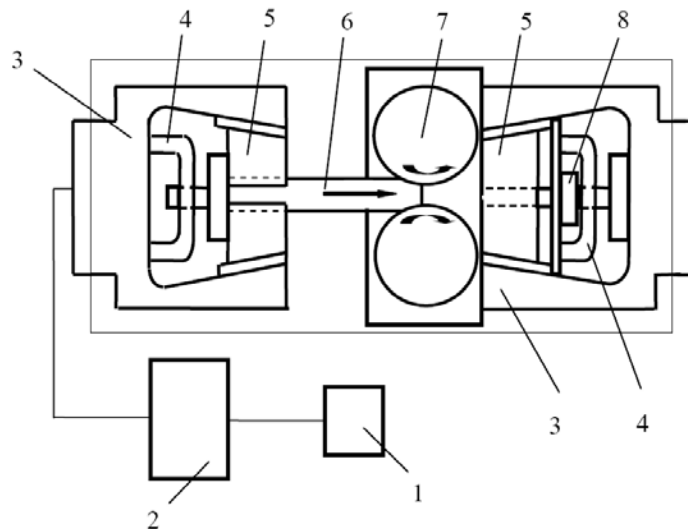


Figure 2.1 Schematic view of the LST mini-mill system.

1 and 2: computer and control system of Gleeble; 3: Gleeble moving side jaw; 4: Gleeble U jack clamp; 5: grips; 6: strip; 7: the mini-mill and its rollers; 8: coupling mount of the mini-mill

The testing parameter is programmed into the Gleeble computer system by inputting the deformation period, strokes, and strain rate. The mill and the materials are installed onto the Gleeble rigs separately. According to the planned reduction, appropriately sized spacers are placed onto the bearing housing to control the roll gap. After the Gleeble system has started the left jaw moves the strip to the right and drives it into the set up roll gap. The computer system measures the driving force during the test.

2.2.3 Configurations of the LST-mill

Figure 2.2 shows the LST-mill configured for a thermo-mechanical simulating test system. The mill comprises a stand, an upper roller (4) and a lower roller (5). Figures 2.3 explains the LST-mill stand which comprises four pulling rods (1), a top cover (2) (as shown in Figure 2.2) and a base (3). The base (3) of the stand is positioned and located at the bottoms of the tie rods (1) by studs and nuts connections. Two side plates (8) are welded on the outside of the pulling rods (1). Each of the upper roller (4) and the lower roller (5) assembly comprises a roller shaft (7) and a cylindrical roller part (4). The test cylindrical part (4) and its mating cylinder (5) are supported by roller bearings (6). The roller shafts (7) are supported by bushings (9) and (11). The upper roller (4) and the lower roller (5) can be repositioned so that for each roller, six to eight tests can be carried out. The upper bushings (9) and lower bushings (11) are mounted between pulling rods (1). The side plates (8) are used for axial positioning of the rollers (4) and (5). The top cover (2) is positioned and fixed on top of the pulling rods (1) by studs and nuts connections. Spacers (12) are positioned between upper

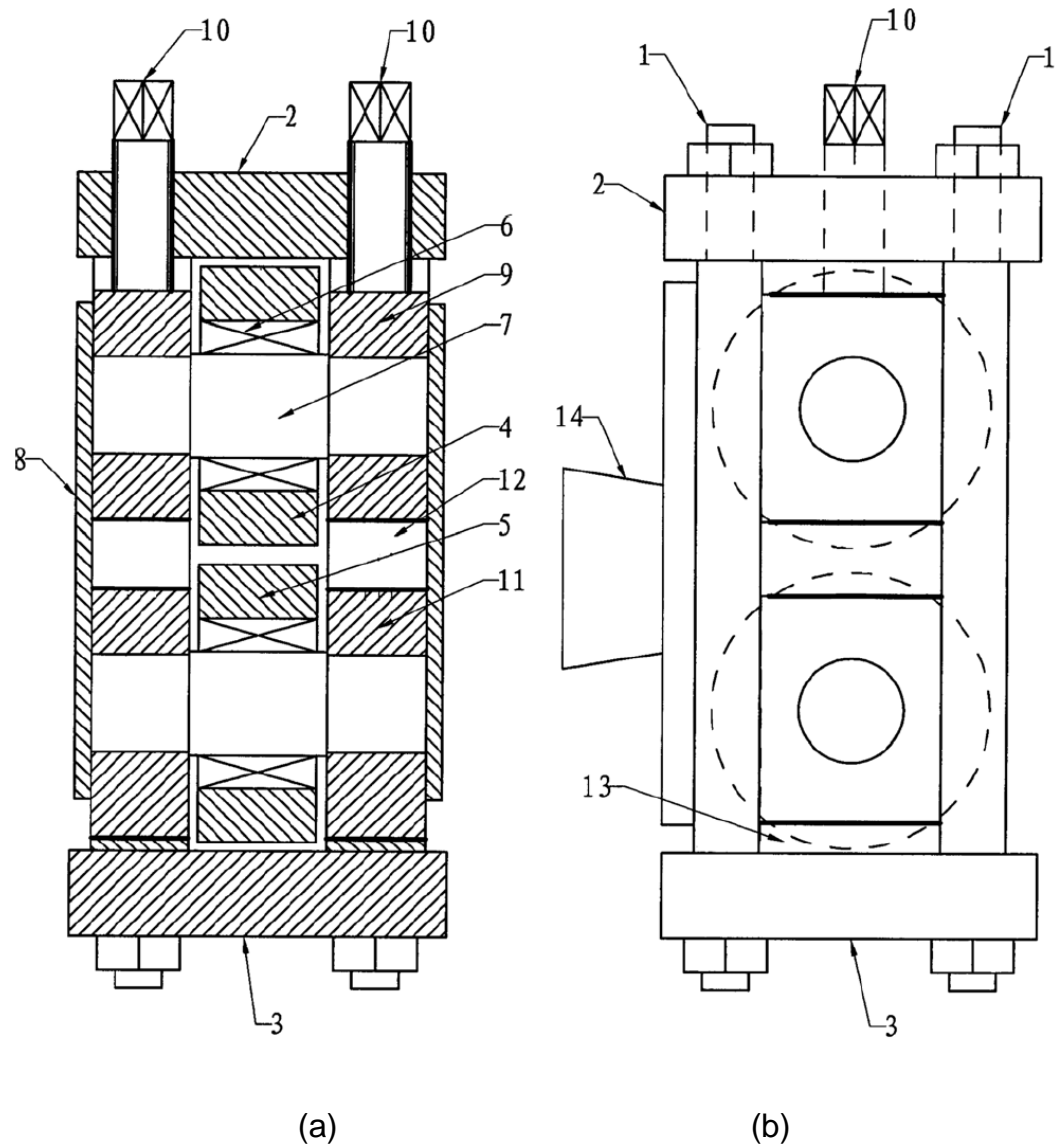


Figure 2.2 Overall view of the LST-mill. (a) Cross-sectional view; (b) Left view of the mill in Figure 2.2 (a).

1: pulling rod; 2: top cover; 3: base; 4: upper roller; 5: lower roller; 6: roller bearing; 7: roller shaft; 8: side plate; 9: upper bushings; 10: holding down bolt; 11: lower bushings; 12 and 13: spacers; 14: coupling mount

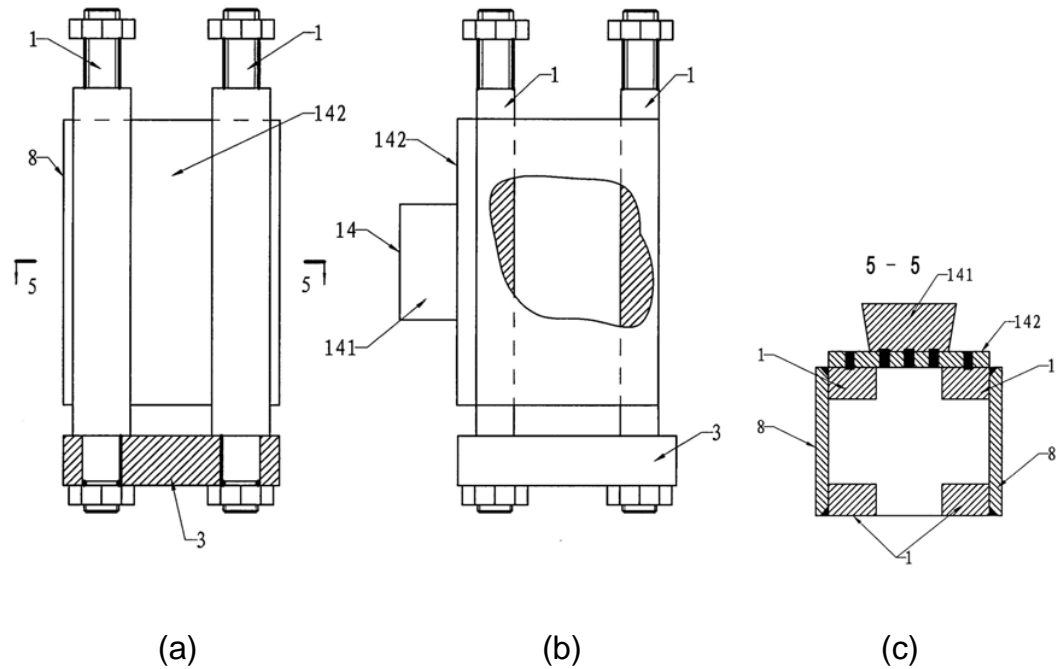


Figure 2.3 Configuration of the LST-mill stands. (a) Front view of the stand in Figure 2.2 (a); (b) left view of the stand in Figure 2.3 (a); (c) a cross-sectional view of the stand along 5-5 in Figure 2.3 (a)

bushings (9) and lower bushings (11), and spacer (13) is located between lower bushings (11) and base (3). The coordination work of pressing down bolts (10), spacers (12) and spacer (13) allow the adjustment of the gap between the upper roller (4) and the lower roller (5). Lower bushings (11) can be moved up and down by adjusting the thickness of spacer (13) and upper bushings (9) can be moved up and down by adjusting pressing down bolts (10).

Figure 2.4 shows the coupling mount (14) that comprises a trapezoid shaped coupling portion (141) and a connecting plate (142) which is integrally welded

thereon. The connecting plate (142) and the pulling rods (1) are connected by plug welding via a number of holes (143) on the connecting plate (142).

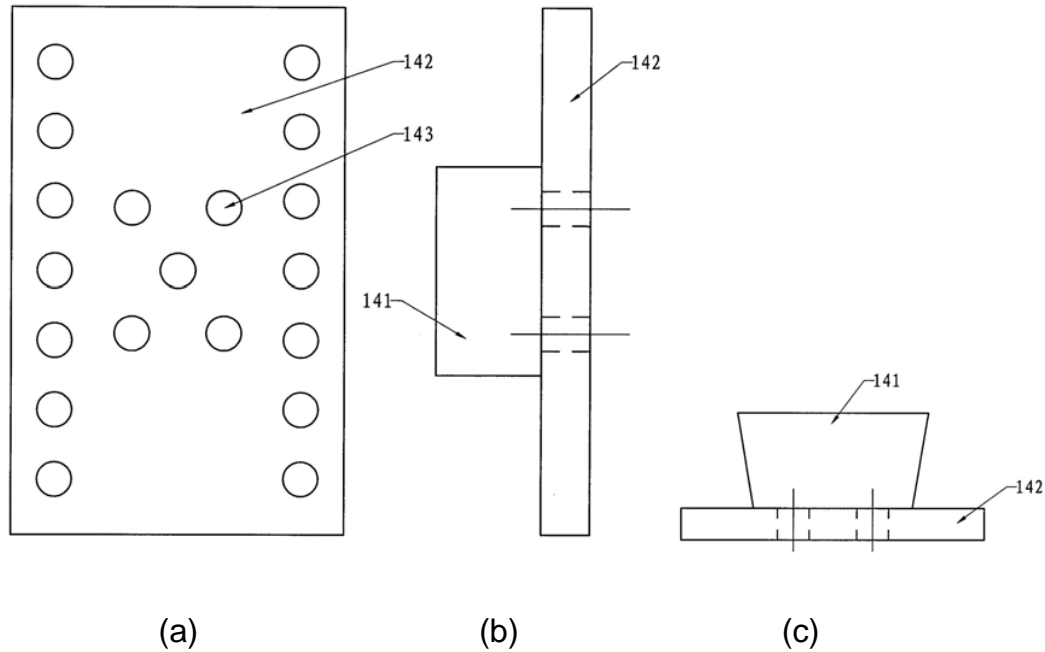


Figure 2.4 Configuration of the coupling mount on the LST-mill stands: (a) structural view of a coupling mount of the mill in Figure 2.2; (b) left view of the coupling mount in Figure 2.4 (a); (c) top view of the coupling mount in Figure 2.4 (a)

When feeding strips between the two rollers, the coupling mount (14) is under pressure and the trapezoidal shaped coupling portion (141) functions mainly to support and position the mini-mill in relation to the Gleeble. The plug welding between the trapezoid shaped coupling portion (141) and the connecting plate (142) can satisfy the resistance requirement when pulling the strip out of the roller after test.

Figure 2.5 illustrates the structure of the strip clamp (15), which is connected to the moving coupling head of the Gleeble test system. The strip clamp is in the shape of a trapezoid, and includes two clamp portions. A rectangular shaped center hole (151) is formed by joining the two clamp portions for clamping strips.

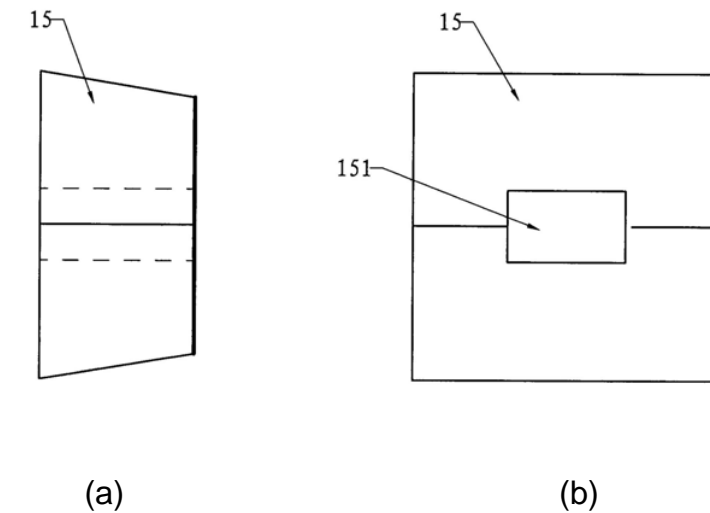


Figure 2.5 Structure of the strip clamp: (a) structural view of a strip clamp; (b) left view of the strip clamp of Figure 2.5 (a)

When performing a test, the cylindrical bearings (6) are placed onto the roller shafts (7), and the two rollers (4), (5) including the cylindrical bearings (6) and the roller shafts (7) are placed inside the stand from the stand top, the top cover (2) is closed and the nuts on top of the pulling rods (1) are screwed down, and the pressing down bolts (10) are screwed downwardly so as to press tightly on the bushings of the upper roller. Then the coupling mount (14) is placed onto the coupling head of a Gleeble thermo-mechanical simulating test system and fastened. Further, the strip is placed into the center of the strip clamp (15) and

fastened. The travel of the coupling head, and hence the travel of the strip, is adjusted and set in the Gleeble system. The strip may be formed of any suitable material. After the installation and adjustment on the mill, strips are driven into rollers (4), (5) to begin the test.

In the future, a load cell will be installed either between the top of the upper bushings (9) and the top cover (2), or disposed between the bottom of the lower bushings (11) and the base (3) in order to observe and record in real-time the changes of the rolling force under various working conditions.

A temperature sensor can also be installed on the stand to record temperature changes under different working conditions. Alternatively, a stand-alone infrared temperature measurement device can be used to measure the surface temperature of the rollers. Accordingly, the load cell and the temperature sensor may be connected to the display system of the Gleeble system so that the test data can be displayed.

2.3 Design of the mill

2.3.1 Basic parameters

a) Overall dimensions

The chamber of the Gleeble system is shown in Figure 2.6 where the maximum stroke is 120 mm, the height 110 mm and the width 290 mm. The minimum length of the strip must not be less than 20 mm. Thus the mill has to fit into the chamber horizontally, as shown in Figure 2.7 which requires the overall dimensions of 95mm wide by 100mm high by 280mm long.



Figure 2.6 Gleeble system chamber (elevated view)

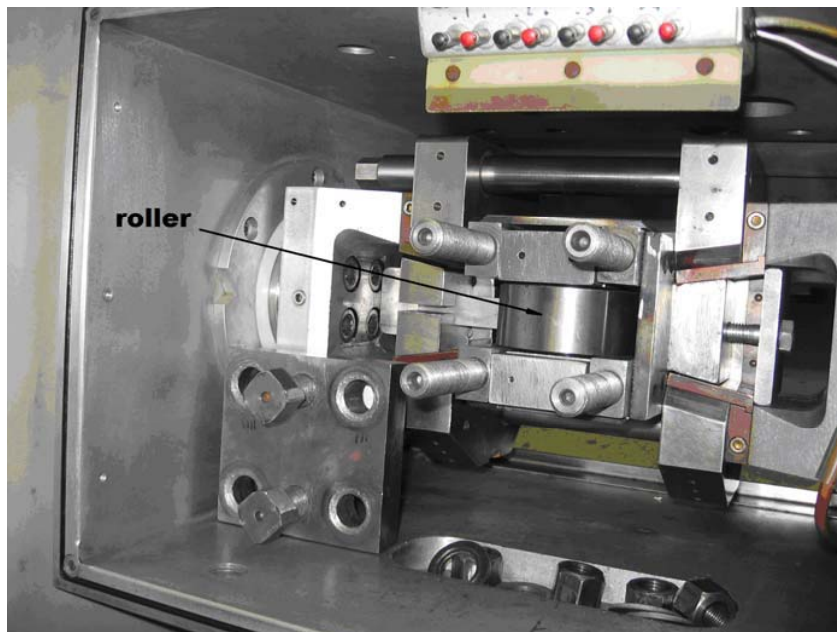


Figure 2.7 Half fixed fitted mini-mill in the Gleeble chamber

b) Dimensions of test materials

In accord with the operation procedures the strip will travel with the stroke and be driven into the roll gap. This creates lateral pressure on the left side and vertical pressure on its free end in the roll gap, as shown in Figure 2.8.

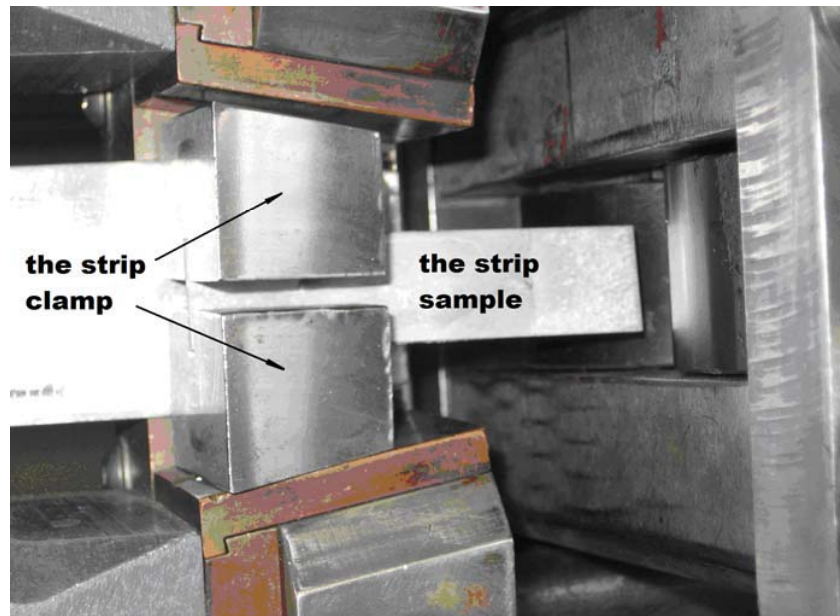


Figure 2.8 Strip undertaken lateral pressure on the left end

The maximum planned reduction in the work is proximately 30%. To fit in the chamber space and achieve the required reduction, the strip dimensions are $6 \times 16 \times 89$ mm.

c) Rolling force

The average rolling pressure p' as estimated by the S. Ekelund [125] was used to design the strength of the roller shaft and bearing:

$$p' = (1 + m)(K + \eta v) \quad (2-1)$$

where m is the influence coefficient of the rolling parameters, K strip deformation resistance in kg/mm^2 , η strip plasticity coefficient in $\text{kg}\cdot\text{s/mm}^2$ and v , the speed of deformation in s^{-1} .

m , K , η and v are determined from equations 2-2 to 2-5.

$$m = \frac{1.6\mu\sqrt{R(h_0 - h_1)} - 1.2(h_0 - h_1)}{h_0 + h_1} \quad (2-2)$$

where m is the influence coefficient of the roller materials, $\mu \approx 1.05$, h_0 , h_1 , thickness of strip (mm) before and after rolling respectively, R , the radius of the roller (mm).

$$K = (14 - 0.01t)(1.4 + C + \text{Mn} + 0.3\text{Cr}) \quad (\text{kg/mm}^2) \quad (2-3)$$

where t is the rolling temperature ($^{\circ}\text{C}$), C , Mn and Cr , the chemical composition of the strip (wt%).

$$\eta = 0.01(14 - 0.1t) \cdot C \quad (\text{kg}\cdot\text{s/mm}^2) \quad (2-4)$$

where C is the influence coefficient for rolling speed on η , when rolling speed is less than 6 m/s, $C = 1$.

$$v \approx 2\nu\sqrt{\frac{\Delta h}{R}} \cdot (h_0 + h_1)^{-1} \quad (\text{s}^{-1}) \quad (2-5)$$

where ν is the rolling speed in mm/s , Δh , the reduction of the strip. Then the rolling force in kgf is calculated as:

$$P = p' \times f \quad (\text{kgf}) \quad (2-6)$$

in which f , the contact area (mm^2), equals the average strip width b_m in the roll bite times the length of the contact arc,

$$L = \sqrt{R \times \Delta h} \quad (\text{mm}) \quad (2-7)$$

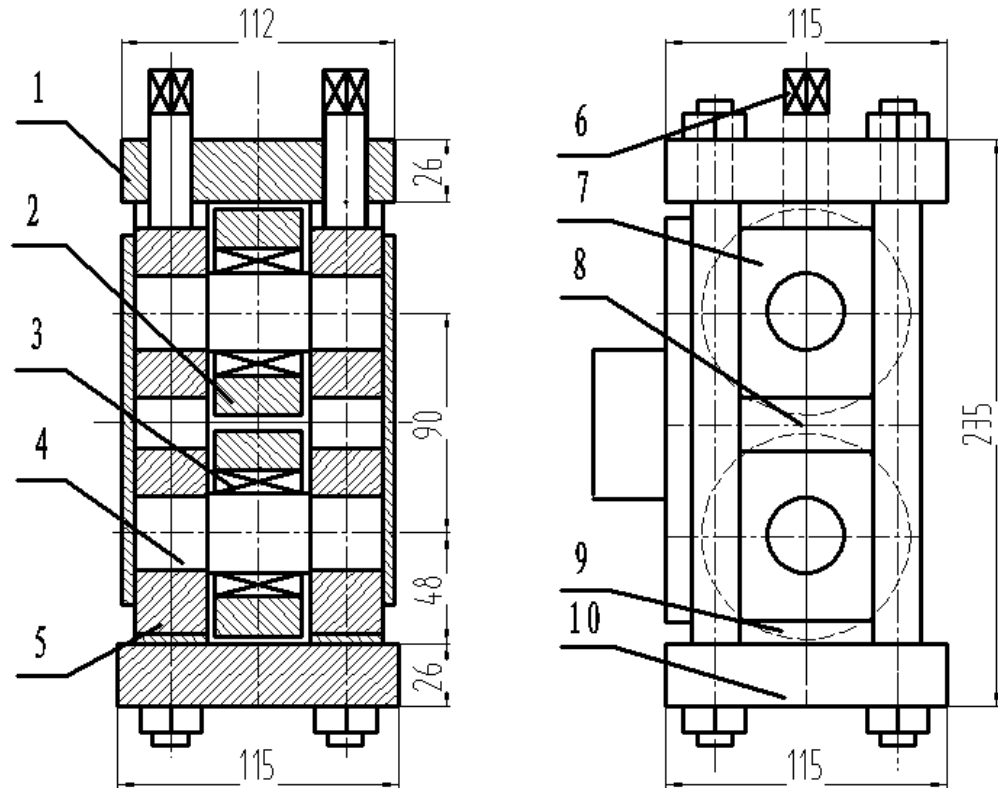


Figure 2.9 Assembly of the mill (dimensions in mm)

1: Top cover; 2: Work roll; 3: Roller bearing; 4: Shaft; 5: Mill housing; 6: The pressing down bolt; 7: Shaft bushings; 8 and 9: Blocks for roll gap adjustment; 10: lower cover

2.3.2 Designs

The LST-mill designed for the Gleeble system must have strong structural parts so that numerous experiments can be carried out. The design and manufacture of the principal parts will now be explained but due to the length limitations of this thesis only the housing, cover, base, coupling mount, work roll, shafts, bearings, method of adjusting the roll gap, will be described in detail. Figure 2.9 illustrates its assembly.

The details of the designs can be found in Appendix I.

2.4 Assembly

The rolling mill is called an LST-mill. It was successfully fitted into the Gleeble 3500 Thermo-mechanical Simulation System at the University of Wollongong and has satisfactorily met the design criteria. Photos in Figure 2.10 give images of the mill house, the roller system, the roll gap adjustment and the connection to the Gleeble machine.

Some experiments made use of the cooling system in the Gleeble machine for lubrication purposes. The system can be used for hot rolling experiments because it is fitted with heating facility. Infra-red heating was used to heat the rollers in order to simulate roll temperature in practical cold rolling.

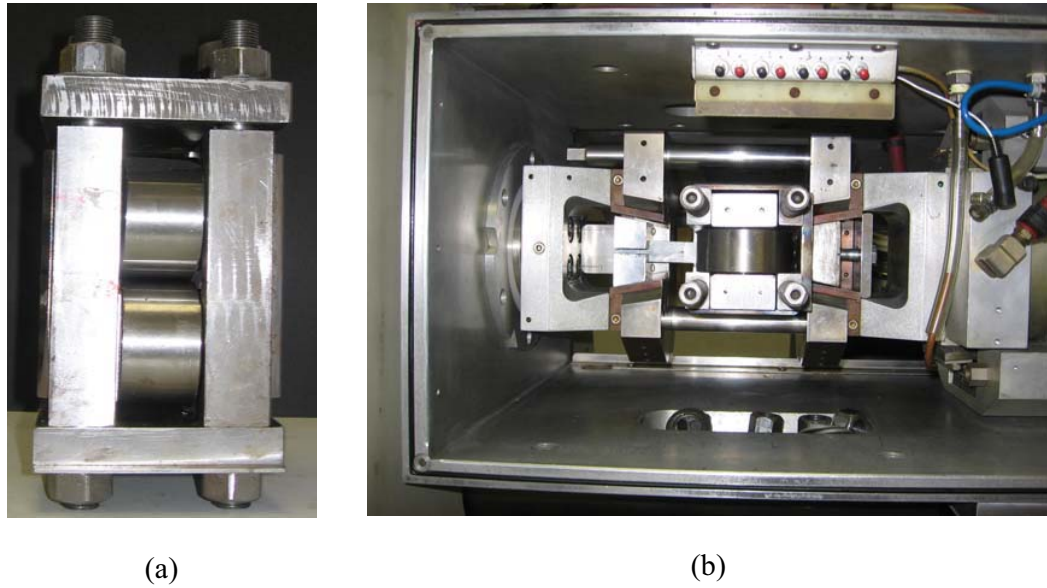


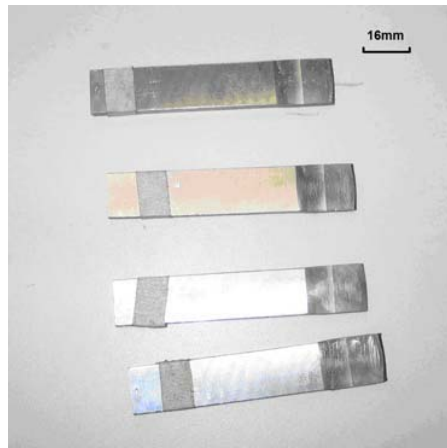
Figure 2.10 Assembly of the LST-mill. (a) LST mill; (b) LST mill assembled in the Gleeble machine

2.5 Application of the LST facility

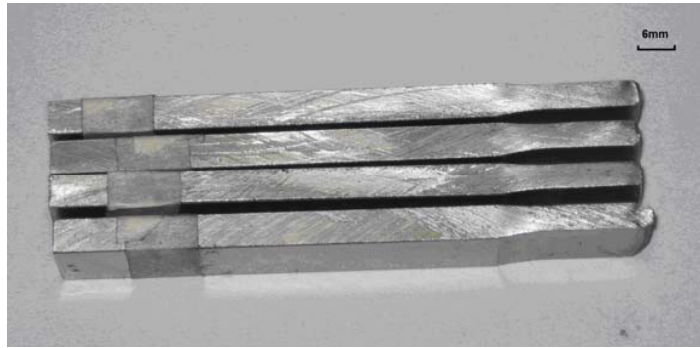
The innovative LST facility was used successfully in the experiments scheduled in the present study. A series of reductions from 7.2% to 30.5% and a sequence of Gleeble stroke speeds up to 0.13m/s were used in these tests. The deformed low-carbon-steel (LCS) strip samples, the roller surfaces and deformation forces were acquired fulfilling the requirements of the desired experiments.

2.5.1 Samples of deformed strips

Figure 2.11 displays the plane view and side view of the samples of deformed strips. They are of uniform thickness and are not twisted which demonstrates that the LST mini-mill connected to the Gleeble system successfully simulated the rolling experiments.



(a)



(b)

Figure 2.11 Photographs of the deformed LCS strip (originally 6mm thick, 16mm wide and 89mm long). (a) plain view; (b) side view

2.5.2 Appearance of the worked roller surface

Figure 2.12 shows photographs of the surface of the roller after 1, 5, 10 and 20 passes. There are distinct imprints of the contact zone visible on the surfaces. When the Gleeble jig moves 20 mm the imprinted curve on the roller is 22mm which implies that the roller and the strip have moved simultaneously by friction

and therefore the LST mini-mill has made it possible to carry out rolling tests that are not available in practical rolling operations, especially in the fundamental wear research on roll materials. The usage of LST mini-mill in conjunction with the Gleeble 3500 machine is a low cost option that can simulate rolling conditions, and facilitate the study of roll wear.

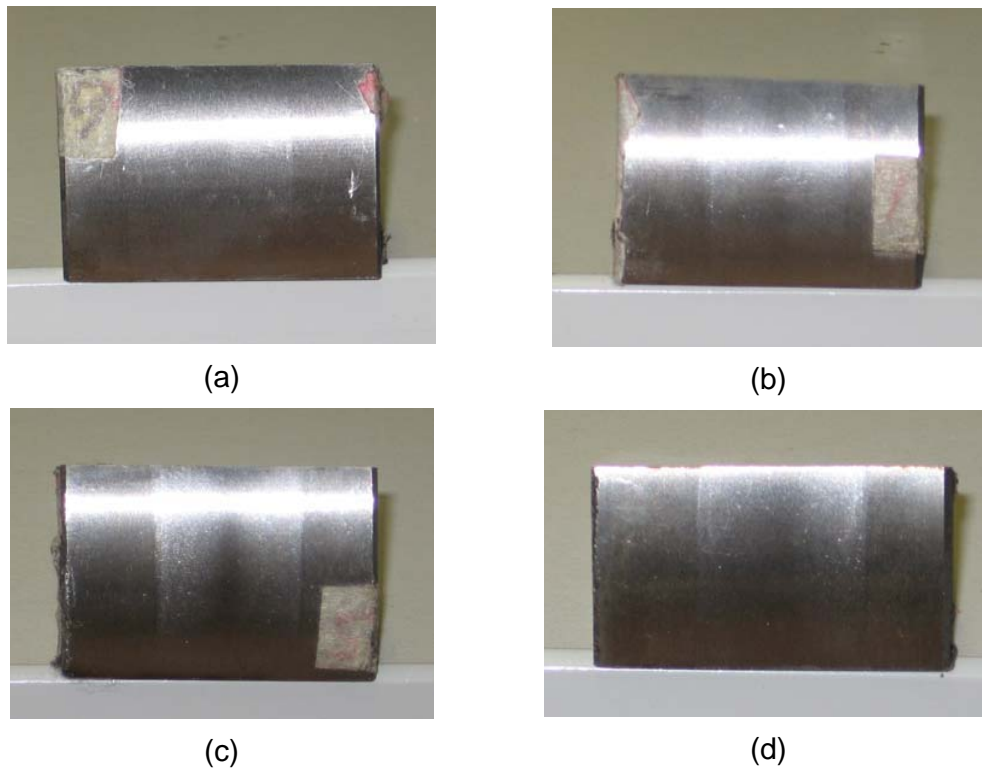


Figure 2.12 Photographs of the surface of a roller after:

(a) a single pass; (b) 5 passes; (c) 10 passes and (d) 20 passes

2.5.3 Force with the Gleeble system

Figure 2.13 shows the driving forces acquired by the Gleeble system at reductions of 7.2% , 17.9% , 26.6% and 30.5% respectively. Figure 2.12

indicates that the LST mini-mill can simulate rolling with steadily increasing forces so it is expected that the experimental data acquired by this system will be useful in future analysis.

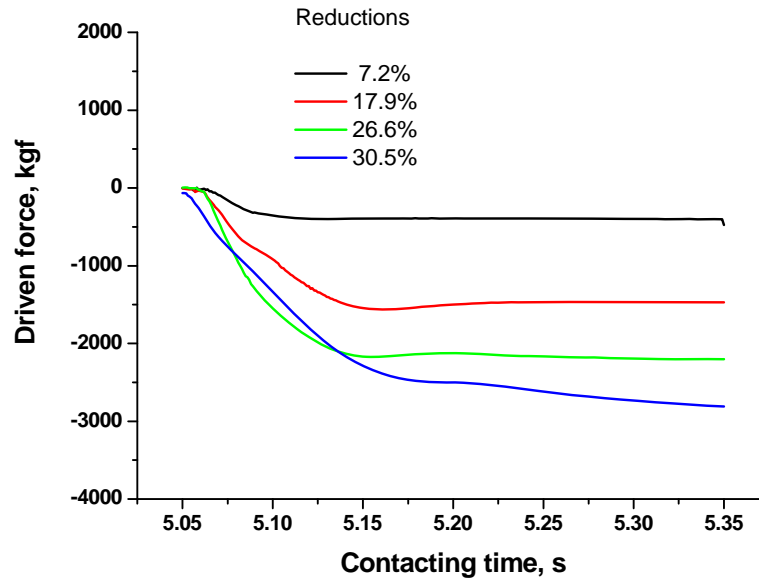


Figure 2.13 Forces acquired by the Gleeble system

2.6 Findings

In this chapter an innovative LST mini-mill attached to a Gleeble 3500 machine is described, it has successfully met the design criteria and has found to be a convenient way of conducting rolling tests and of studying of the roll surface.

2.7 Summary

1. The LST-mill is driven by the Gleeble machine and useful experimental data have been acquired by the inherent function of the machine. It is 115mm wide by

115mm long by 235mm high.

2. The roller comprises a shaft, a bearing, and a roller-ring. The chemical composition of the shaft and roller-ring may be different from each other. The shaft is made of high-chromium medium carbon steel while the material for the roll ring is determined by the scheduled experiments.

3. It is expected that the LST-mill tests can be successfully carried out in single pass and/or in multiple passes of simulated stalled rolling experiments and wear mechanisms of the work roll surfaces during cold rolling of steel can be thoroughly and conveniently investigated.

Chapter 3 Experimental Instruments and Methodology

3.1 Introduction

The lateral-setting test (LST) mini-mill described in Chapter 2 was used to carry out single-and multi-pass rolling with a view to obtaining information on the evolution of worn roll surface while cold rolling. A series of wear tests were conducted with an MMS-2B disc-to-disc friction and wear testing machine. The surfaces of the discs were evaluated after the tests by surface profile-meter, SEM microscopy, and (AFM) technology. An electronic analytical balance was used to weigh the samples before and after each test to calculate the weight loss and characterize the wear properties.

In this chapter the test materials, equipment and experimental processes are described in detail.

3.2 Test materials

Conventional high chromium 4%Cr, which is similar to the forged work roll in a cold mill plant, and 4%Cr +0.11%Ti materials were the principal test materials in the present study. Paired rolls in the disc-to-disc wear tests and strips used in LST experiments are low-carbon steels.

a) Chemical compositions of materials in the experiments

Table 3.1 and 3.2 show the chemical compositions of the low-carbon steel and the roll materials respectively. The low-carbon steel was a 6mm thick hot rolled low carbon steel (LCS) strip. The samples were ground to 6mm thickness \times 18mm width \times 90 mm length and the required surface roughness varying from 0.8 μ m to 3.05 μ m. The hardness is from HB 87 to 92.

The roll size is shown earlier in Fig. 2.7, the hardness were from HRC 58 to 65.

Table 3.1 Chemical composition of the low-carbon steel (wt%)

<i>C</i>	<i>Si</i>	<i>Mn</i>	<i>P</i>	<i>S</i>	<i>Al (soluble)</i>
0.05~0.06	≤ 0.03	0.25~0.40	≤ 0.008	≤ 0.003	0.015~0.045

Table 3.2 Chemical Composition of the roll materials (wt%)

<i>Elements</i>	<i>C</i>	<i>Si</i>	<i>Mn</i>	<i>Cr</i>	<i>Ni</i>	<i>Mo</i>	<i>Ti</i>	<i>P</i>	<i>S</i>
4%Cr	0.84	0.41	0.36	3.99	0.27	0.51	--	0.009	0.004
4%Cr + Ti	0.80	0.45	0.40	4.0	0.30	0.50	0.11	0.01	0.005

b) Preparation of the roll materials

The roll materials were melted in a 200kg vacuum induction furnace and poured into a metallic mould to produce 200mm \times 200mm ingots. They were then reheated to 1200°C in a nitrogen protected atmosphere, forged into Φ 85mm bars and allowed to cool in air. Spheroidising annealing was carried out at 780°C for 2.5 hours. After

rough machining to $\Phi 52$ and 62mm the bars were further hardened and tempered (austenitisation for one hour at 920°C and tempered at 150°C for 2 hours). They were then turned into discs and rollers as required for the disc-to-disc wear tests and LST experiments. The surface roughness of the roller or disc was controlled to satisfy the scheduled experiments. Figure 3.1 shows the flow chart of disc and roller manufacture process. The microstructure and mechanical properties of the experimental rollers and discs are described in Chapter 6.

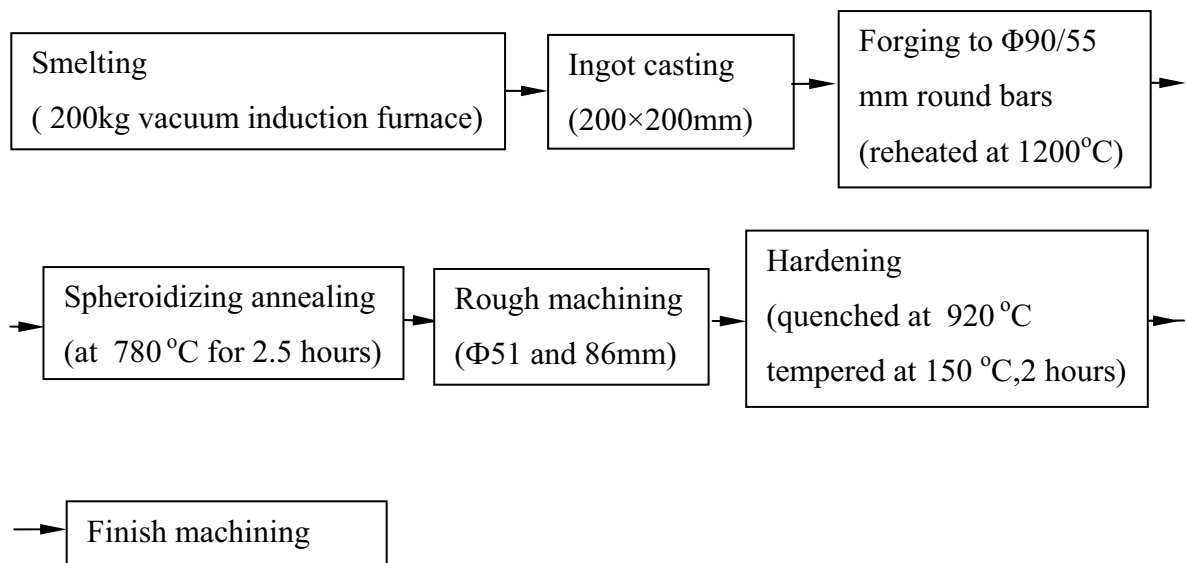


Figure 3.1 A schematic diagram showing the manufacturing of roll and disc

3.3 Single and multi-pass rolling tests by LST

Single and multi-pass rolling tests, also called LST (Lateral Setting Test), were carried out by the mini-mill fitted to the Gleeble 3500 Thermo-Mechanical

Simulating system, as described previously in section 2.2.2.

3.3.1 Gleeble 3500 Thermo-Mechanical Simulator

The Gleeble 3500 is a digital, fully integrated, closed loop control, thermal and mechanical testing system. This system is a complete, hydraulic servo system capable of exerting up to 10 tons of static force in tension or compression. Displacement rates as fast as 1000mm/second can be achieved. Linear velocity displacement transducers, load cells, and a non-contact laser extensometer provided feedback to ensure accurate execution and repeatability of the test program.

The system can be changed from one control mode to another and the program switched between control variables as often as required during the test. Control modes available include stroke displacement, force, various extensometers, stress, and strain.

3.3.2 Lateral Setting Test procedure

The two rollers were 58mm diameter, as described in Appendix I. Both materials were tested under dry contact and oil-mist lubricating conditions. The experimental schedule included tests with different values of roller and strip surface roughness, traversing speeds and reductions.

a) Strip reduction

Four reductions from 7.2% to 30.5% were selected in the single pass rolling tests. The Gleeble 3500 stroke speeds were controlled from 15 to 127mm/s. The surface

roughness of the strip was from 0.8 to 1.0 μm before rolling while the roller surface has a roughness from 0.6 to 0.8 μm .

b) Testing at different roller surface roughness

Values of surface roughness ranging from 0.5 to 3.0 μm were tested at a reduction of 26.6%. The Gleeble machine stroke speeds and strip surface roughness were the same as in the strip reduction tests.

c) Testing at different strip surface roughness

In these tests, the strips were surface-ground to give a range of surface roughness values from 0.9 to 3.0 μm . The roller surface was from 0.6 to 0.8 μm and a reduction of 26.6% was applied.

d) Multi-pass rolling tests

Up to 20 tests were carried out on the two roll materials under dry and oil-mist lubricating conditions respectively. The same reduction of approximately 26.6% was used for each pass, at a fixed speed of 64mm/s. The roll surface roughness was from 0.6 to 0.8 μm and the work-piece was 1.2 to 2.4 μm before rolling.

3.4 Disc-to-disc wearing tests

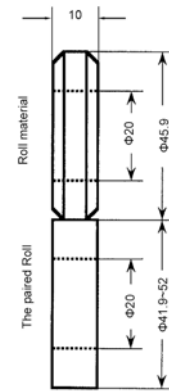
3.4.1 Equipment

A MMS-2B model wear machine supplied by Jinan Yihua Tribology Testing Technology Co.,Ltd, China, was used for these tests, and Figures 3.2 to 3.4 illustrate the settings.

The test machine can carry out wear resisting tests under rolling and combined rolling and sliding movements. Simulated material can be tested under dry lubricated and abrasive wear conditions. A computer system controls the required torque, coefficient of friction, and test time, during the test.



Figure 3.2 MMS-2B disc-to-disc test system



The roll material is made by the material used in rollers. The paired roll is made with the LCS strip material.

Figure 3.3 Schematic view of the disc-to-disc setting

Wear tests can be carried out at a maximum load of up to 2000N. The maximum moving distance of the upper sample is -4 to +4mm. Friction torque can be measured in a range up to 22N·m. Friction tests may last from 1s to 9999min.

The surface roughness of the paired discs were 0.8 to 1.0 μ m and 0.6 to 1.0 μ m respectively. The dimensions are illustrated in Figure 3.3. The roughness of the contact face was 0.6-0.8 μ m. The paired material disc was a low carbon steel 10mm thick.

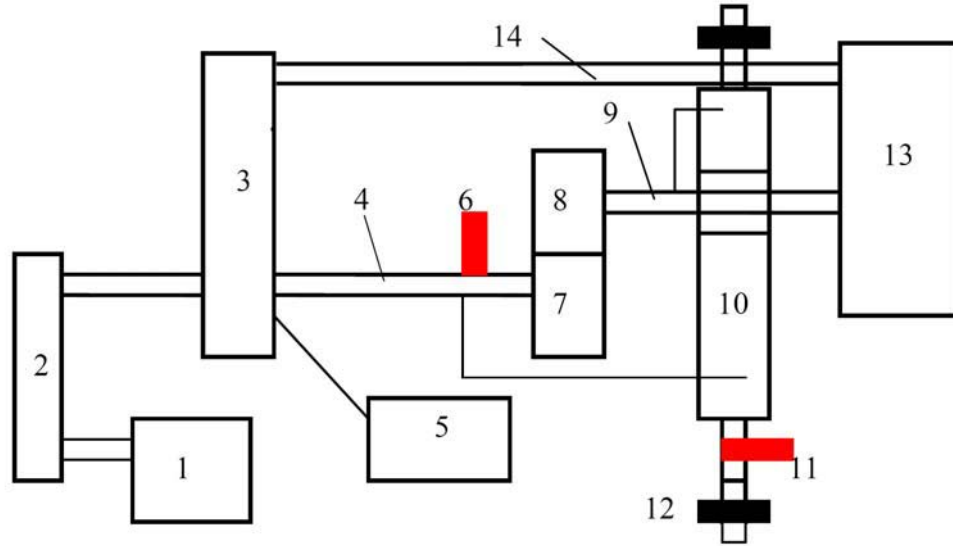


Figure 3.4 Schematic view of the disc-to-disc test system.

1: motor; 2: transmission belt; 3: gear box 1; 4: paired disc driving shaft; 5: torque measuring weight; 6: rotating speed sensor; 7: paired disc; 8: sample disc; 9: sample disc driving shaft; 10: load adjustment spring; 11: load sensor; 12: load adjustment bolt; 13: gear box 2; 14: driving shaft

3.4.2 Wear test procedure

A series of tests were carried out under dry contact and lubrication for the two roll materials. The lubricant, an emulsion with 3.9% Quakerol N680-2-DPD (details shown in chapter 5), was from an industrial cold rolling mill plant. A rolling-sliding wear test configuration was applied because it closely simulates the conditions found in service for work rolls in cold mills. Wear in this configuration may result from the high alternating stresses experienced during rolling or from the relative motion between the paired roll surface and specimen. Thus the experiments on roll

materials wear included:

- a) Wearing-in under loads from 500N up to 2000N;
- b) the duration of test cycles: for dry contact from 10 up to 390 minutes and with lubrication from 5 to 480 minutes at a maximum distance of approximately 4000m;
- c) at speeds ranging from 214 revolutions per minute (rpm) to 757 rpm testing at different slip rate from -2% to 6.3%. Four pairs of discs, 52, 44, 43 and 42mm outside diameters, were selected according to the requirement in the slip rate tests. The slippage was determined by the following equation:[128]

$$s\% = \frac{R_1 W_1 - R_2 W_2}{R_1 W_1} \times 100 \quad (3.1)$$

where R is the roll radius, W is the roll speed (rpm), and 1 refers to the upper roll and 2 to the lower roll.

Generally, load, speed, test duration, and slip rate were controlled at 1000N, 597rpm, 30 minutes and 1.5% resp. in the above series unless a specific test parameter was indicated.

Wear was evaluated by measuring the weight loss with the FA Series Electronic Analytical Balance (EAB), which had a capacity of 200g with an accuracy of 0.0001g.

3.5 Facilities and approaches to evaluate experimental samples

In the present study, the samples tested were examined and evaluated for surface roughness, surface topography, surface morphology and the mass change. Thus the surface profile meter and some microscopic approaches need to be explained.

3.5.1 Atomic Force Microscopy (AFM)

A Multi-Mode Scanning Probe Microscope (SPM) from Digital Instruments operating in contact AFM mode (Nanoscope IIIA AFM) [1] was used to obtain topographic images of the surfaces of the samples. This AFM has a lateral resolution of 1–5 nm and a vertical resolution of 0.08 nm. Figure 3.5 illustrates the design of the probes and the cantilever spring constants.

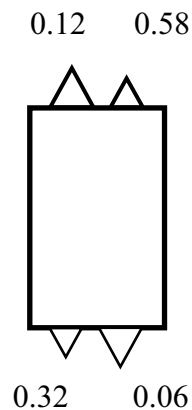


Figure 3.5 Design of the probe and its four silicon nitride cantilevers showing spring constants (N/m)

The V-shaped nano-probe cantilevers were made of silicon nitride (Si_3N_4) with a nominal tip radius of 20 - 60 nm. The length of each cantilever is 100 and 200 μm .

The tips are shaped like a pyramid with an included angle of 35° on all four sides.

The tip with 0.12m/s spring constant was used in the present study.

AFM was principally used in the assessment of the roll surface from the LST tests.

The tested rolls were carefully cut around the wear marks that were imprinted on the roll surface before rolling. The samples were cleaned before testing to ensure they were free of contamination. Each sample was scanned at 6 points around the area as illustrated in Figure 3.6, including the raw surface, inlet and exit site, left and right site, and the middle point. The location corresponds to the steady state rolling condition.

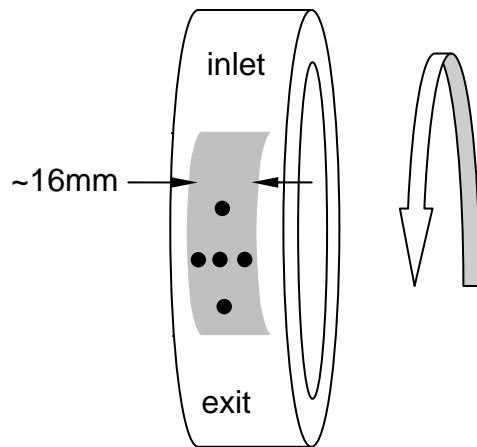


Figure 3.6 AFM scanned positions on each roller surface after the LST tests

3.5.2 Hommel Tester T1000 for roughness measurement

The Hommel Tester T1000 is a modern, easy to handle, portable instrument. It can characterise the periphery of a roll with a resolution of $0.01\mu\text{m}$.

A number of standard surface roughness parameters (R_a , R_z , R_t , R_{max} , t_{pi} , t_{pa}) are available for determining the magnitude of surface flaws and characterising the surface profile. These can be calculated from the unfiltered measured profile, the filtered roughness profile, or the filtered waviness profile, depending on the type of parameter measured. The instrument is shown in Figure 3.7.

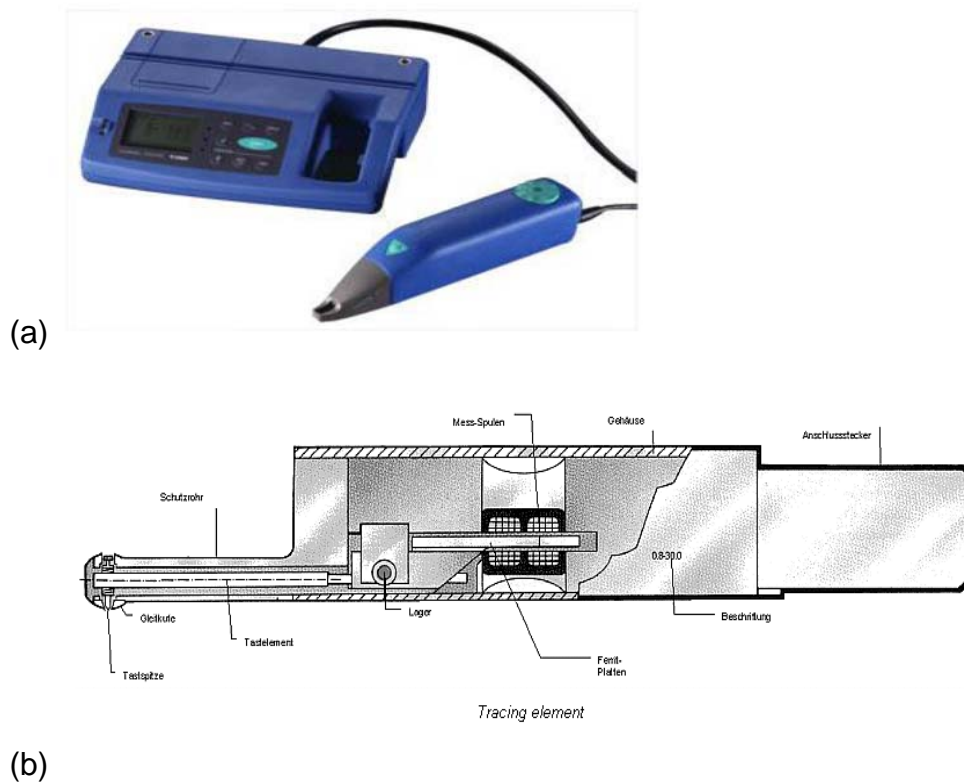


Figure 3.7 Hommel Tester T 1000 instrument: (a) an outline of the profile meter; (b) details of tracing elements

The Hommel Tester T1000 can carry out profile measurements in a range from 80 to 320 μm . Its tip radius is 5 μm at an angle of 90° . The engaging force is 0.8mN when the measurement is carried out.

When carrying out surface roughness tests, 5 points were measured on each sample, keeping the tip moving vertical to the rolling direction.

3.5.3 Philips XL30 Scanning Electron Microscope (SEM)

The Philips XL30 SEM was used to analyse the roller surface and microstructure of the materials tested. The fine electron source of the lanthanum hexaboride single crystal system gives a much brighter source with higher resolution than a conventional tungsten filament SEM. Useful magnification in excess of 200,000 times are obtainable which translates to a resolution of 3.5 nm at an accelerating voltage of 30 kV.

The XL30 SEM can be used for both imaging and micro-analysis of conductive and/or coated specimens. This microscope is also equipped with a quantitative Energy Dispersive Spectrometer capable of chemical analysis with a detectable element range from B-U. An X-ray Mapping facility is also available. An Electron Back-Scattered Diffraction (EBSD) Pattern Camera is available which can determine sample grain orientation together with a Mapping Facility that is able to provide details such as sample normal, coincident lattice sites, grain boundary mis-orientation, sample normal, pole Figures, and diffraction pattern maps.

3.6 Summary

In this chapter the principle instruments and experimental methodology are described.

Chapter 4 Study on Roll Surface Profile Changes by Single and Multi-Pass Stalled Rolling

4.1 Introduction

Investigations on the evolution of a work roll surface profile were carried out by studying the surface of a work piece. It is anticipated that a detailed study of the changes to the roll surface profile should provide an understanding of the process of surface deterioration. The objective of this chapter was to examine the effects of cold rolling parameters, namely, strip to roll surface contact mode, and the initial workpiece surface states on the changing profile of the roll surface.

In this chapter stalled rolling was introduced via a mini-mill fixed into the Gleeble 3500 Mechanical Simulation System. This makes it possible to carry out an investigation into the effects that several rolling parameters have on the changes in the roll surface profile after single pass and multiple-pass rolling. Roll materials and the chemical composition of the strip are outlined in Chapter 3. Dry contact and oil mist lubrication were used to compare surface deterioration. The experiments are divided into the following groups that consider:

- i. the effect of surface roughness of both the roll and the strip;
- ii. different lubricating conditions, and
- iii. the effect of pass reduction and rolling speed.

The rolling tests were performed at a nominal reduction range of 5-30% at ambient temperature. Due to the low stiffness of the sample and the capability of the Gleeble, the simulated experimental rolling speeds were set within the range

of 0.05-0.13 m/s. Multi-pass rolling under a defined rolling condition was also carried out to make an extensive investigation of the deterioration of the roll surface.

To quantify changes to the surface profile a Hommel Tester T1000, that can measure the circumference, and the AFM were used to characterise the surface after rolling. The average surface roughness (R_a), skewness (S_k), kurtosis (K_{ur}) and power spectrum density (PSD) were analysed to examine the effect of rolling parameters on the surface profile.

4.2 Change in surface morphology after a single pass of rolling

4.2.1 Surface roughness

Figures 4.1 to 4.3 illustrate the changes in surface roughness R_a after a single pass under conditions given in Table 4.1. The initial surface roughness values were not always the same due to grinding, and are marked in the Figures when the initial surface roughness is not a factor to be tested. Both the 4%Cr rolls and 4%Cr+Ti rolls were tested under dry contact mode and oil mist lubricating conditions.

Table 4.1 Rolling parameters of the mini-mill tests

Testing groups and parameters	Reduction (%)	Speed (10^{-2} m/s)	Strip R_a (μ m)	Roll R_a (μ m)
Strip reductions (%): 7.2, 17.9, 26.6, 30.5	--	1.5, 3.0, 6.2, 12.7	0.8 to 1.0	0.3-0.6
Effect of roll surface (μ m): 0.53, 0.73, 1.05, 170	26.6	1.5, 3.0, 6.2, 12.7	0.8 to 1.0	-
Effect of strip surface (μ m): 0.93, 1.40, 1.95, 3.05	26.6	1.5, 3.0, 6.2, 12.7	-	0.3-0.6

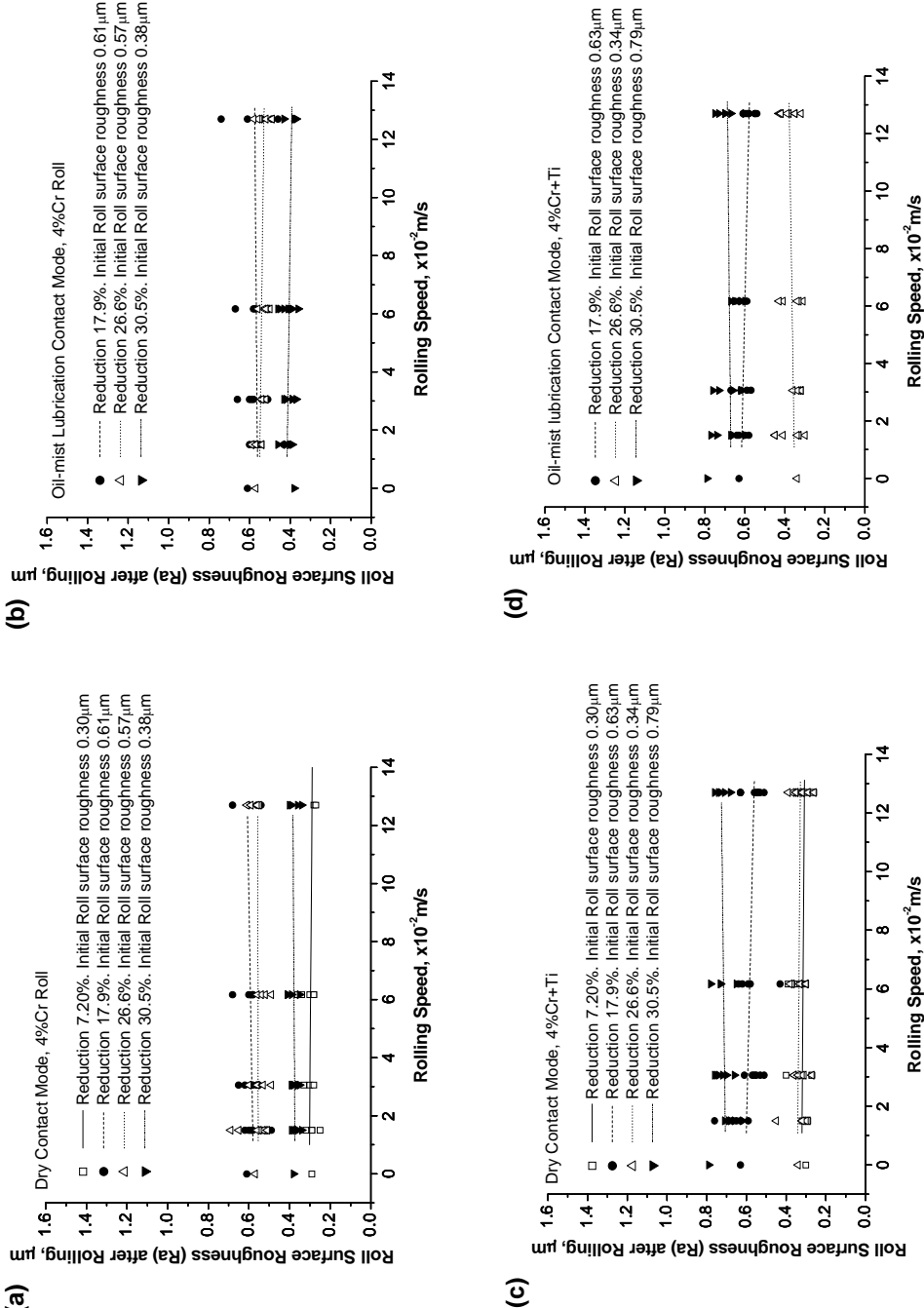


Figure 4.1 Effect of reduction on roll surface roughness

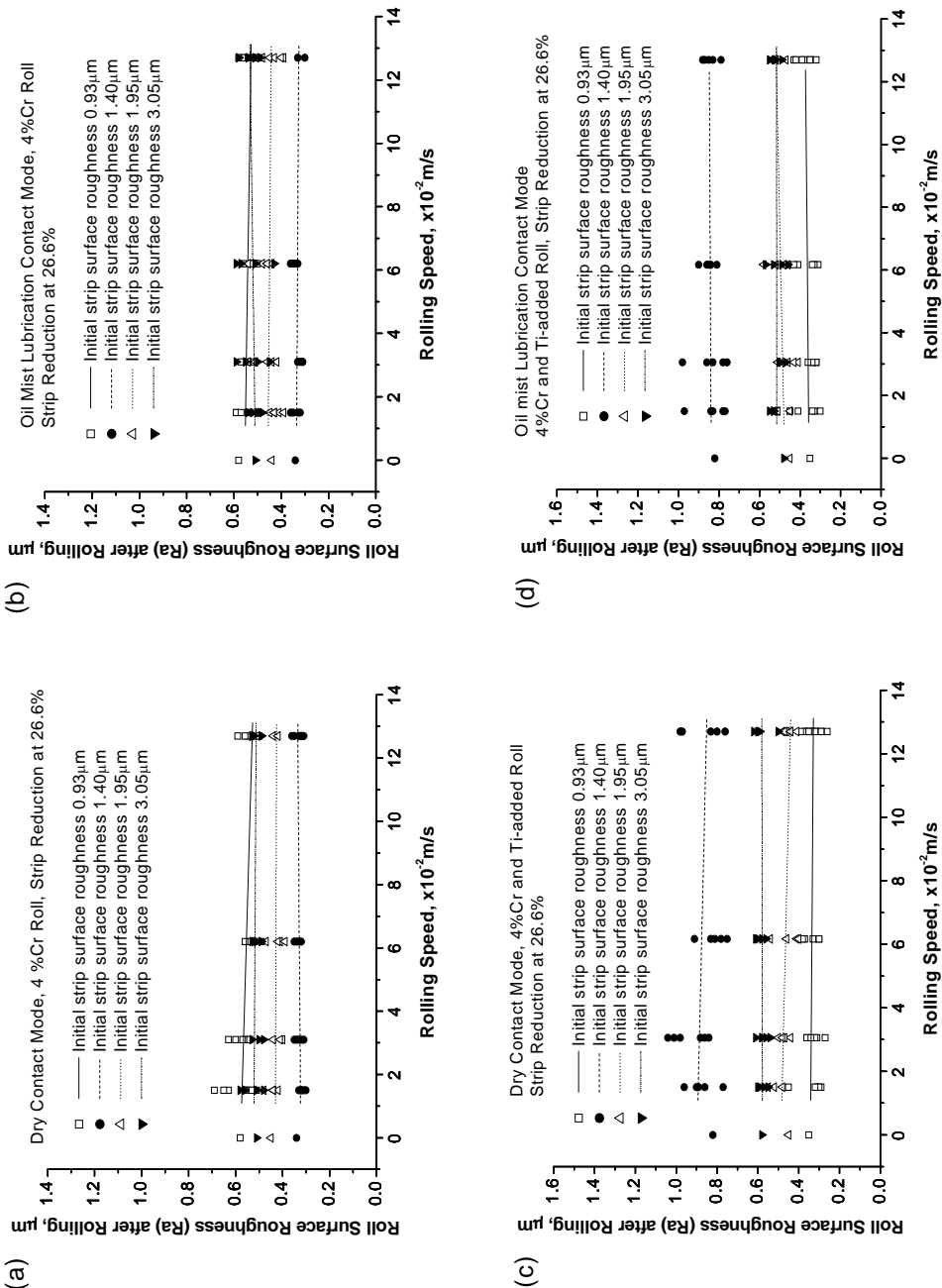


Figure 4.2 Influence of strip sample roughness on roll surface roughness

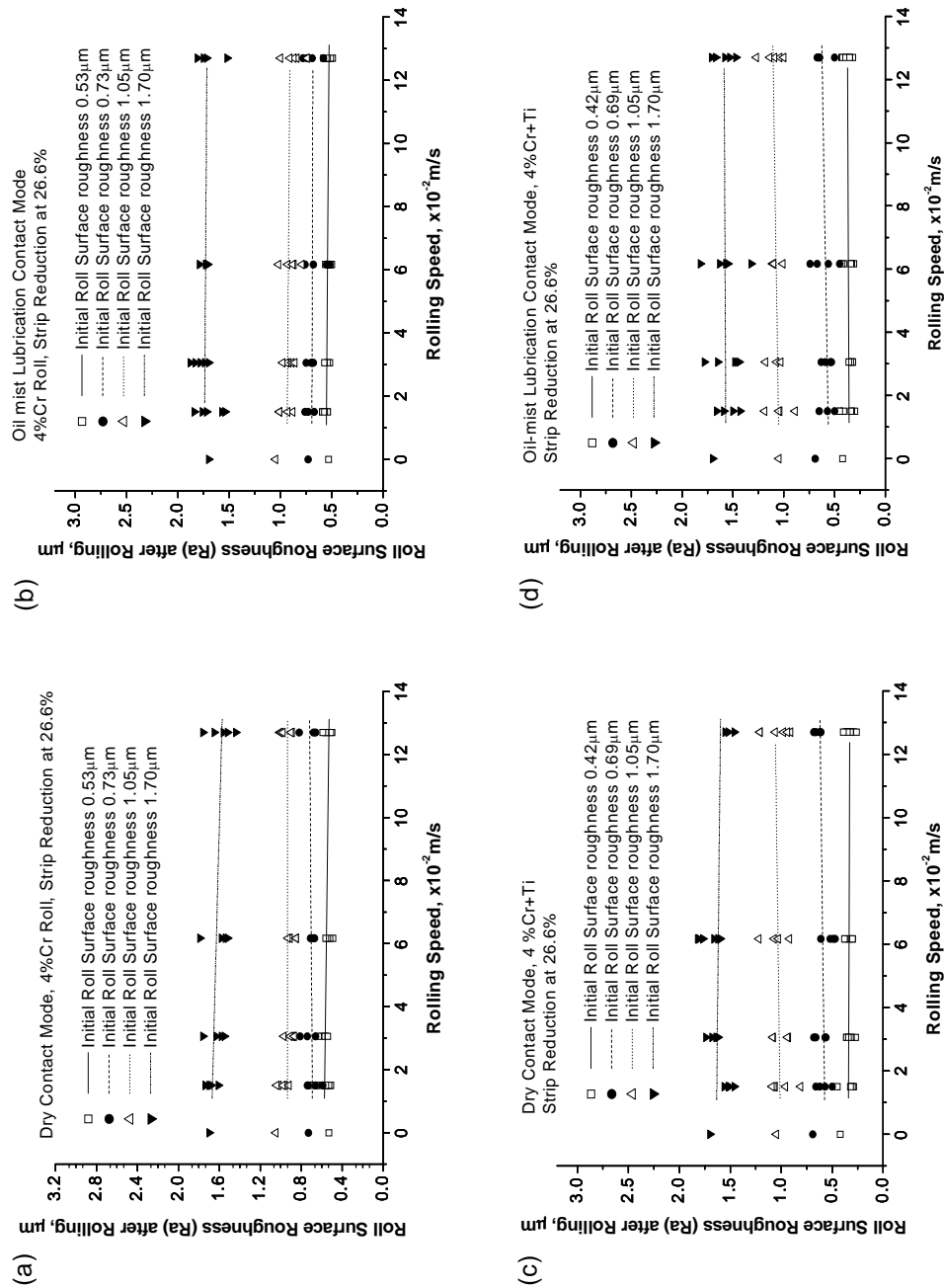


Figure 4. 3 Roll surface roughness compared to its initial surface profile

From Figures 4.1 to 4.3, one cannot conclude that the roll surface is affected significantly by reductions, initial surface roughness and surface profile of the workpiece after a single pass of rolling.

Reduction alters the surface roughness of the roll insignificantly after a single pass reduction. The surface roughness values of the roll used are very close after rolling reductions of 7.2% and 26.6% for the rolls with 4%Cr and with 4%Cr+Ti when their initial surface roughness are 0.30 and 0.34 μm respectively (Figure 4.1 (c)). The roughness of 0.57 μm and 0.63 μm of the 4%Cr roll produced about similar results when they respectively accomplished 26.6% and 17.9% reduction under dry contact and oil mist lubrication conditions (Figure 4.1 (a) and (b)). In all cases the values of the worked roll surface roughness are almost the same as their initial roughness values.

The roll surface roughness is not modulated after rolling by the strip surface roughness. For example, the 4%Cr roll with 0.58 and 0.51 μm roughness produced approximately similar values after they respectively encountered the workpiece at 0.93 and 3.05 μm roughness under both contact modes (Figure 4.2 (a) and (b)). With 0.45 and 0.48 μm initial surface roughness, the 4%Cr with 4%Cr+Ti rolls produced similar results when they worked with 3.05 and 1.95 μm workpieces under lubricating conditions (Figure 4.2 (d)).

With the surface roughness of the 4%Cr roll changes from 0.53 to 1.70 μm and from 0.42 to 1.70 μm for 4%Cr+Ti rolls, the roll surfaces after rolling show no change in roughness from their initial ones at 26.6% reduction under both dry and lubricated contacts. This indicates that the surface of the roll is not affected

by a single pass of rolling.

As for the rest of the roll with minor differences in initial surface roughness, neither the 4%Cr roll nor the roll with 4%Cr+Ti changed their surface roughness when they were rolled under the same operating conditions. There was also no change of roughness as the rolling speed increased.

However, the above analysis does not indicate that the surface profile is not modified by a single pass reduction, in fact statistical measurements such as average roughness or root mean square roughness, have limitations for characterising the primary information of a given surface topography [166].

4.2.2 3-D roller surface topography after a single-pass of rolling

Figures 4.4 and 4.5 illustrate 3-D roller surface topographies by AFM before and after a single-pass of rolling for the 4%Cr and the 4%Cr+Ti materials respectively. The tests were carried out at 0.015m/s reduction under a 26.6% reduction. Roller surface roughness values were respectively 0.34 μ m and 0.53 μ m for the 4%Cr+Ti and the 4%Cr materials. The strip surface roughness used in these tests was approximately 0.9 μ m.

From Figures 4.4 and 4.5 it can be seen that the roll surface changes little after one pass of rolling. Nevertheless, the 4%Cr+Ti roller surface seems less influenced than the 4%Cr roller at both dry-contacting and lubricated conditions. Meanwhile, the 4%Cr roller surface exhibits some difference between dry-contacting and lubricated conditions, indicating the effects of lubricating condition and/or roller material on the surface features even after a

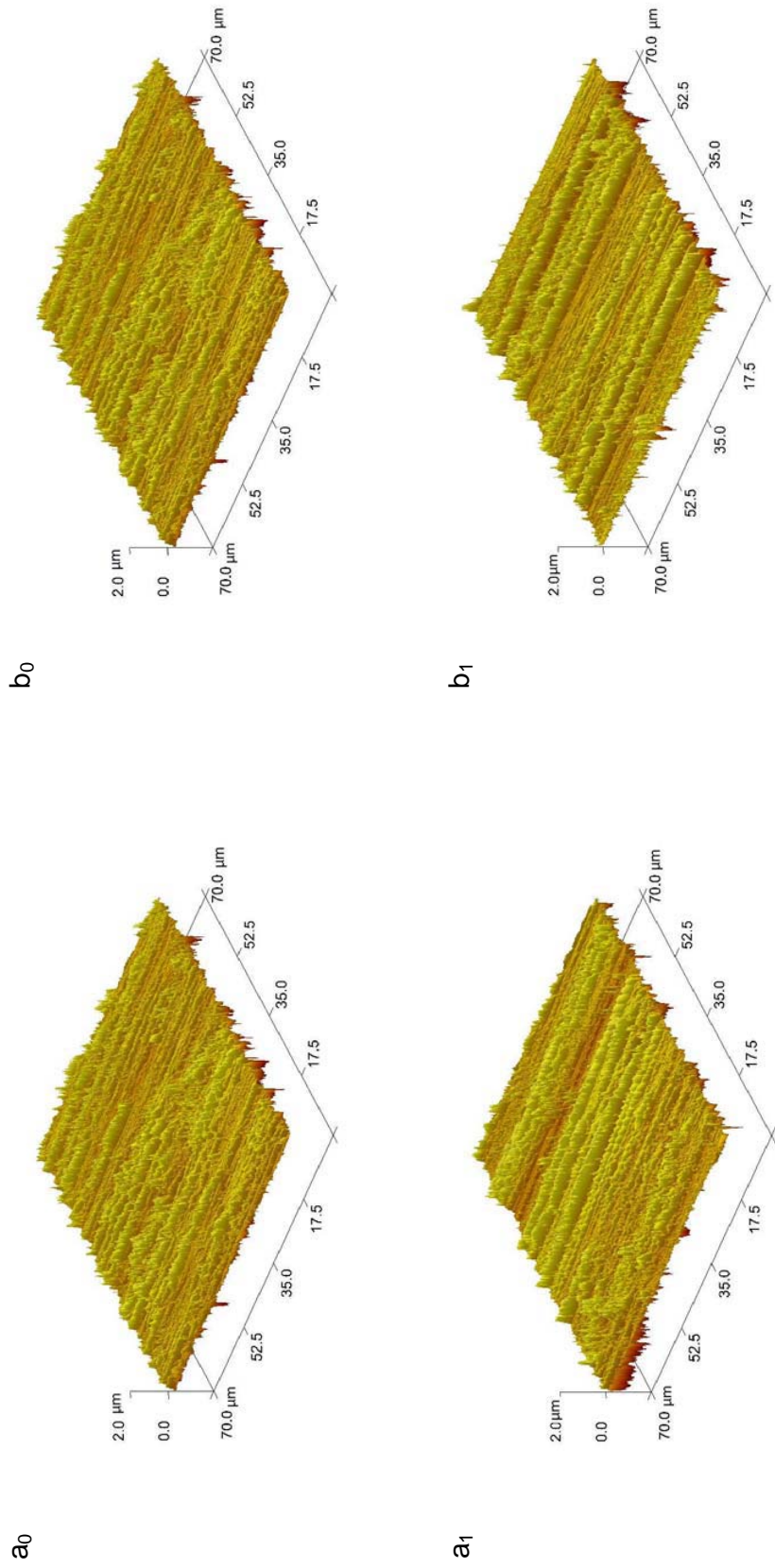


Figure 4.4 Surface topographies of the 4%Cr roller before test (a_0 and b_0) and after one pass of rolling at 26.6% reduction. (a_1 at dry-contacting; b_1 , at oil-lubricating)

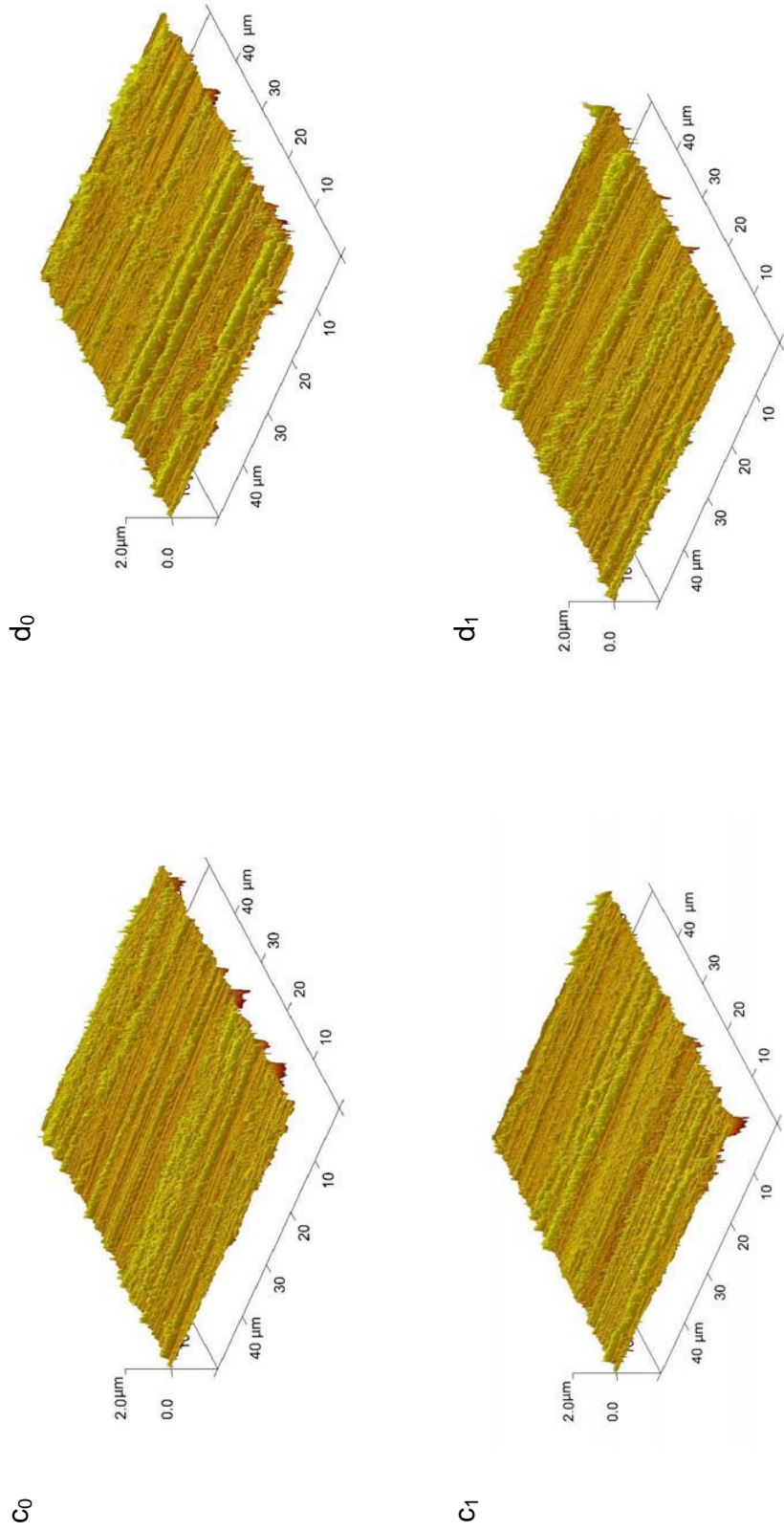


Figure 4.5 Surface topographies of the 4%Cr+Ti rollers before test (c_0 and d_0) and after one pass of rolling at 26.6% reduction. (c_1 at dry-contacting; d_1 , at oil-lubricating)

single pass of rolling. Thus, an in-depth investigation of the information about the distribution or intrinsic roughness and transverse properties of the surface profile was carried out to determine changes in surface morphology under defined rolling conditions.

4.3 Enhanced surface feature analysis using Fast Fourier Transform (FFT) and Power Spectrum Density (PSD)

4.3.1 Definitions of FFT and PSD

The traditional roughness parameter, such as average roughness or root mean square roughness only contains the vertical direction information. Therefore it neglects important in-plane spatial information. The power spectral density (PSD) decomposes the surface profile into its Fourier components or spatial frequencies (F). It is the most appropriate way to characterize the micro roughness of a surface with a spatial wavelength range from several centimeters to a few hundred nanometers.

Definitions for FFT and PSD and their use in analysing surface features can be found in Appendix I. PSD hereafter is defined as power spectral density in either the direction perpendicular or parallel to the rolling direction while a 2D-PSD is an in-plane power spectral density.

4.3.2 Surface profiles after different reduction of the workpiece

Figure 4.6 displays the results of the PSD analysis of the surface of the 4%Cr roll at 7.2, 17.9, 26.6 and 30.5% reductions. The roughness Ra is from 0.35 to 0.42 μm at a rolling speed of 0.127m/s. The roughness of the workpiece before

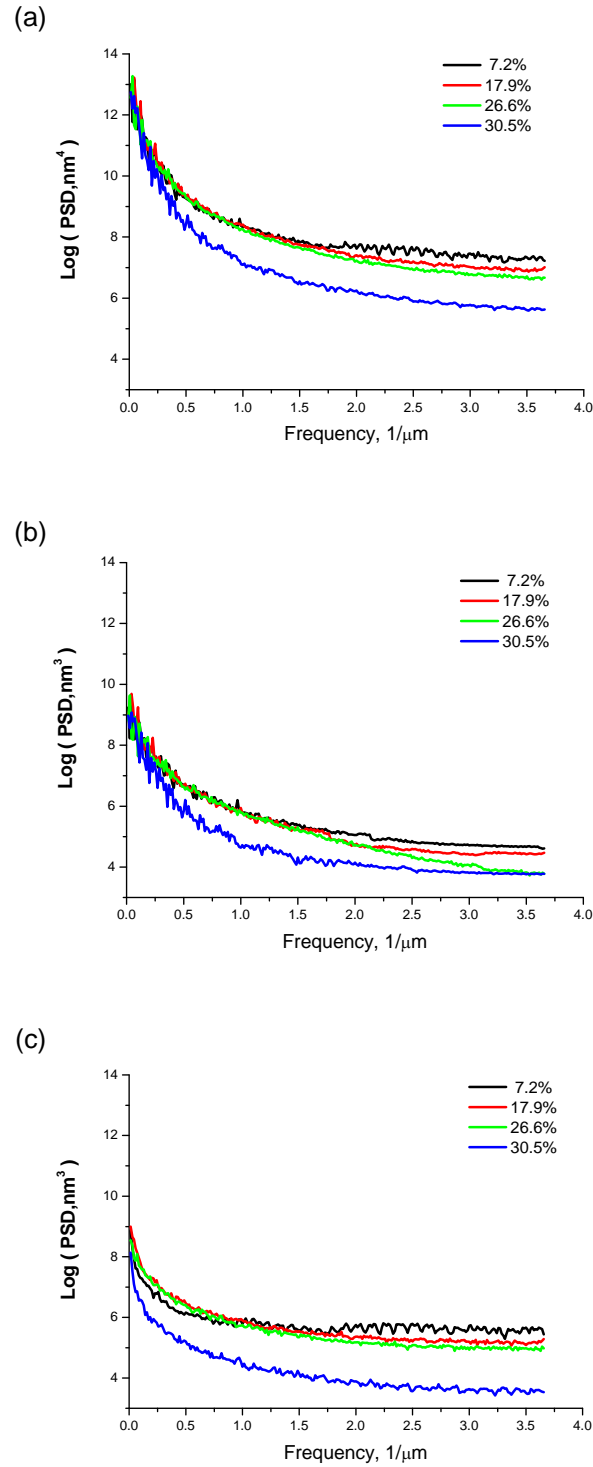


Figure 4.6 PSD analysis of roller surface at different reductions in the workpiece: (a) 2D PSD; (b) 1D-PSD, perpendicular to the direction of rolling; (c) 1D-PSD, parallel to the direction of rolling.

rolling is approximately 0.8 to 1.0 μm . The rolling operations were carried out under dry contact conditions.

Since the initial roughness was limited to 0.35 to 0.42 μm , it is assumed that all the surface profiles are characterised with a similar original PSD distribution in all frequency domains. The results of the PSD analysis reveal that for reductions from 7.2 to 26.6%, the surface profile at a larger amplitude- frequency domain is affected. When the frequency is higher than 1.25 kHz both the 2D-PSD and PSD of the roller surface decrease circumferentially and axially as reduction increases.

However, the 30.5% reduction shows a significant influence on the power spectrum density, especially in the axial direction. One should bear in mind that the property of a given surface profile is dominated by the axial feature due to grinding. Nevertheless the PSD perpendicular to the rolling direction is affected more in a larger wavelength domain (small frequency) at 30.5% reduction than with smaller reductions. Thus a further examination of the section analysis on the surface perpendicular to the rolling direction could be useful in explaining the above circumstances.

Figure 4.7 shows a comparison of the results of a section analysis in the axial direction on the roller surface after rolling at reductions of 26.6% and 30.5%. It can be seen in Figure 4.7 (a) and (c) that the roll peaks were flattened more extensively at 30.5% reduction than at 26.6%.

FFT analysis shown in Figures 4.7 (b) and (d) indicates that substantial differences exist between the two surface features after 26.6% and 30.5% reductions. Table 4.2 summarizes the roll surface FFT features before and after

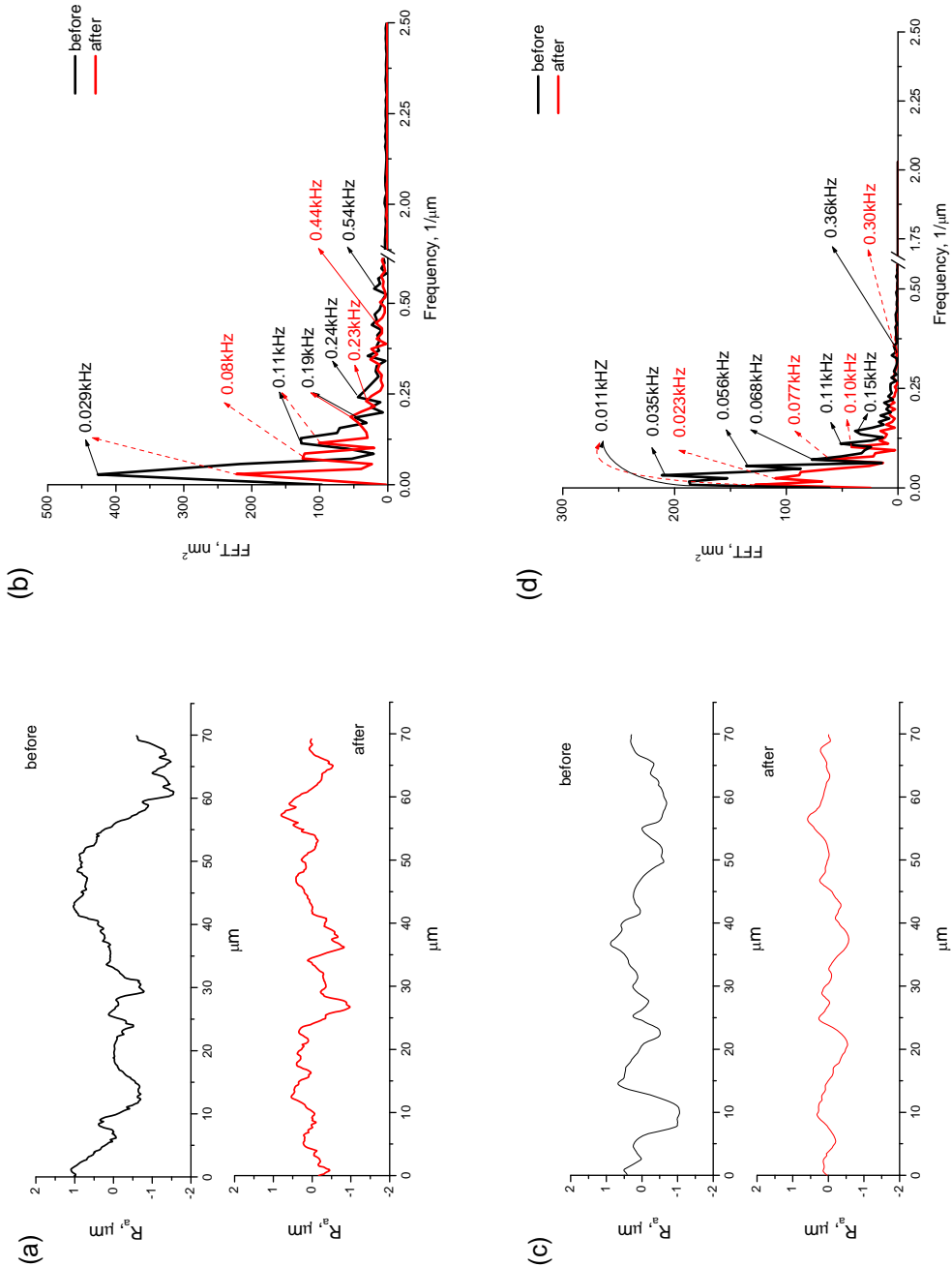


Figure 4.7 Comparison of section analysis of the 4%Cr roller surface at reductions of 26.6% and 30.5%. (a) Cross section profile at reduction 26.6%; (b) FFT of (a); (c) Cross section profile at reduction 30.5%; (d) FFT of (c)

Table 4.2 The 4%Cr roll surface FFT features before and after rolling at 26.6% and 30.5% reductions

Reduction	Rolling condition	FFT features						
		Up to 0.15 kHz						above 0.15 kHz
26.6%	Before rolling	0.029				0.11		0.54
	After rolling	0.029			0.08	0.11		0.45
30.5%	Before rolling	0.011	0.035	0.056	0.068	0.11	0.15	0.36
	After rolling	0.011	0.023		0.077	0.10		0.30

rolling. In the 26.6% reduction, the original surface is composed of two principal long waves at 0.029kHz and 0.11kHz with a series of short waves up to 1.01kHz (only 0.54kHz is marked in Figure 4.7 (b)-previously). After rolling an additional long wave at 0.08 kHz appeared with the main waves at approximately 0.029 kHz and 0.11 kHz, which have lower amplitudes than before rolling. Short waves after rolling are up to 0.68 kHz (only 0.44 kHz was marked in Figure 4.7 (b)-after). With 30.5% reduction the original roll surface is composed of a dominant wave at 0.011 kHz and a series of subsidiary waves at 0.035, 0.056, 0.068, 0.11, and 0.15 kHz, with some small, substantially functional waves up to 0.36 kHz. After rolling the dominant wave is at 0.011 kHz with subsidiary waves at 0.023, 0.077 and 0.10 kHz, along with short waves up to 0.30 kHz. These results imply that the surface has shorter waviness with heavier reduction rather than lighter reductions.

4.3.3 Surface profiles of different initial roller surface roughness after rolling

Figure 4.8 shows the results of PSD analysis of the 4%Cr roll with different initial surface profiles after rolling a workpiece with roughness from 0.8 to

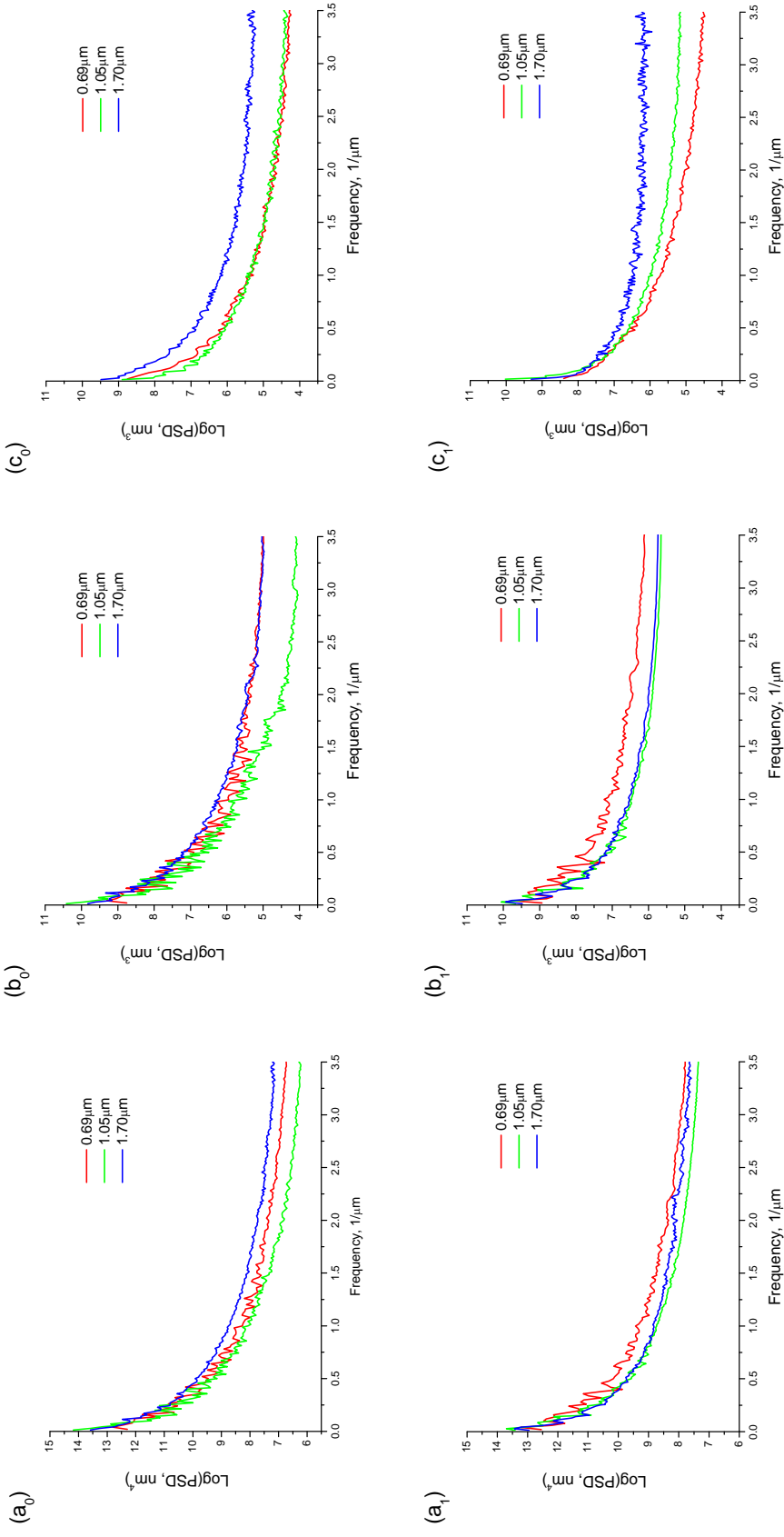


Figure 4.8 PSD analysis of roller surface after rolling with different initial surface roughness: (a) 2D PSD; (b) PSD, perpendicular to the rolling; (c) PSD, parallel with the rolling; subscript 0 and 1: before and after rolling

1.0 μ m. The initial surface roughness values of the rolls were 0.69, 1.05 and 1.70 μ m. Reduction was 26.6% at a rolling speed of 0.031m/s and the operations were carried out under dry contact conditions.

Within the initial roughness range from 0.69 μ m to 1.70 μ m, the one-dimensional PSDs exhibit larger values after rolling than before, both circumferentially and axially in the shorter waviness domain where the frequency is smaller than 0.45 kHz. Similar results were found for the 2-D PSDs.

Over the circumference the PSD amplitudes distribute in an inverse order to surface roughness at high frequency domain. When the frequency is higher than 0.45 kHz the short wave becomes more dominant on the 1.05 μ m surface than the 0.69 μ m surface while for the 1.70 μ m initial surface, PSD becomes stronger than the 1.05 μ m surface when the frequency is higher than 0.20 kHz (See Figure 4.8 (c₀) and (c₁)). This result implies that short waves play a more dominant role for heavy reduction. Even though there is some difference among the PSD values on the original roller surface, the PSD features of the surface after one pass do not follow their original ones.

The PSD along the axis characterises the surface after rolling in the described frequency domain for the roller with 0.69 μ m to 1.70 μ m roughness (Figure 4.8 (b₁)). Figure 4.9 exhibits a section analysing comparison between the roll at 1.05 μ m and that at 1.70 μ m. From Figure 4.9 (a) and (c), the original surfaces of these rollers are quite different, exhibiting different PSD distribution along the frequency (Figure 4.8 (b₀)). Table 4.3 summaries FFT analysing results before and after rolling for the rolls with 1.05 μ m and 1.70 μ m roughness.

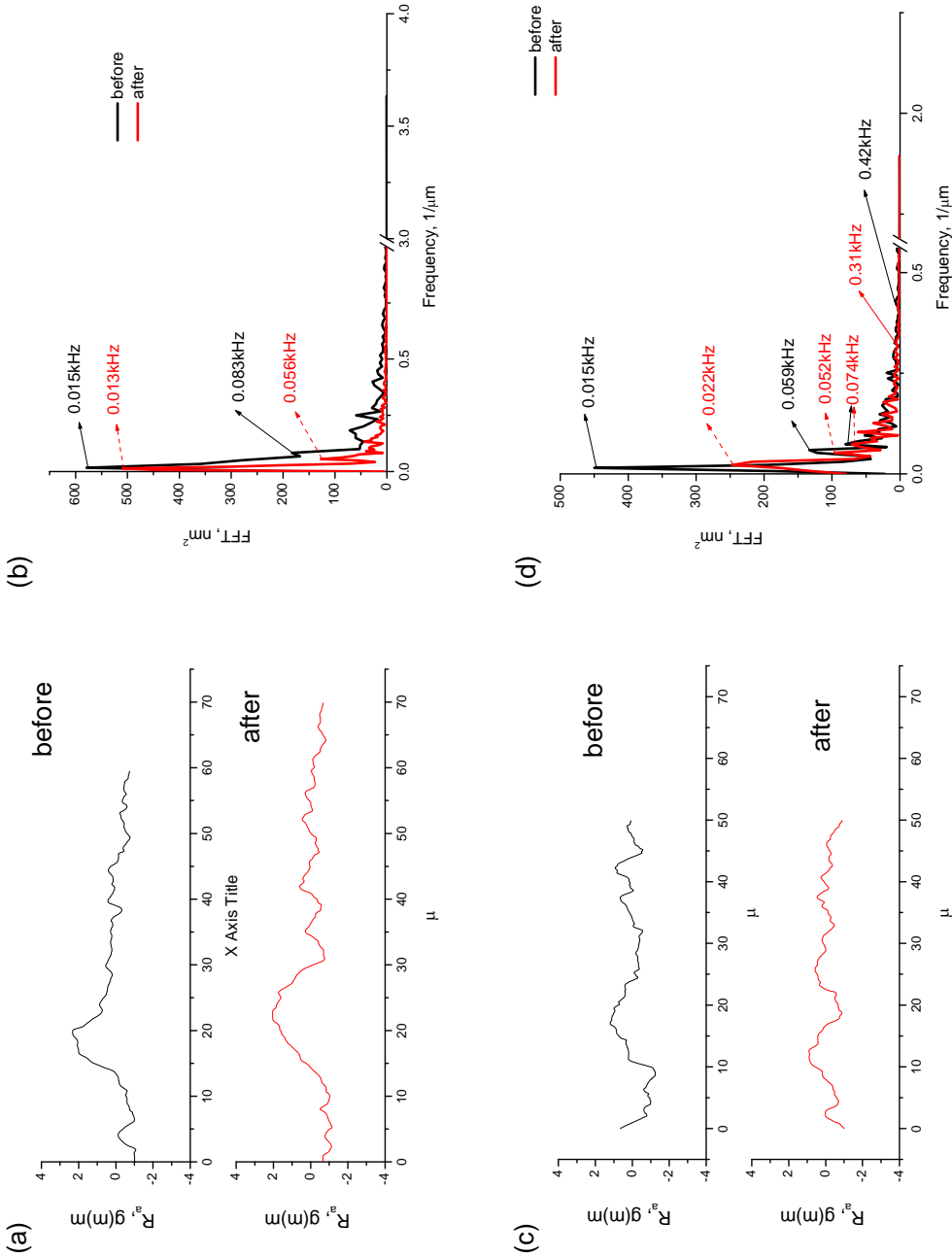


Figure 4.9 Cross section analysis of surface after rolling: (a) Original roll surface roughness at 1.05 μ m; (b) FFT of (a); (c) Roll with original surface roughness at 1.70 μ m; (d) FFT of (c)

Table 4.3 The 4%Cr roll surface FFT features before and after rolling at 26.6% and 30.5% reductions

Initial roughness	Rolling condition	FFT features		
		Up to 0.15 kHz		above 0.15 kHz
1.05 μ m	Before rolling	0.015	0.083	0.51
	After rolling	0.013	0.056	0.27
1.70 μ m	Before rolling	0.015	0.059	0.074
	After rolling	0.022	0.052	0.074

The initial surface of the roller at 1.05 μ m had a dominant long wave at 0.015 kHz with some subsidiary small waves from 0.083 to 0.51 kHz. After rolling the dominant wave is at 0.013 kHz and sub-waves range from 0.056 to 0.27 kHz.

The roller with 1.7 μ m roughness is quite different, its dominant amplitudes is at 0.022 kHz after rolling while its original one is at 0.015 kHz. A second amplitudes at 0.052 kHz appears after rolling between 0.022 and 0.074 kHz that are assumed to be inherited from 0.015 and 0.059 kHz waves on its original surface. Subsidiary waves are intense up to 0.31 kHz after rolling. These results confirm the PSD property analysis in Figure 4.8 (b₁).

4.3.4 Surface profiles with different workpiece roughness

Figure 4.10 displays the results of the PSD analysis of the surface of the 4%Cr roll after rolling on a workpiece with a roughness of 1.40, 1.95 and 3.05 μ m respectively. The rolling reduction is 26.6% at a rolling speed of 12.7 cm/s. The initial surface roughness is from 0.35 to 0.45 μ m while the rolling operations were

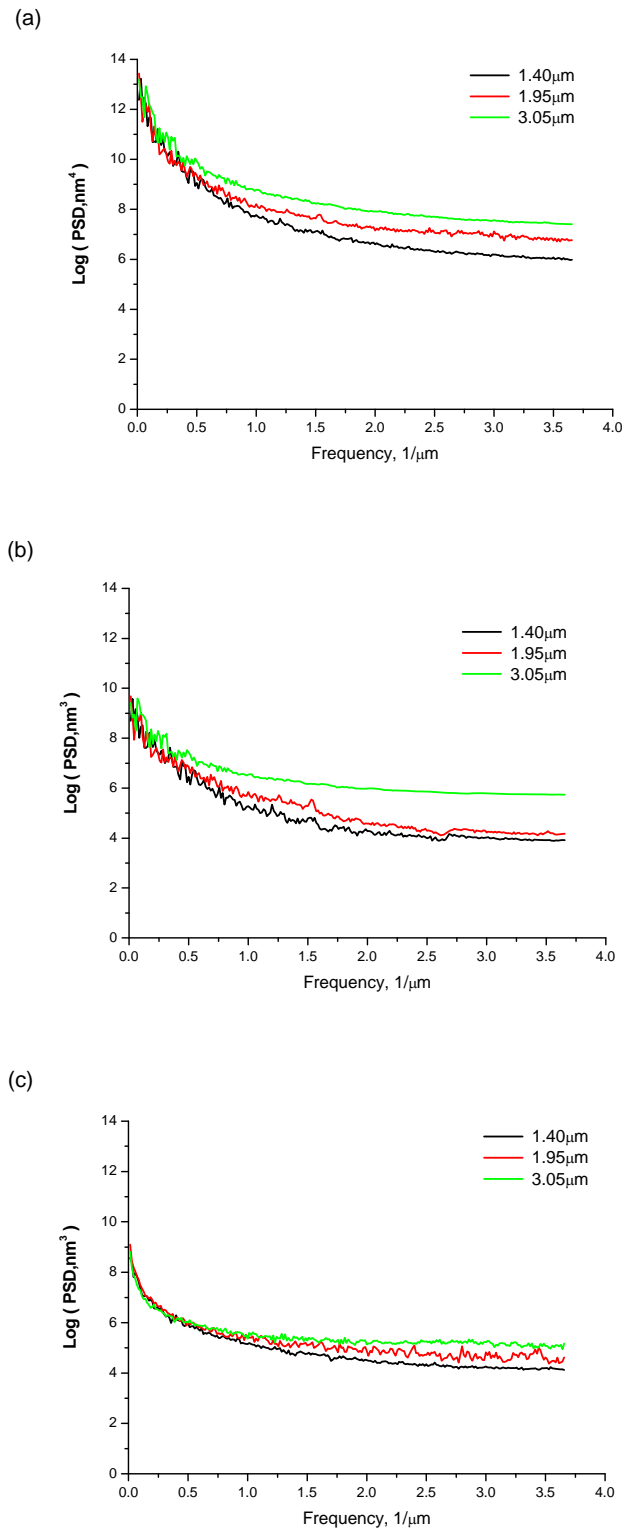


Figure 4.10 PSD analysis of the surface with different workpiece roughness:
(a) 2D PSD; (b) PSD, parallel to the rolling, (c) PSD ,
perpendicular to the rolling.

carried out under dry contact conditions.

The results indicate that a rougher workpiece produces a larger power spectrum of the surface profile through all frequencies. Along the roller circumference, PSD amplitude is profoundly influenced at higher frequency domain, as can be seen in Figure 4.10 (b).

4.4 Surface profiles of the roll after multi-pass rolling

Multi-pass rolling was carried out to help understand the evolution of the surface at a specified pass for the two roller materials, under different contacting conditions. Reduction was controlled to approximately 26.6% at a speed of 6.4 cm/s. The original surface roughness was 0.6 to 0.8 μm respectively for the two rollers tested and the workpiece was 1.2 to 2.4 μm .

4.4.1 Effect of lubrication on the evolution of surface roughness

Figure 4.11 and 4.12 describe changes in surface roughness for the rollers with 4%Cr and Ti-enhanced 4%Cr after 1 pass, and 5 to 20 passes under dry contact and oil mist lubrication conditions.

As discussed in Section 4.2, surface roughness does not reveal any obvious change after one rolling pass but lubrication significantly affects surface deterioration after 20 rolling passes (See Figure 4.11). The surface roughness of the roller with 4%Cr decreases as the number of the rolling pass increases. Under dry contact conditions the surface roughness decreases from 0.60 to 0.50 μm respectively after the roller is subjected to 1, 5, 10 and 20 passes of rolling

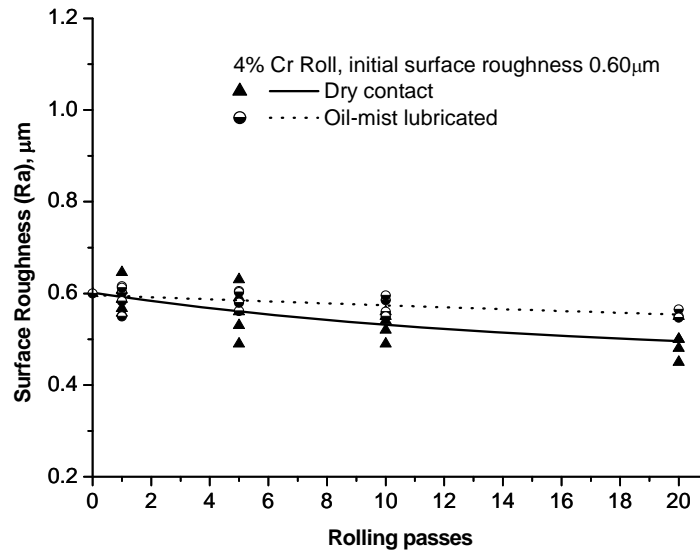


Figure 4.11 Evolution of surface roughness of the roller with 4%Cr

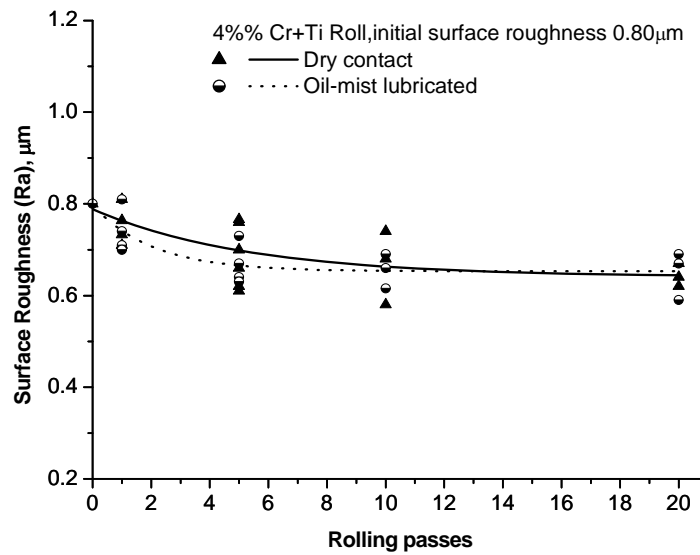


Figure 4.12 Evolution of Surface roughness for the 4%Cr+Ti roller

operations while the amplitudes of surface roughness are 0.60, 0.58, 0.57 and 0.55 μm with oil mist lubrication. It seems that surface roughness deteriorates substantially even after 20 passes under dry contact conditions which suggests

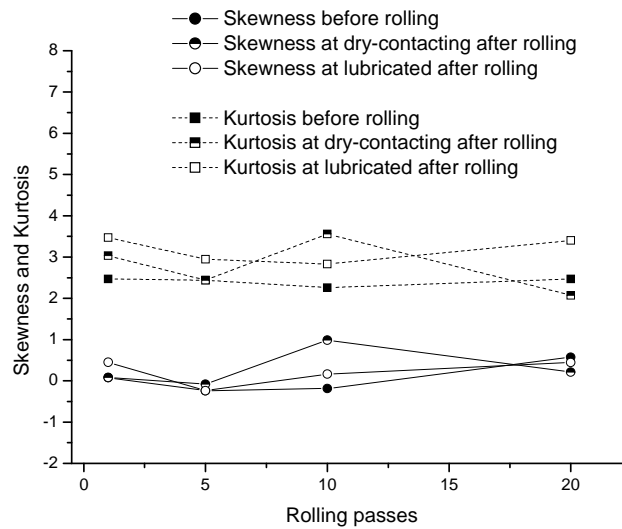
that lubrication plays a significant role.

As for the roller with 4%Cr+Ti 4%Cr, the surface roughness was 0.71, 0.66, 0.65 and 0.64 μm after 1, 5, 10 and 20 passes of rolling under dry contact. but is 0.73, 0.69, 0.67 and 0.65 μm respectively with lubrication. These results suggest that lubrication has less influence on surface roughness than the roller without Ti-enhancement. Tables 4.4 summarises the maximum vertical distance between the highest and lowest data points (R_{max}) by the Hommel Tester T1000. R_{max} decreases for the roller with 4%Cr under both lubrication conditions while the roller with Ti-additive shows a roughness jump after a certain number of passes which implies that the roller with 4%Cr+Ti wears differently to the roller with 4%Cr. This will be discussed in Chapter 6.

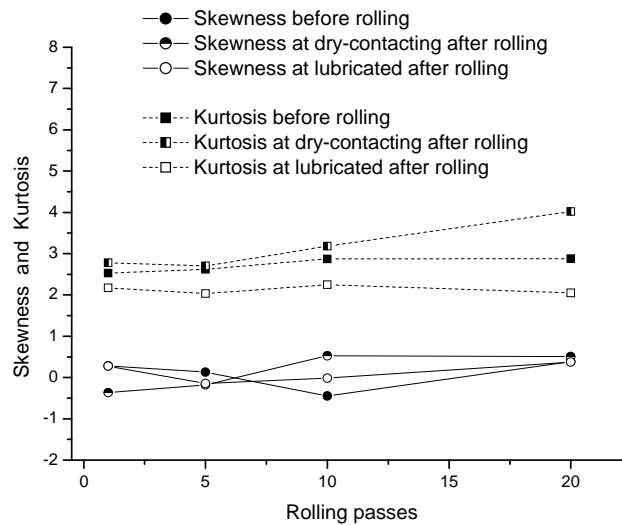
Table 4.4 R_{max} by Hommel Tester T1000

Material/lubrication	R_{max} , μm		
	original	5 passes	20 passes
4%Cr Dry-contact	2.374	2.332	2.168
4%Cr Lubricating	2.074	1.913	1.882
4%Cr with Ti, Dry-contact	1.965	1.413	1.58
4%Cr with Ti, Lubricated	2.557	2.588	2.848

Figures 4.13 and 4.14 display the skewness and kurtosis before and after rolling for the 4%Cr and 4%Cr+Ti rollers. Skewness and kurtosis are statistical parameters to describe the amplitude distribution function (ADF) which indicate the probability that a profile of the surface has a certain height at any position.



Figures 4.13 Skewness and kurtosis before and after rolling (4%Cr).



Figures 4.14 Skewness and kurtosis before and after rolling (4%Cr+Ti).

Detailed definition on skewness and kurtosis may be found in the A00endix II.

Surfaces with negative skewness, such as porous surfaces, have fairly deep valleys in a smoother plateau. More random (e.g. ground) surfaces have a skewness near zero. A value of R_{sk} greater than 1.5 indicates that the surface does

not have a simple shape. Kurtosis relates to the uniformity of the ADF or, to the spikiness of the profile. A Gaussian distribution has a kurtosis of 3. If $R_{ku} < 3$, the distribution has few high peaks and low valleys, which means a relatively flat surface. If $R_{ku} > 3$, the distribution has many high peaks and low valleys, which means a relatively sharp surface [29].

From Figures 4.13 and 4.14, it is evident that the 4%Cr and 4%Cr+Ti rolls exhibit different surface topography evolution under the same contact condition and under different lubricated contact conditions. For the 4%Cr roller, as the number of passes increase under lubricated conditions, kurtosis values change little, being approximately 0.5 larger in amplitude than before rolling. The skewness is very close to its initial value before rolling. AFM images in Figure 4.15 (b₀) to (b₂₀) show the topography changes with increasing numbers of rolling passes. Under dry-contacting condition, both the skewness and kurtosis are very close to their values before rolling except for the 10th pass of rolling, at which each of them exhibits significant deviation, as shown in Figures 4.15 (a₀) to (a₂₀).

For the 4%Cr+Ti rollers, both skewness and kurtosis increase as the rolling pass number increases for dry-contacting condition. The kurtosis at the 20th pass of rolling, is the highest of the samples tested while its skewness displays very little change. For the lubricated condition, the kurtosis amplitude changes little with rolling pass number while skewness values experience a minor increase except for at the 1st pass of rolling. The AFM topographies in Figures 4.16 and

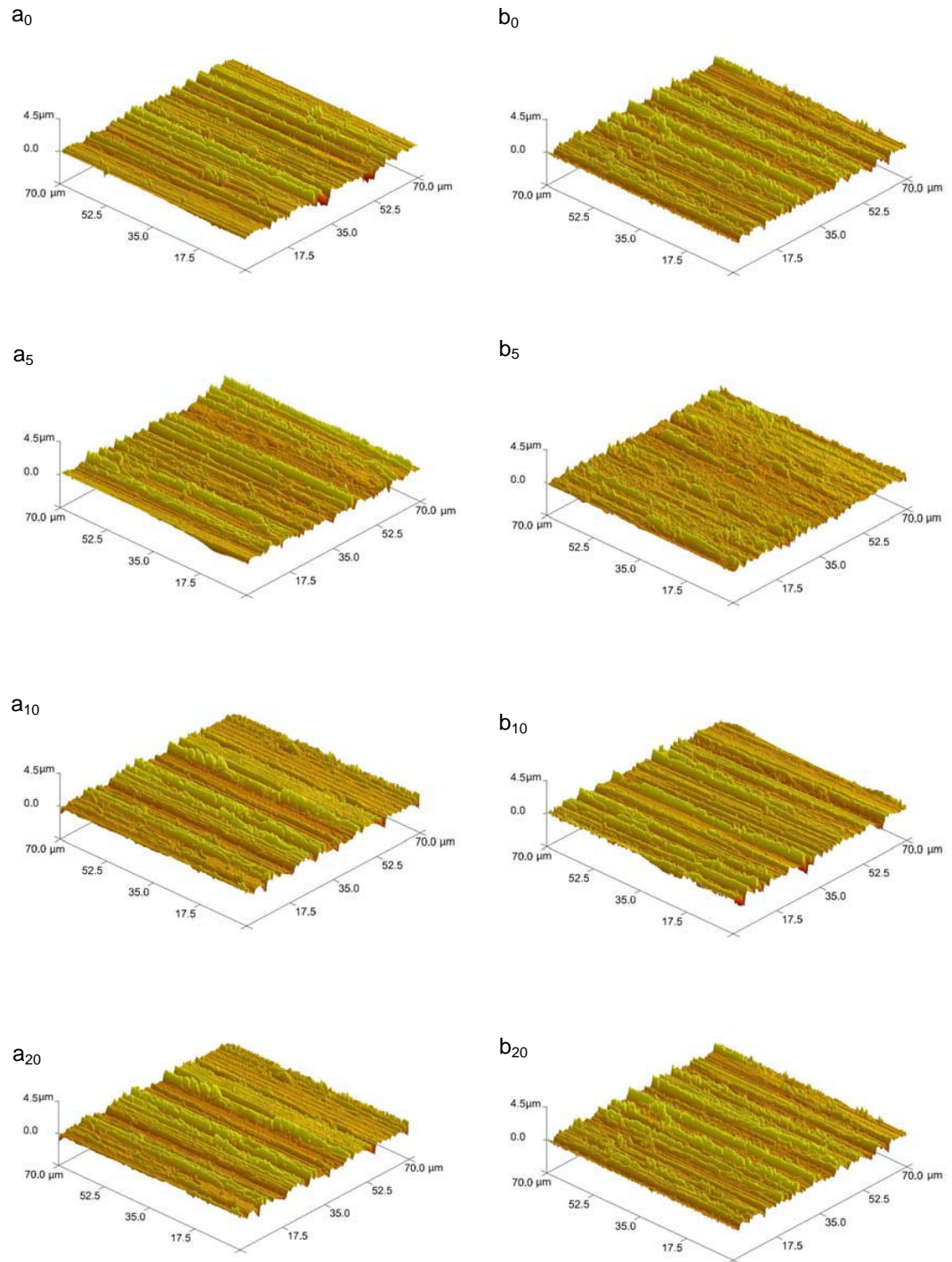


Figure 4.15 Surface morphologies of the 4%Cr rollers before (subscript '0') and after 5, 10 and 20 passes of rolling tests at: (a) dry-contact and (b) oil-lubricating

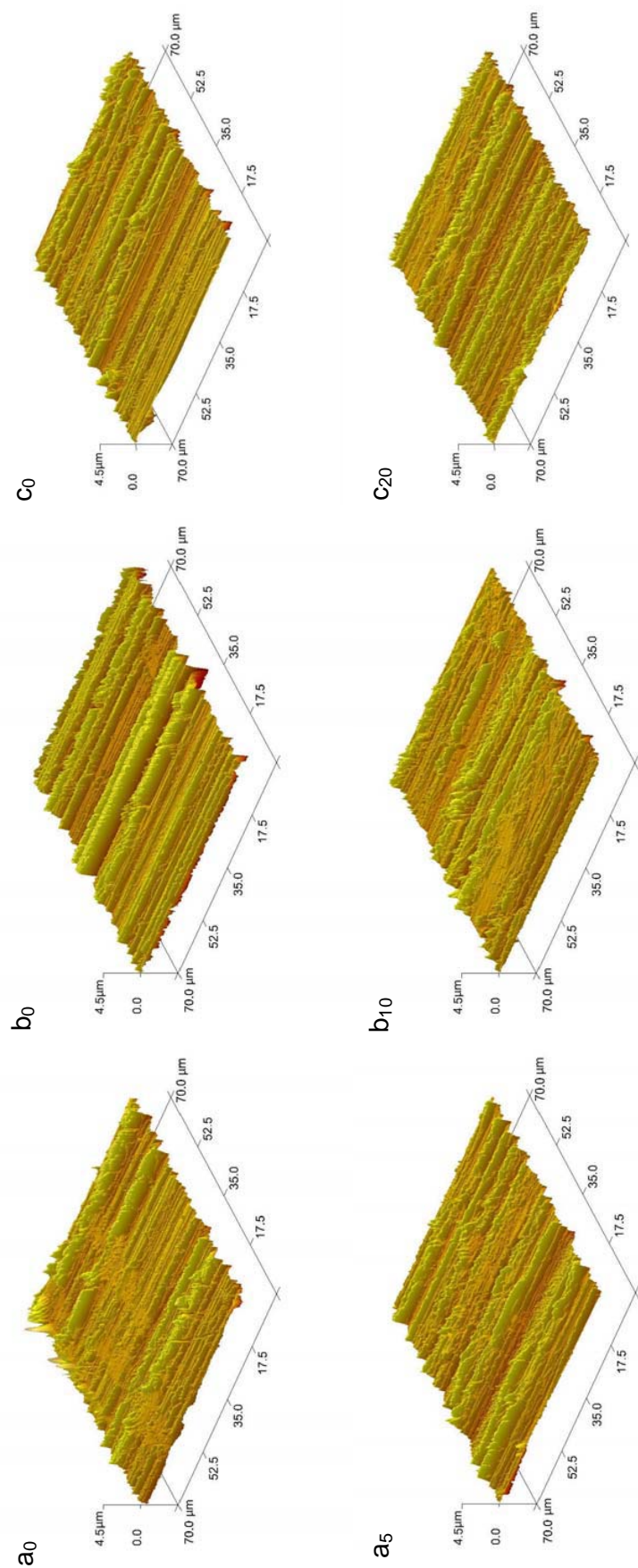


Figure 4.16 Surface morphologies of the 4%Cr+Ti rollers before (subscription ‘0’) and after 5, 10 and 20 passes of rolling at dry-contact

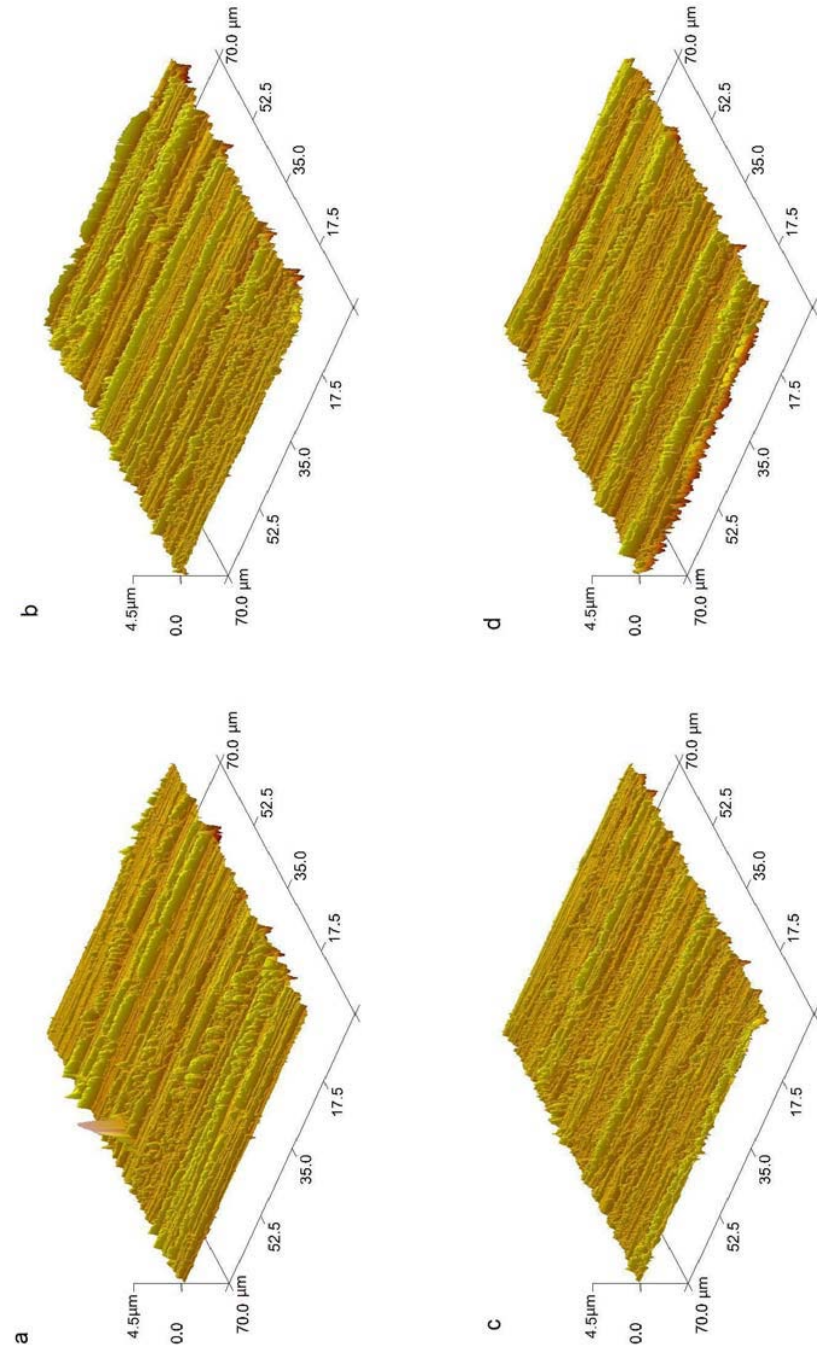


Figure 4.17 Surface morphologies of the 4%Cr+Ti rollers at oil-lubricating before (a) and after (b) 5, (c) 10 and (d) 20 passes of rolling tests.

4.17 display the 4%Cr+Ti roller surface characteristics. Figures 4.15 to 4.17 also indicate that asperities on the roller surface experience inhomogeneous variation. They also indicate that deterioration of surface roughness points to a difference in the response of the two materials (4% Cr-Roll & 4%Cr+Ti).

4.4.2 Effect of Ti-enhancement on the roller surface after multi-pass rolling

Figures 4.18 to 4.20 display the PSD analysis and cross section of the worked roller surface under dry and lubricated conditions for the two rollers material. Tables 4.5 summarises the FFT feature of roll surface profiles by the Hommel Tester T1000.

Table 4.5 PSD features by Hommel Tester T1000

Material/lubrication		FFT features				
		Up to 0.15 kHz				above 0.15 kHz
4%Cr at Dry-contact	Before rolling	0.033	0.058	0.11	0.18	0.97
	After 5 passes	0.044				0.86
	After 20 passes	0.013	0.062			0.31
4%Cr at Lubricating	Before rolling	0.044			0.11	0.72
	After 5 passes	0.021	0.041	0.055	0.62	
	After 20 passes	0.016	0.031	0.048	0.35	
4%Cr+Ti at Dry-contact	Before rolling	0.024	0.049	0.061	0.081	0.44
	After 5 passes	0.015	0.034	0.060	0.42	
	After 20 passes	0.015	0.034	0.060	0.32	
4%Cr+ Ti at Lubricating	Before rolling	0.014	0.028	0.061	0.12	0.71
	After 5 passes	0.013	0.036	0.061	0.12	0.71
	After 20 passes	0.014	0.036	0.053	0.11	0.68

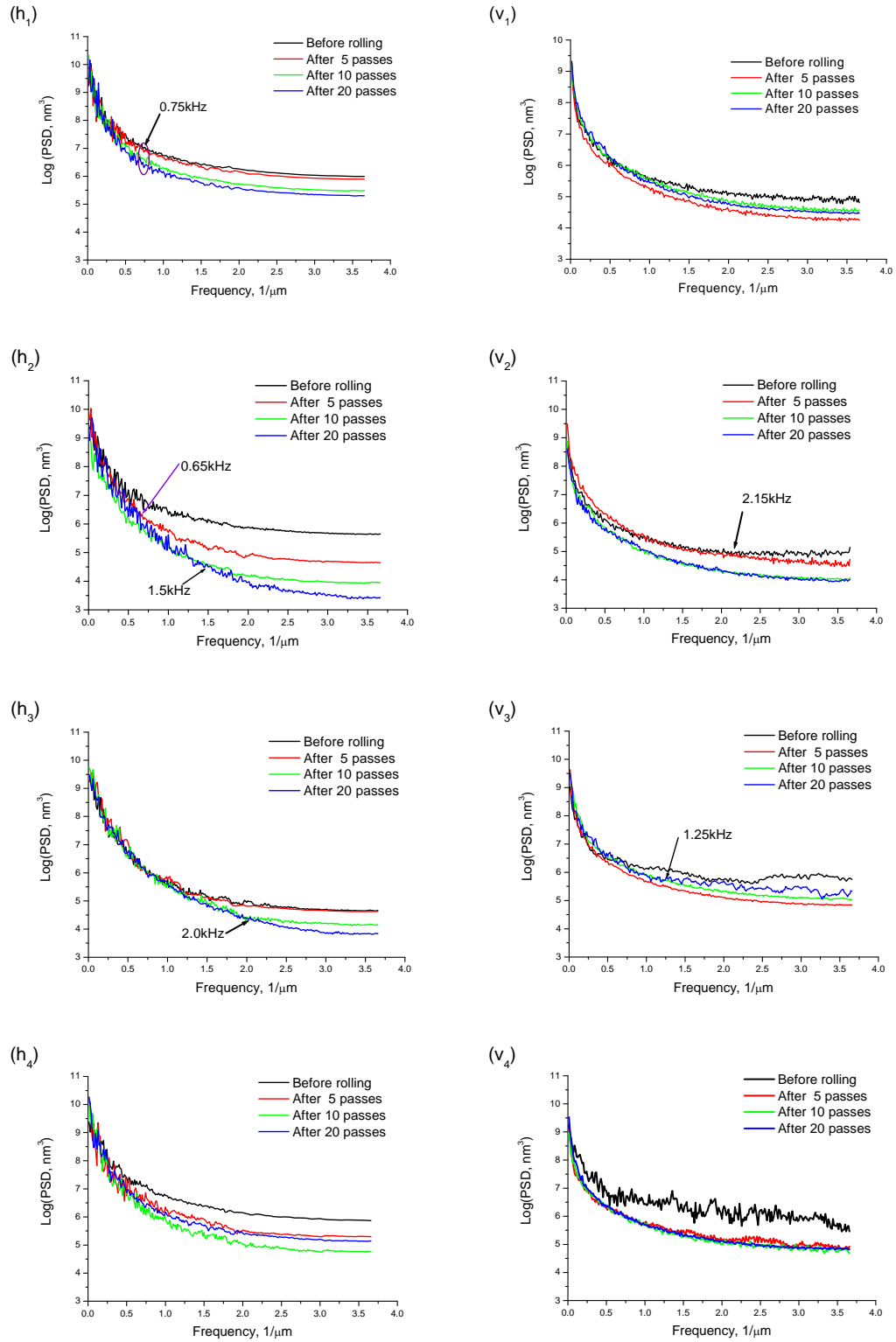


Figure 4.18 Roll surface PSD analysis: h , axial and v , circumferential; ‘1’ and ‘3’, dry contact, ‘2’ and ‘4’ oil-mist lubrication; ‘1’ and ‘2’: 4% Cr; ‘3’ and ‘4’: 4%Cr+Ti

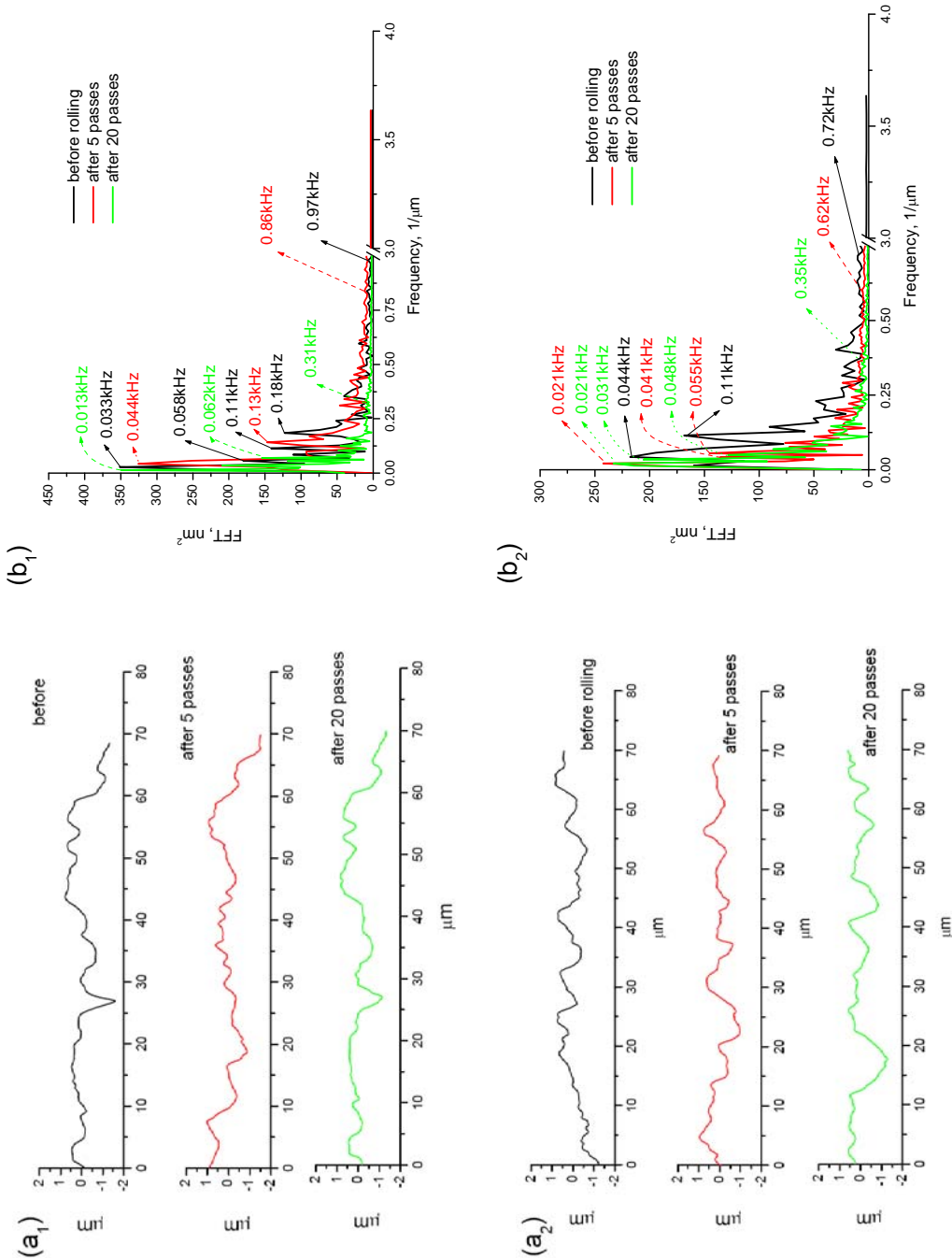


Figure 4.19 4% Cr roll surface section analysis.
a, surface profile;
b, FFT distribution;
‘1’ dry contact,
‘2’ oil-mist lubrication

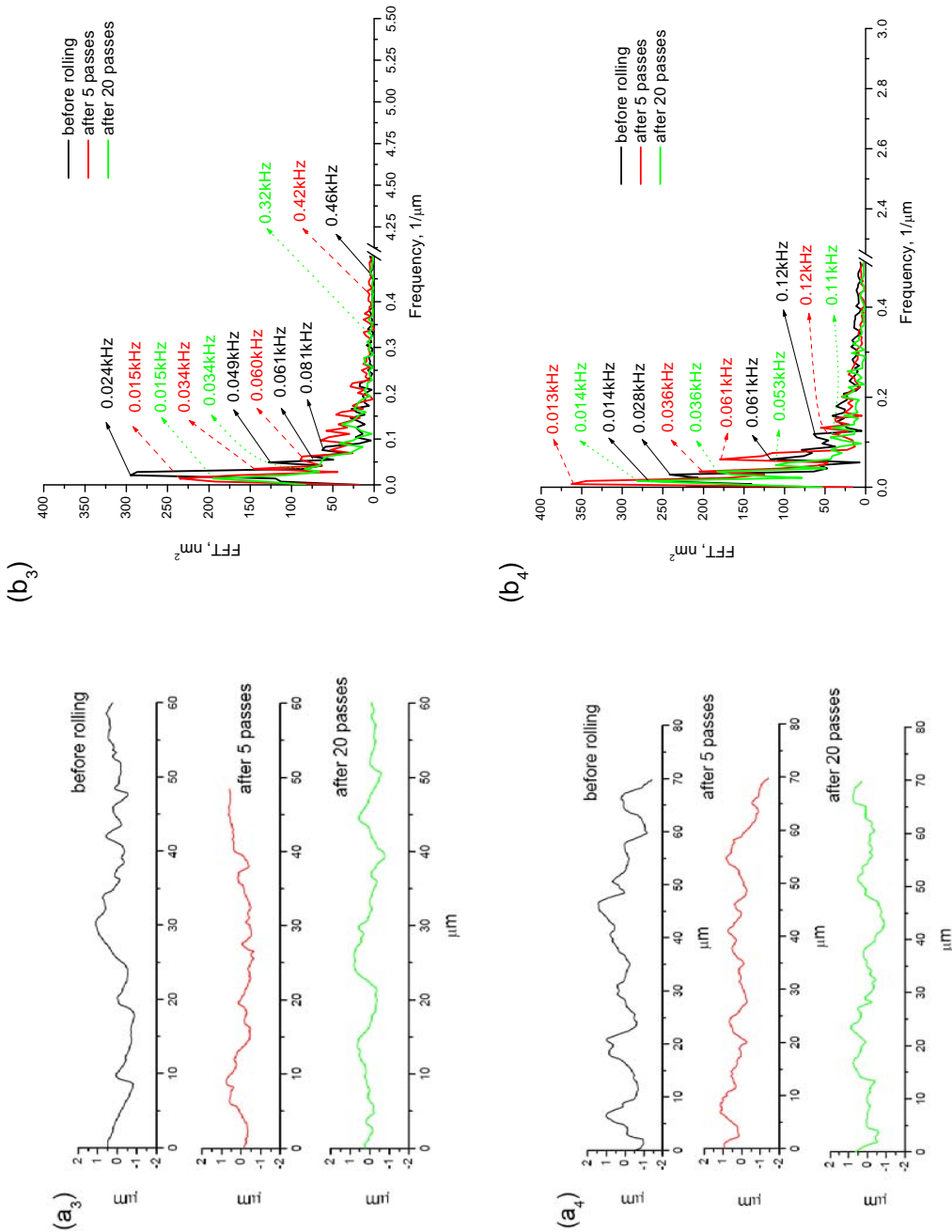


Figure 4.20 4% Cr+Ti roll
surface section analysis.
a, surface profile;
b, FFT distribution;
‘3’ dry contact,
‘4’ oil-mist lubrication

a) In dry contact

Circumferentially the PSD values are lower than the original surface after 5, 10, and 20 passes of rolling but do not exhibit a similar characteristics with the number of rolling passes (Figure 4.18 (v_1) and (v_3)). This result is different from the case of one pass rolling discussed in 4.3.3. It implies that the waviness along the rolling direction is reduced after several passes of rolling. The PSD amplitudes are close together for the roller with 4%Cr, especially after 10 and 20 passes of rolling. But the roller with 4%Cr+Ti reveals a different distribution of PSD which varies with the rolling pass. The more rolling passes there are the higher the PSD amplitude will become. This indicates that as the number of rolling passes increases, waviness shorter than $0.8\mu\text{m}$ on the 4%Cr+Ti surface will increase at higher frequencies domain, indicating regeneration of waviness in the rolling direction.

The PSD amplitudes along the axial direction of both materials are close but decrease as the number of rolling passes increase in the high frequency domain (Figure 4.18 h_1 and h_3). The large difference in amplitude of the PSD on the roller with 4% Cr appears at frequencies higher than 0.75 kHz ($1.3\mu\text{m}$ wavelength), as can be seen in Figure 4.18 (h_1).

For the roller with 4%Cr+Ti, axial PSD after 5 passes is at almost the same level as the original (Figures 4.18 (h_1) and (h_3)). The results in Table 4.5 and Figures 4.19 (b_1) and 4.20 (b_3) indicate that the FFT amplitude ‘peaks’ have been ‘shifted’ to the longer wavelength (low frequency) domain at a further distance

for the roller with 4%Cr than the roller with Ti-additive. Further, more additional wavelengths lose power for the roller with 4%Cr than with 4%Cr+Ti.

It may be concluded from the above analysis that as the number of rolling passes increase, the roller with 4%Cr+Ti is better able to retain PSD power in a short wavelength domain than the traditional roller with 4%Cr during dry contact rolling.

b) The oil mist lubricating case

In the rolling direction the PSD values are lower for both materials after 5 to 20 passes. In every frequency domain the PSD amplitudes display similar power for the surface with 4%Cr at its 5th and 20th pass (Figure 4.18 (v_2)), and the 5th, 10th, and 20th pass for the Ti-additive (Figure 4.18 (v_4)).

For the two materials under lubricated conditions, the PSD is quite different in the axial direction. In all cases, the PSD has a lower amplitude after rolling than before but when the frequency is higher than 0.65 kHz (Figure 4.18 (h_2)), the surface with 4%Cr rolling affects the PSD amplitude significantly. For frequency larger than 0.65kHz PSD power decreases with the number of rolling passes but the surface with 4%Cr+Ti appears to be less sensitive. The FFT analysis in Table 4.5 and Figures 4.19 (b_2) and 4.20 (b_4) further indicate that the dominant and effective wavelength deteriorates to a lesser extent for the surface with Ti-additive than with only 4%Cr.

4.5 Findings

It was found that the experiments with the LST mini-mill are helpful for single

pass and multi-pass stalled rolling tests and make it feasible to apply FFT methodology on different roughness parameters to evaluate surface changes during sequential rolling.

4.6 Summary

In this Chapter the surface deterioration of the two material rollers mentioned were tested by single and multi-pass cold rolling under dry contact and lubricated conditions. Roller surface roughness, PSD features, and FFT properties were analysed on the surfaces of the rollers that were tested.

1. It was found that statistical measurements such as average roughness or root mean square roughness, are limited methods for characterising the primary information of the surface topography after a single pass rolling. The findings in this thesis support previous workers who have also concluded that average surface roughness measurements are of limited value.
2. A rougher work piece results in a larger spectrum power of the roller surface profile through all frequencies. Significant effects of rougher workpiece have been found on PSD amplitude along the axis especially in higher frequency domains.
3. The PSD amplitude over the circumference is more sensitive to the original surface roughness of the roller and it decreases with original surface roughness increasing at a higher frequency domain.
4. Lubrication significantly affects the surface roughness of the 4%Cr roller but less so on the roller with Ti-enhancement.

5. The surface deterioration of the added Ti roller is obviously different as the number of rolling passes increases,

a) the PSD amplitude ‘peaks’ have been ‘shifted’ further to the longer wavelength domain for the roller with 4%Cr than that with the Ti-additive.

Furthermore, subsidiary wavelengths diminish further on the roller with 4%Cr than the 4%Cr+Ti;

b) the roller with 4%Cr+Ti is better able to retain short wavelengths than the 4%Cr roller under dry contact rolling and the ability to regenerate roughness in the rolling direction when the number of rolling passes increases;

c) the dominant and effective wavelength deteriorates to a smaller extent for the roller with added Ti than the one with 4%Cr.

Chapter 5 Tribological Behaviour of Roll Materials by Disc-to-Disc experiments

5.1 Introduction

In cold rolling of steel, the work-roll is one of the principal components in the running the plant. Surface deterioration and work roll wear is always a topic of interest to many researchers. Schey [131] outlined the principles of laboratory simulation methods and processes for tribological experimental purposes. The usual facility for simulating rolling is the disc-to-disc set-up [132-136] which can reveal the phenomenon at the interface between the workpiece and roll [131].

In this chapter, results obtained from disc to disc experiments are presented. The experiments are carried out to investigate the effect of duration, load, disk speed and slip on roll wear, friction and torque.

The materials used to simulate the rolls were again 4%Cr steel and 4%Cr+Ti steel, the compositions of which are described in Chapter 3. The partnered disc was a low carbon steel, the chemical composition of which is given in Table 5.1.

Table 5.1 Chemical composition of the partnered disc (wt%)

C	Si	Mn	P	S	Al (soluble)
0.05	0.02	0.25	0.008	0.003	0.032

The disc-to-disc wear experiments were carried out under dry contact and lubrication by emulsion conditions. An emulsion with 3.9% Quakerol N680-2-DPD from a cold rolling plant was used as a lubricant at the interface between the roll and workpiece. Table 5.2 details the properties of the emulsion.

Table 5.2 Emulsion used in the experiments

concentration	pH	conductance	saponification	acid number	Fe+	Cl-	ash	ESI
%		$\mu\text{s/cm}$	mgKOH/g	mgKOH/g	mg/L	mg/L	mg/L	%
3~5	5.5~7	<300	155~180	9~13	100~300	5~20	<500	50~75

The diameter of the disc for the roll material was 45.9mm, while the workpiece disc was 45.2mm. i.e., the positive slip difference in speed between the roll material disc and the workpiece was normally controlled at 1.5%, except for the controlled tests. The surface finish of the workpiece was 0.8 to 1 μm . The duration of contact, contact loads, differential initial surface roughness of the roll disc and difference in speed between the two discs were introduced in the experiments.

To quantify the wear properties of the roll, the weight loss was measured and the surfaces characterised by SEM to identify the experimental results under different testing conditions.

5.2 Effect of wear duration

The tests hereafter were carried out under dry contact and lubricated conditions.

The speed was held at 597rpm under a 1000N load and there were 7 test intervals, 10, 30, 60, 90, 180, 270 and 390 minutes for both the 4%Cr and 4%Cr+Ti discs. When lubricating was introduced tests lasted between 5 minutes to 480 minutes.

The initial surface roughness was determined before testing to provide a reference point.

5.2.1 Weight loss

Figures 5.1 and 5.2 display the roll material weight loss versus test duration under both dry contact and lubricated emulsion conditions.

Under dry conditions the weight loss increases over time for both types of materials but as the contact time increases this slows down for both materials. In the first 60 minutes the disc with 4%Cr+Ti loses more weight than the 4%Cr, but after that the weight decreases much slower for the 4%Cr+Ti than the 4%Cr. When the duration of contact is longer than 180 minutes the 4%Cr+Ti roll experiences further slight weight loss while the 4%Cr roll continue to lose weight.

With lubrication, however, the weight loss is much less for both materials. During the first 120 minutes the weight loss for both rolls is very close but the 4%Cr+Ti material loses more weight than the 4%Cr roll. When the discs are in contact for a longer period, however, the 4%Cr+Ti shows almost no further

weight loss, indicating better wear properties than the 4%Cr.

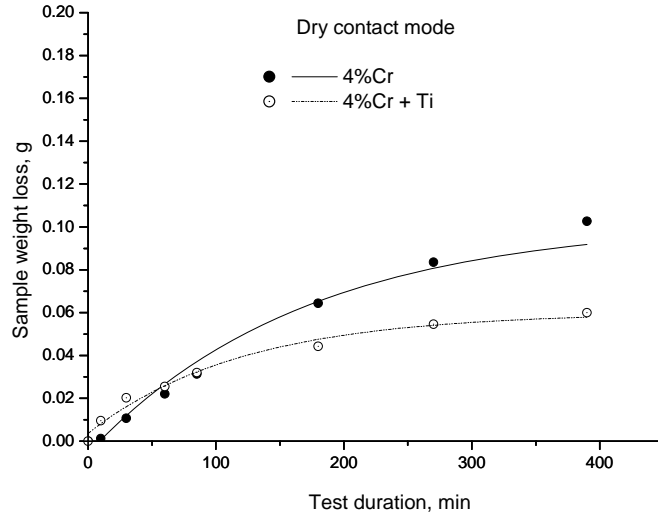


Figure 5.1 weight loss versus test duration under dry contact conditions

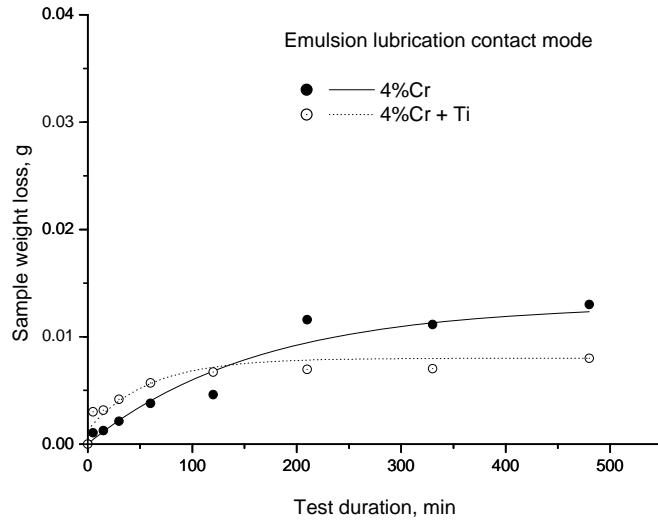


Figure 5.2 Weight loss versus test duration with lubrication

5.2.2 Changes in surface roughness

Figures 5.3 and 5.4 show the changes in surface roughness with test duration for

materials with 4%Cr and 4%Cr+Ti under dry contact and lubricating contact. The initial surface roughness for 4%Cr and 4%Cr+Ti materials was 0.66 and 0.75 μm respectively in the dry contact wear tests and 1.0 and 1.03 μm under lubricated condition. Figures 5.5 and 5.6 illustrate microscope of the initial surface of the discs with 4%Cr and 4%Cr+Ti before the test.

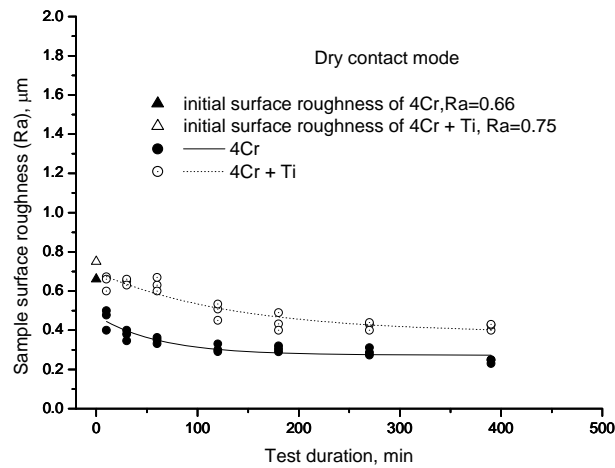


Figure 5.3 Surface roughness versus test duration at dry contact conditions

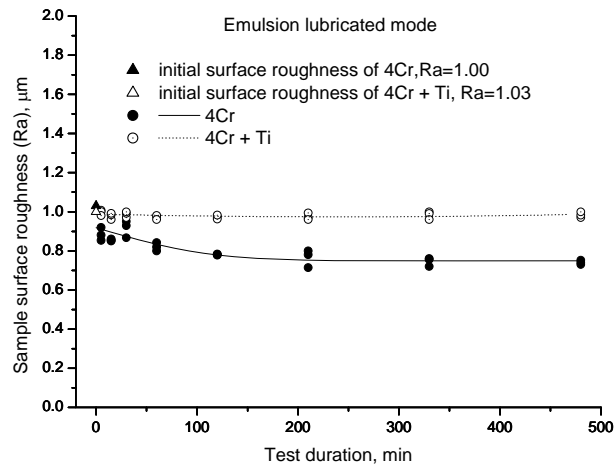


Figure 5.4 Surface roughness versus test duration with lubrication

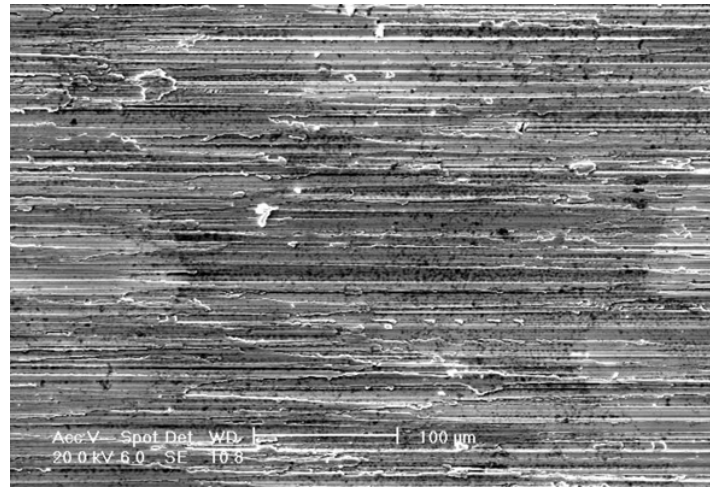


Figure 5.5 Initial surface of the 4%Cr disc ($R_a=0.66\mu\text{m}$)

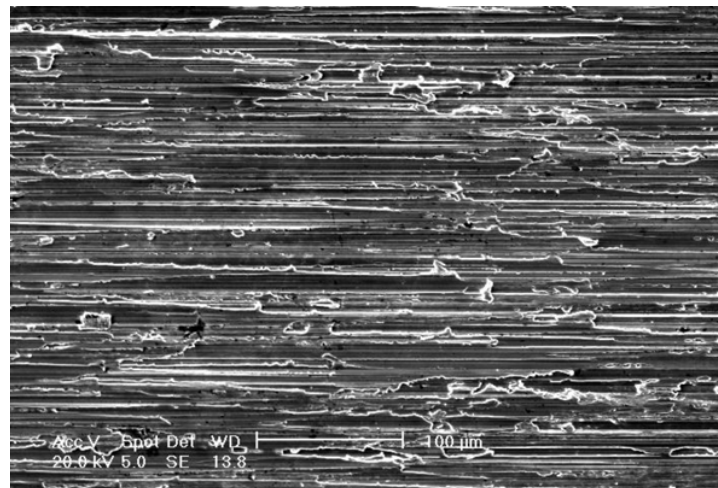


Figure 5.6 Initial surface of the Ti-added 4%Cr+Ti disc ($R_a=1.0\mu\text{m}$)

The surface roughness of the discs with 4%Cr decreases significantly in the first 120 minutes under both contact conditions but was slower when lubrication was added. These results are consistent with Shimizu et al [17] where it is concluded that a convention 5%Cr roll on the finishing stand roughness reduction is fast in the early stage and decreases gradually but roughness changes very small in the

early stage for the Ti-roll. However the different rates of deterioration was a characteristic of the disc with 4%Cr+Ti under different lubricating conditions. When lubrication was used there was very little change in surface roughness during the eight hours of testing (as shown in Figure 5.4). Scanning electron micrographs in Figures 5.7 and 5.8, which display the surface morphology after the discs worked at different intervals. In dry contact the grooves on the surfaces of both discs generated by grinding (See Figures 5.5 and 5.6), were removed after only a few cycles of wear, leaving a smoother surface. When lubricating emulsion was used, the grinding grooves remained even after 480 minutes of rolling/sliding.

It is evident from the above figures that the material with 4%Cr+Ti has better anti-abrasive properties than the roll with only 4%Cr. When lubrication is applied the surface roughness of the material with 4%Cr+Ti deteriorates much slower than the 4%Cr.

5.3 Effect of load on roll wear

Experiments were carried out on the disc at 597rpm under loads varying from 500N to 2000N depending on the materials and contact duration which was 30 minutes for each pair of discs. The weight loss and surface roughness was measured to determine the effect that load has on the wear of the materials.

5.3.1 Weight loss to experimental loads

Figures 5.9 to 5.10 show the weight loss as a function of load.

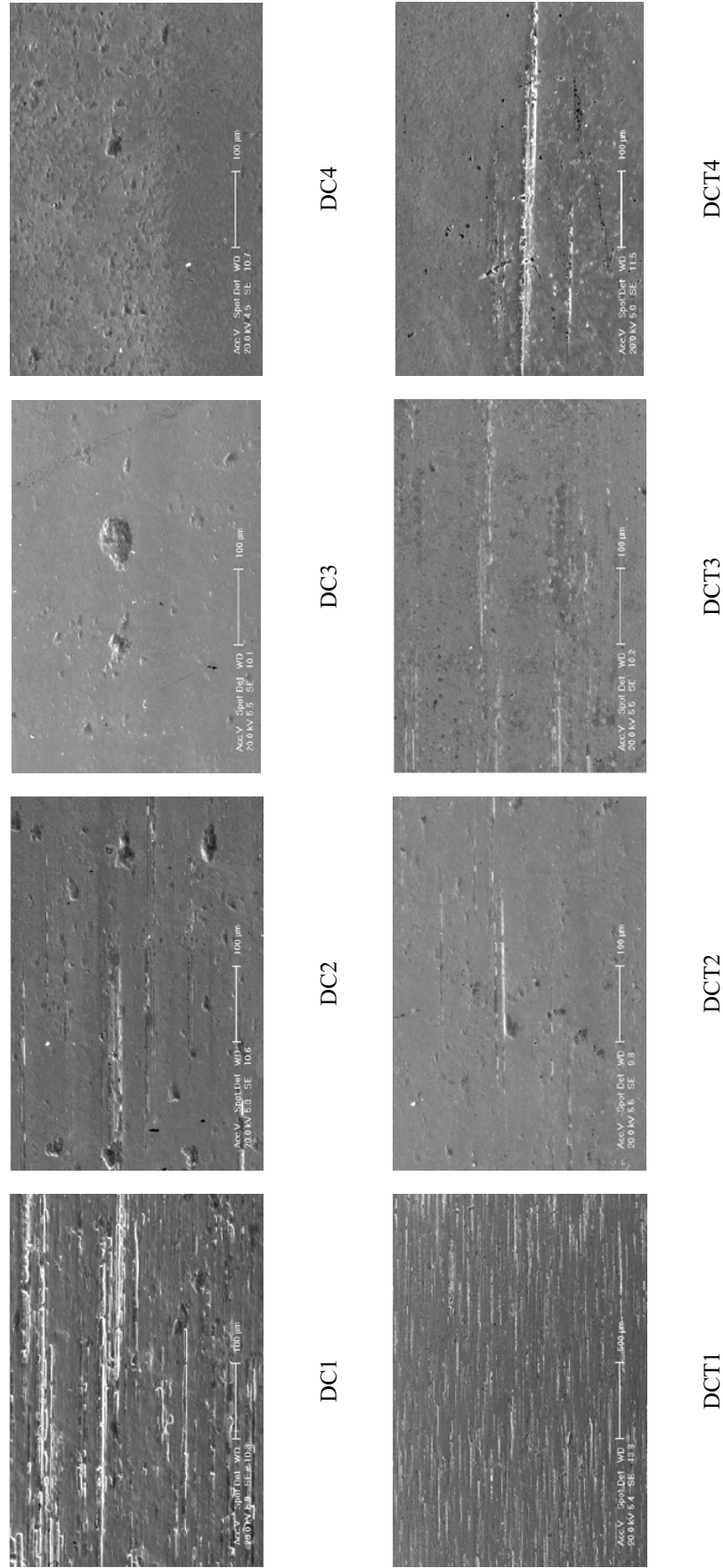


Figure 5.7 Surface morphology of discs in dry contact after a series of wear intervals: D-dry, C-4%Cr material, CT-4%Cr+Ti material, 1 to 4: 10, 30, 120 and 390 minutes respectively.

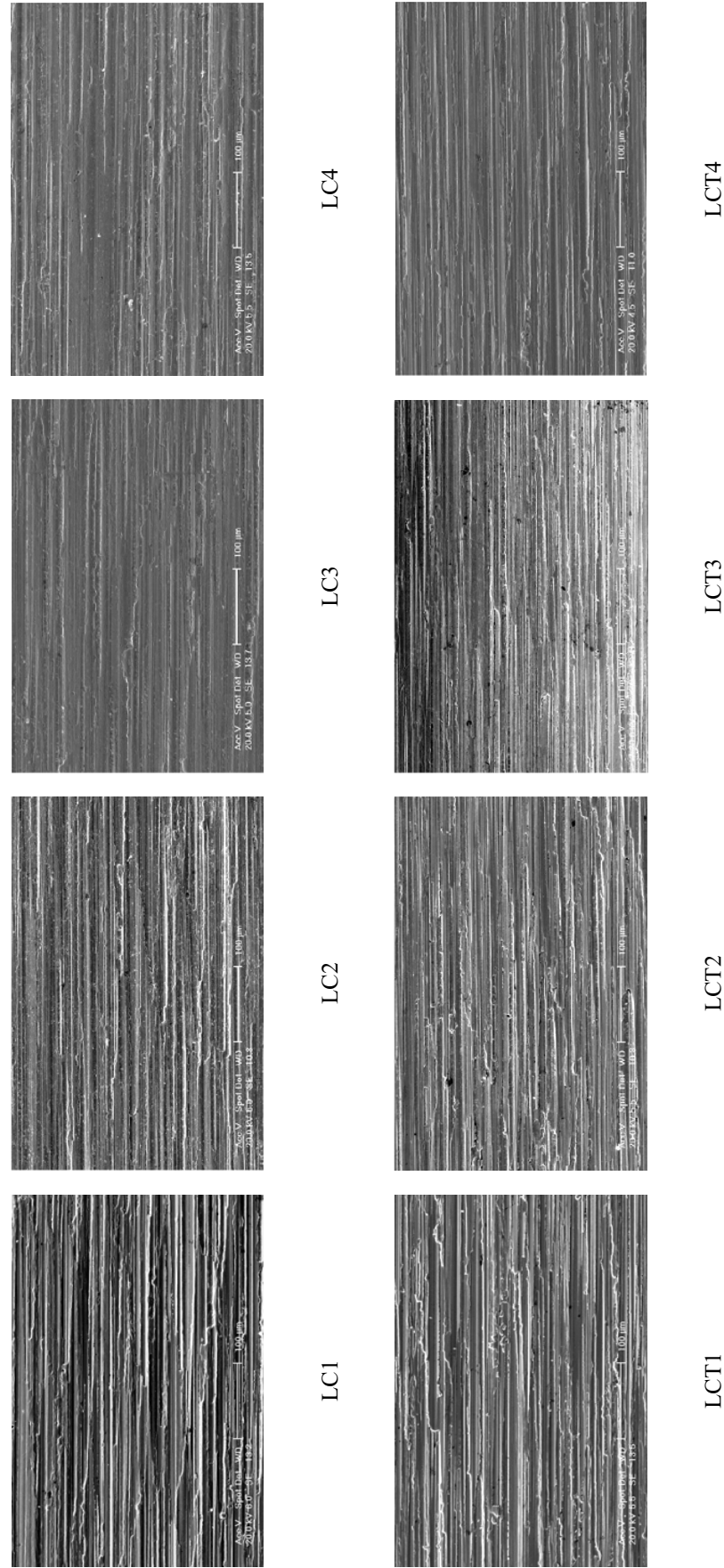


Figure 5.8 Surface morphology of discs with lubrication after a series of wear intervals: L-emulsion lubrication, C-4%Cr material, CT-4%Cr+Ti material, 1 to 4: 15, 60, 210 and 480 minutes respectively.

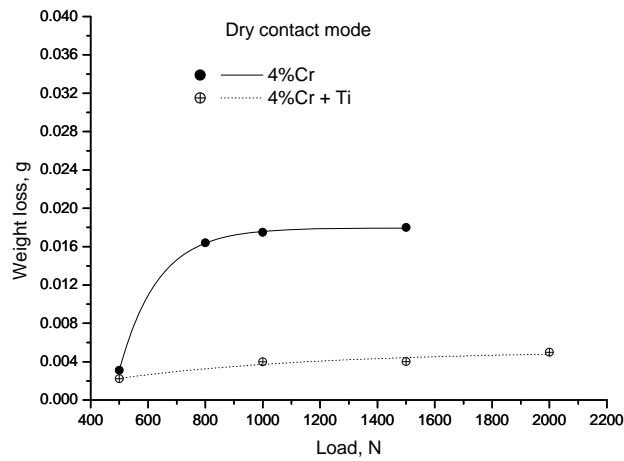


Figure 5.9 Weight loss to loads under dry contact

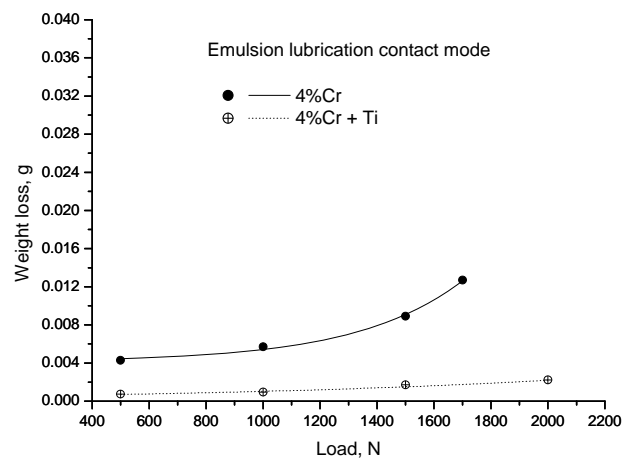


Figure 5.10 Weight loss to load with lubrication

The 4%Cr+Ti material loses weight at a lower rate under dry contact as the load increased but when lubrication is applied the weight loss is smaller in amount than at dry contact.

When lubrication is used (See Figure 5.10) the weight loss of the material with 4%Cr increased gradually as the load increased but rose considerably when the load exceeded 1500N. Under dry contact conditions, when the load is raised to

800N the loss of weight increases to a high value but then levels to a steady state value. As the load increases further the weight loss becomes insignificant. A comparison of the images in Figure 5.11 may provide an explanation: under dry contact the grinding grooves were removed and the surface was flattened after 30

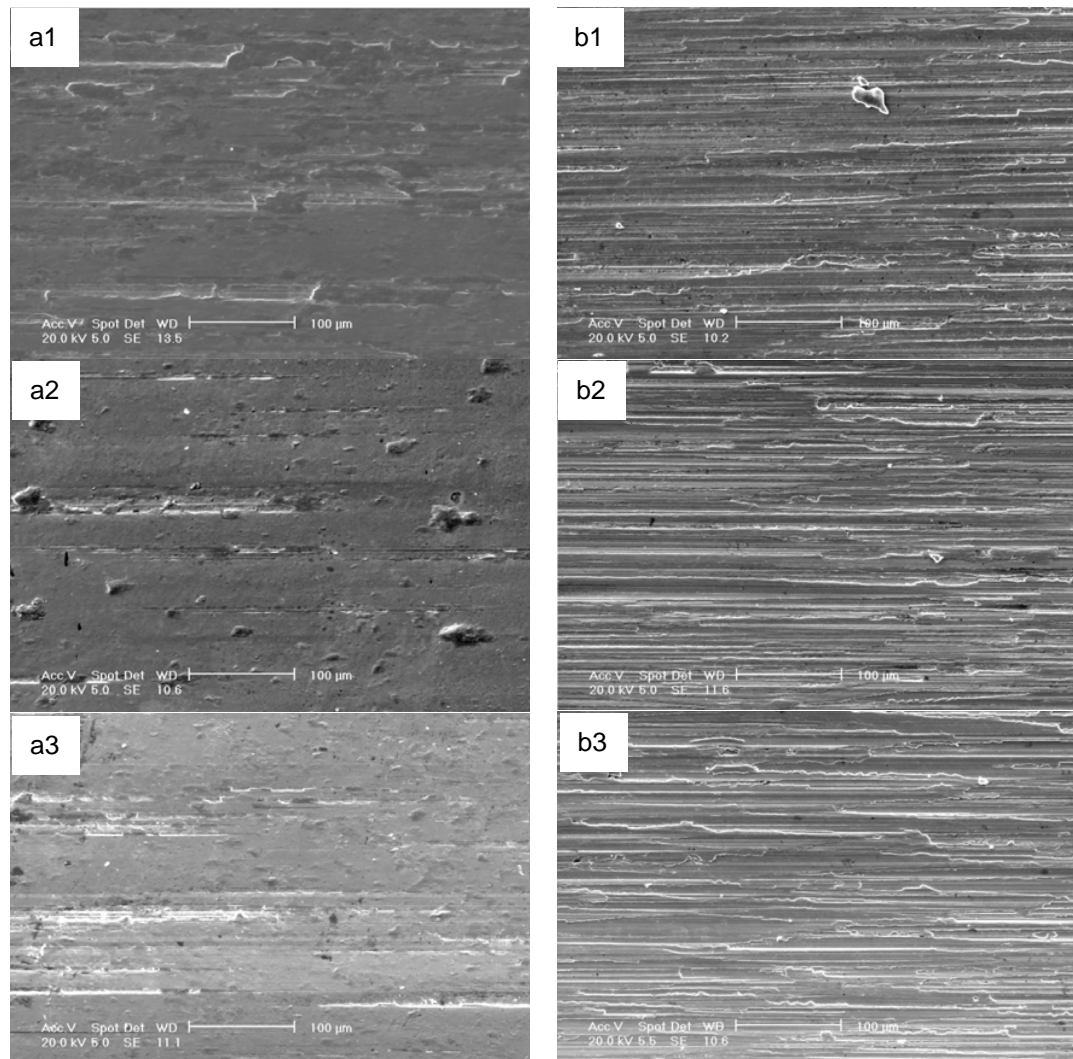


Figure 5.11 Comparison between dry and lubricating contacts of 4%Cr discs under different loads. a: dry and b: lubricated; 1 to 3: 500, 1000 and 1700N respectively.

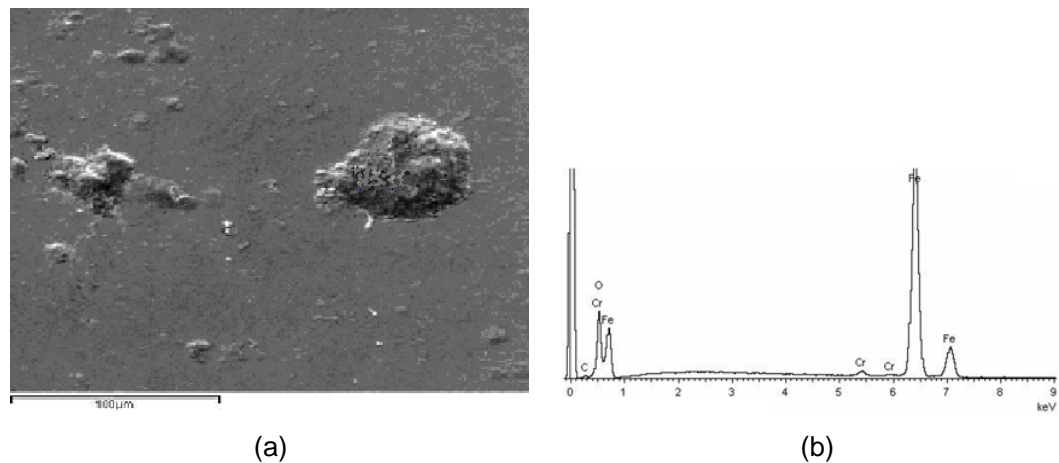


Figure 5.12 Roll surface after 30min under 1000N under dry contact and slip =1.5%: (a) SEM spot; (b) spot chemical composition

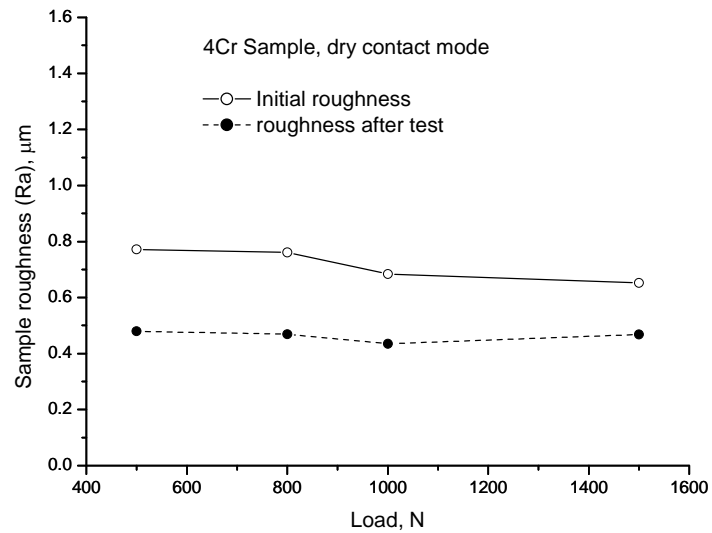
minutes of test duration at 500N (Figure 5.11 (a1)). When the load increased to 1000N the surface humps appear and suggest they could be due to the presence of oxides, according to SEM, as can be seen in Figure 5.12 (b). At the same time the surface began to exhibit grooves and when the load was increased further, more humps and grooves appeared. This implies that adhesive wear occurs and material adhered to the surface under dry contact. Although the surface appeared to be flatter under lubrication, no new grooves appeared at corresponding loads.

5.3.2 Surface roughness to loads

Figures 5.13 to 5.14 show a comparison of changes in surface roughness before and after the experiments. The figures show that the changes were less with lubrication for the materials with 4%Cr and 4%Cr+Ti respectively. Under dry contact the 4%Cr surface roughness deteriorated with an amount varying from 0.18 to 0.30 μm when the samples were loaded from 500 to 1500N. The change in

surface roughness of the material with 4%Cr and 4%Cr+Ti were at a lower level, ie, from 0.14 to 0.2 μm when the loads were from 500 to 1700N under dry contact.

(a)



(b)

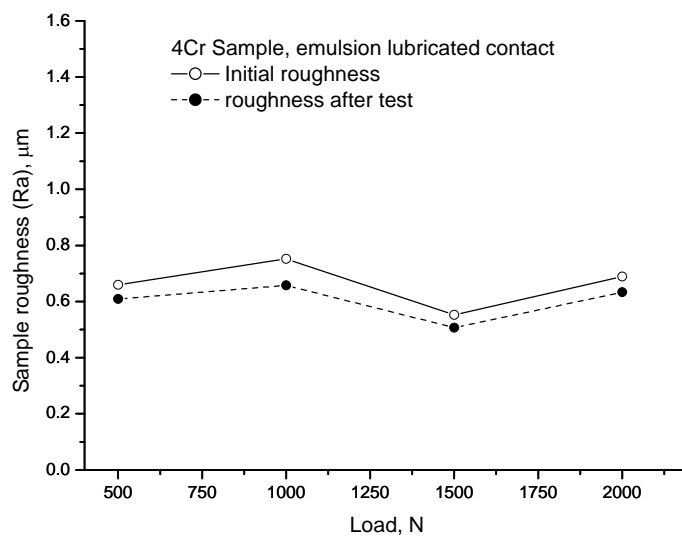


Figure 5.13 Change in surface roughness to load under dry contact

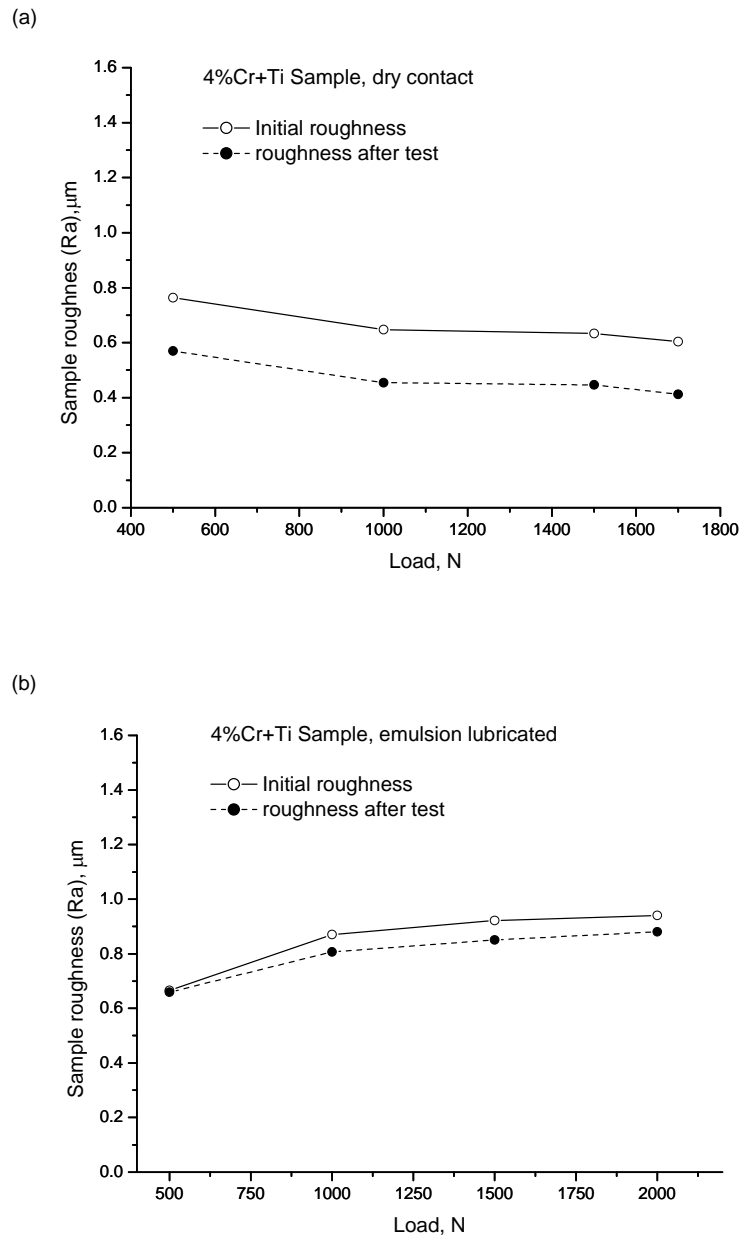


Figure 5.14 Changes in surface roughness to load with lubrication

The above figures indicate that the material with 4%Cr and 4%Cr+Ti deteriorated less than that with 4%Cr under dry or lubricated conditions but the initial surface roughness of each differed slightly due to the difficulties to control

the roughness during grinding. This fact must be considered as part of the deterioration process. Figures 5.13 (b) and 5.14 (b) show there is a less roughness drop on a rougher surface with lubrication under each load. A possible reason for this is that more lubricant is trapped on a rougher surface.

5.4 Surface profile as function of disk speed

Four speeds, 214, 428, 597 and 757rpm were run to investigate its effect on surface roughness. The slip was 1.5% and load 1000N.

Figures 5.15 and 5.16 display the weight loss as a function of speed; with dry contact the speed plays a significant role in the wear of both materials. The material with 4%Cr+Ti loses less material than that with 4%Cr and the 4%Cr+Ti material is less sensitive to speed than the other as the speed increases.

Scanning electron micrographs in Figure 5.17 illustrate a comparison of surface morphology after testing at the given speeds. As speed increases the grinding grooves are removed and ploughings appeared on the materials for both discs under dry contact.

Similarly, the tests under lubricated contact revealed that the material with 4%Cr were worn more than that with 4%Cr+Ti. The changes in surface roughness vs. speed with lubrication for both materials is illustrated in Figure 5.18 and show that the 4%Cr+Ti material exhibits less roughness drop than that with 4%Cr.

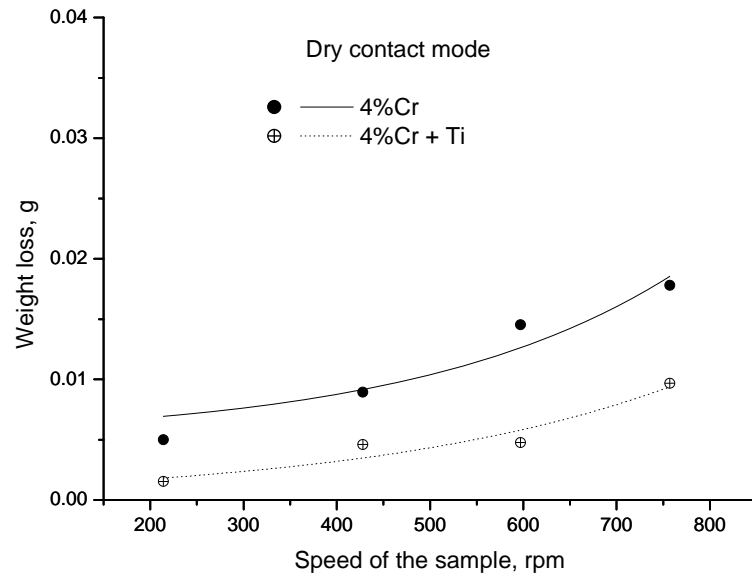


Figure 5.15 Weight loss vs speed at dry mode

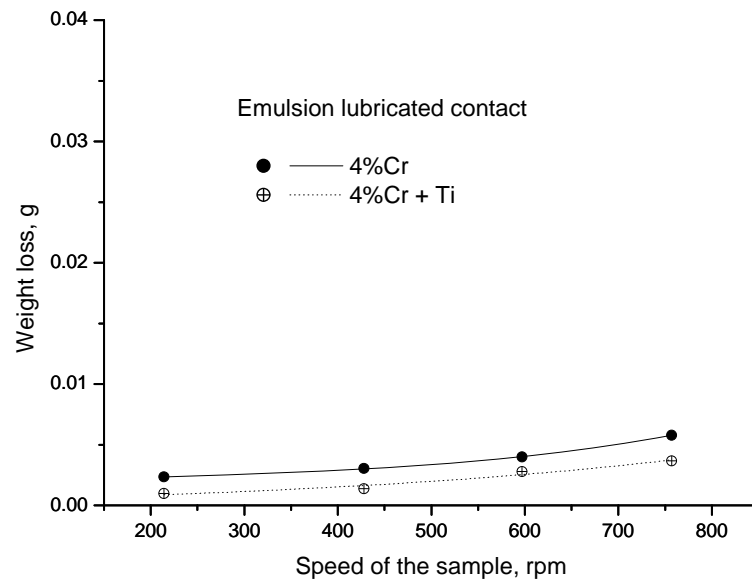


Figure 5.16 Weight loss vs speed at lubricating mode

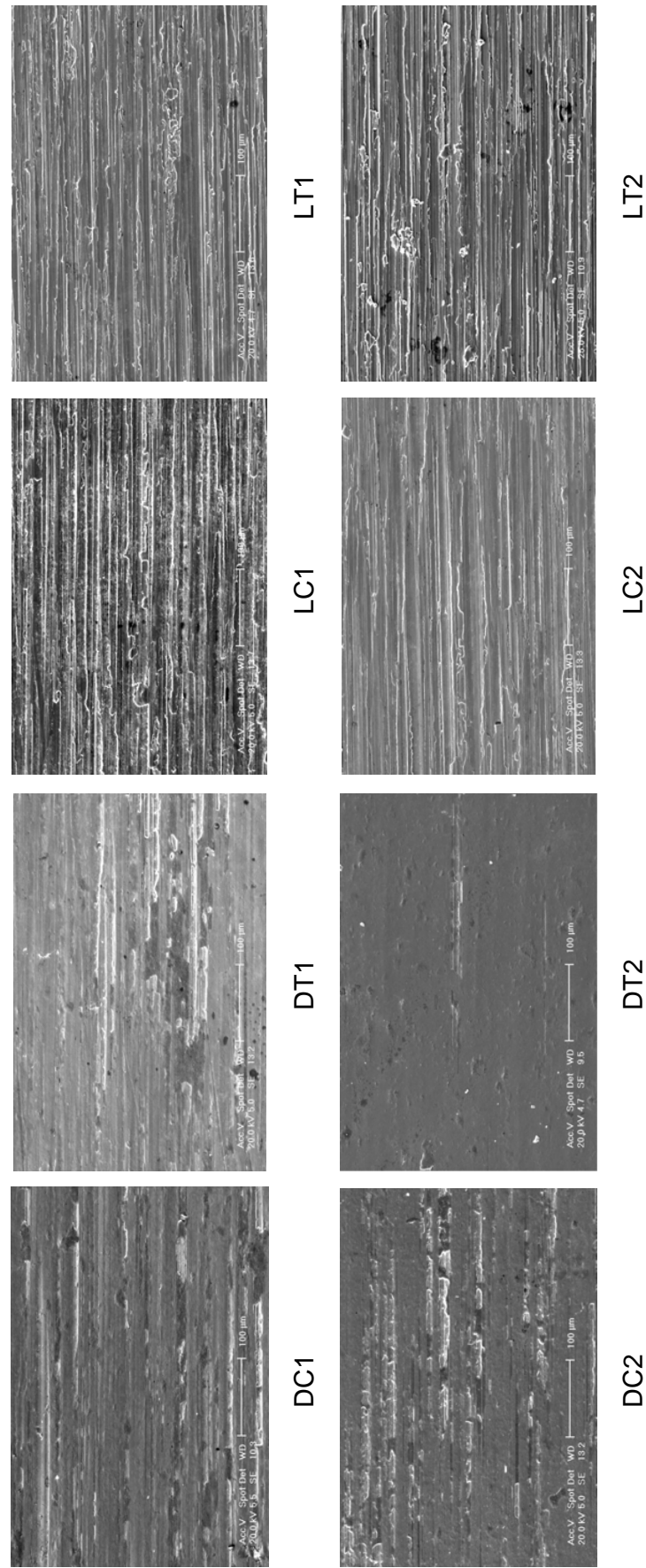


Figure 5.17 Surface of discs after testing at each speed: D, dry; L, lubricating; C, 4%Cr material; T, 4%Cr+Ti material; 1 to 4: rotating speed at 214, 428, 597 and 757rpm respectively (To be continued)

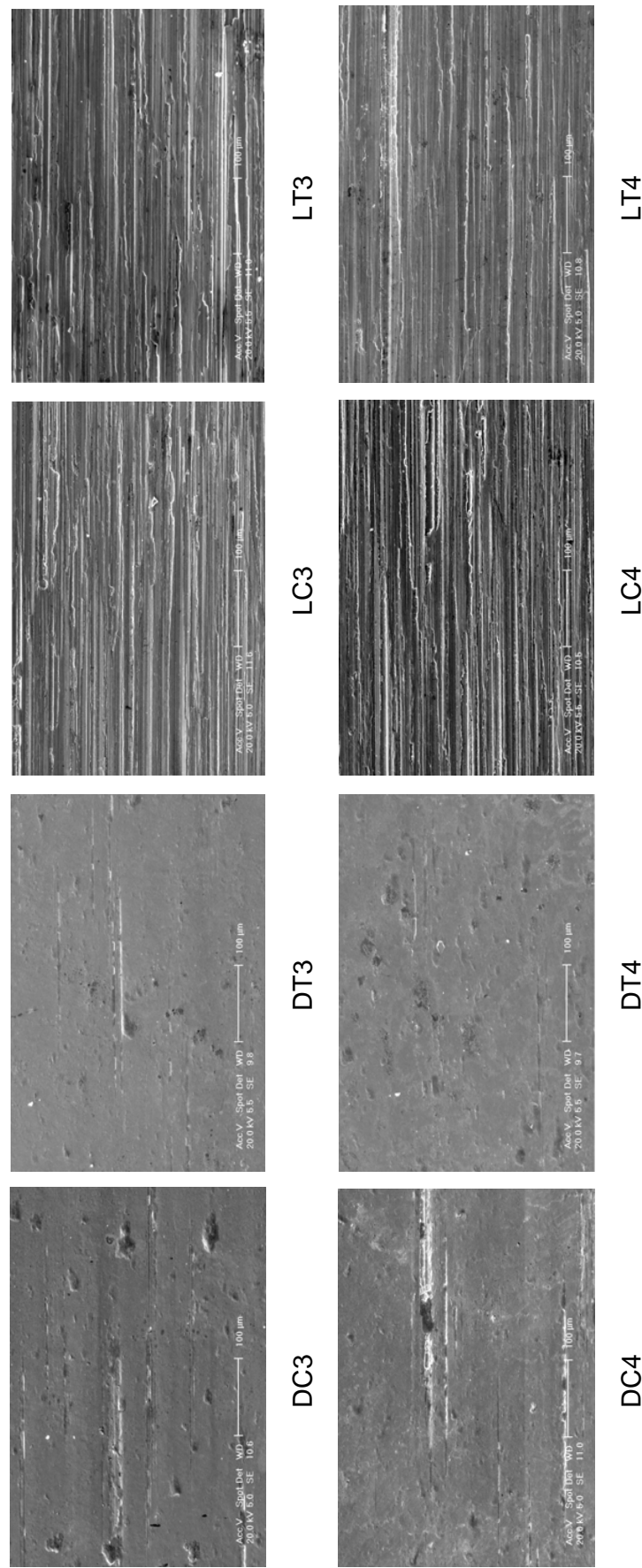


Figure 5.17 (Continued) Surface of discs after testing at each speed: D, dry; L, lubricating; C, 4%Cr material; T, 4%Cr+Ti material; 1 to 4: rotating speed at 214, 428, 597 and 757rpm respectively

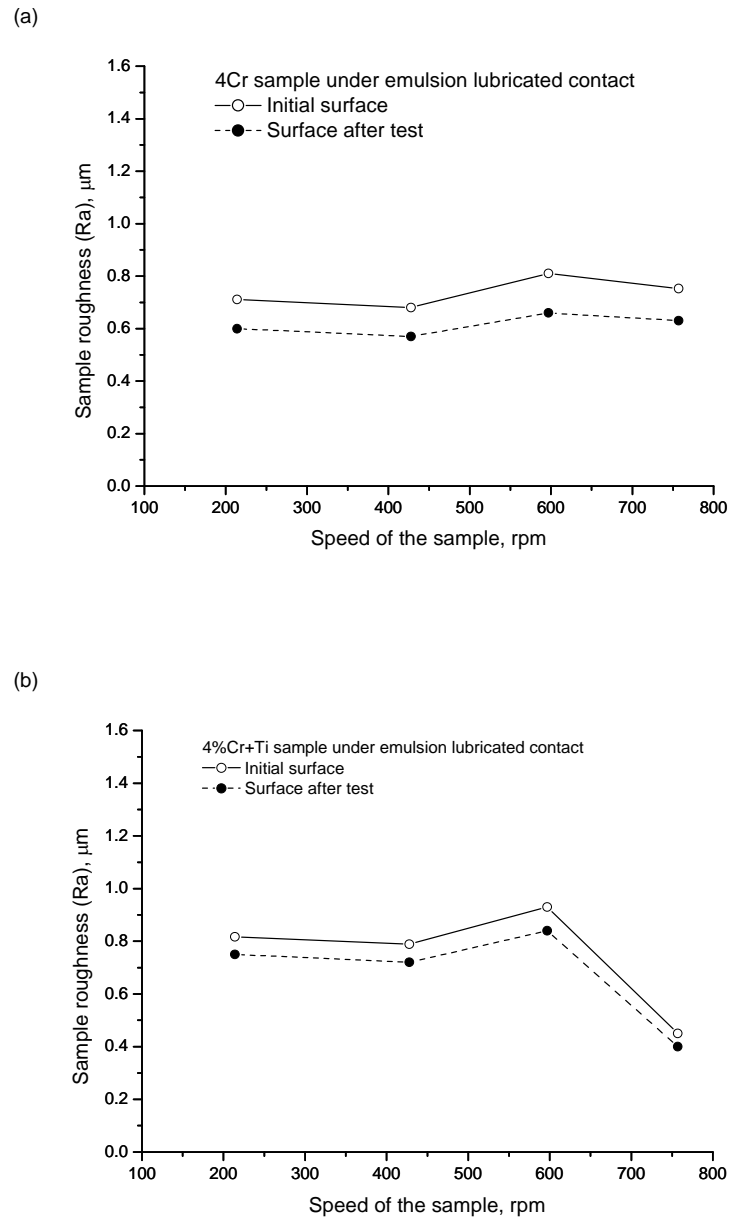


Figure 5.18 Surface roughness to disc speed with lubrication

5.5 Difference in speed between sample and material

In this section tests were only carried out for dry contact. Sample speed was 597rpm and the load 1000N. A negative slip -2% and positive slip from 1.5 to

6% were used to compare how the difference in speed between the sample and material affects wear. The results are shown in Figures 5.19 to 5.20.

Figure 5.19 shows that minimum loss of weight occurs at the negative slip of -2% but it increases significantly with the positive slip from 1.5% to 6%, although the disc with 4%Cr+Ti loses less than the disc with only 4%Cr.

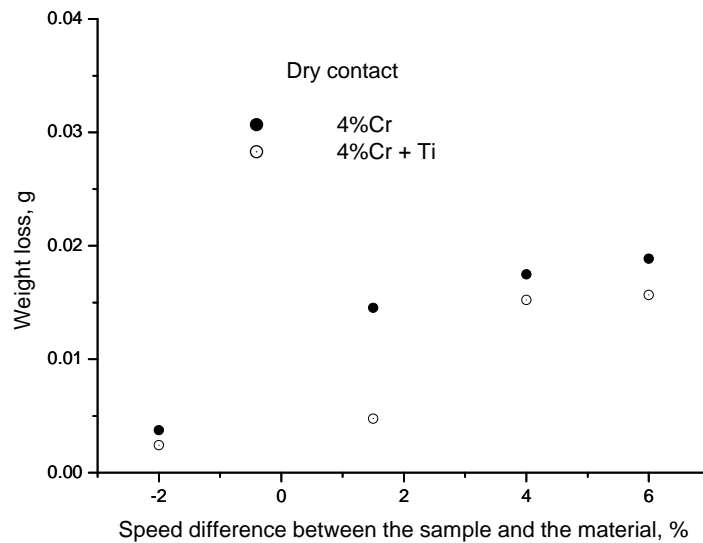


Figure 5.19 Weight loss to speed difference under dry contact

Figure 5.20 indicates that there is a minor surface roughness drop of the 4%Cr disc when slip increases from 1.5% to 6.0% but under test conditions it was difficult to find any change of roughness drop with slip on the disc with 4%Cr+Ti.

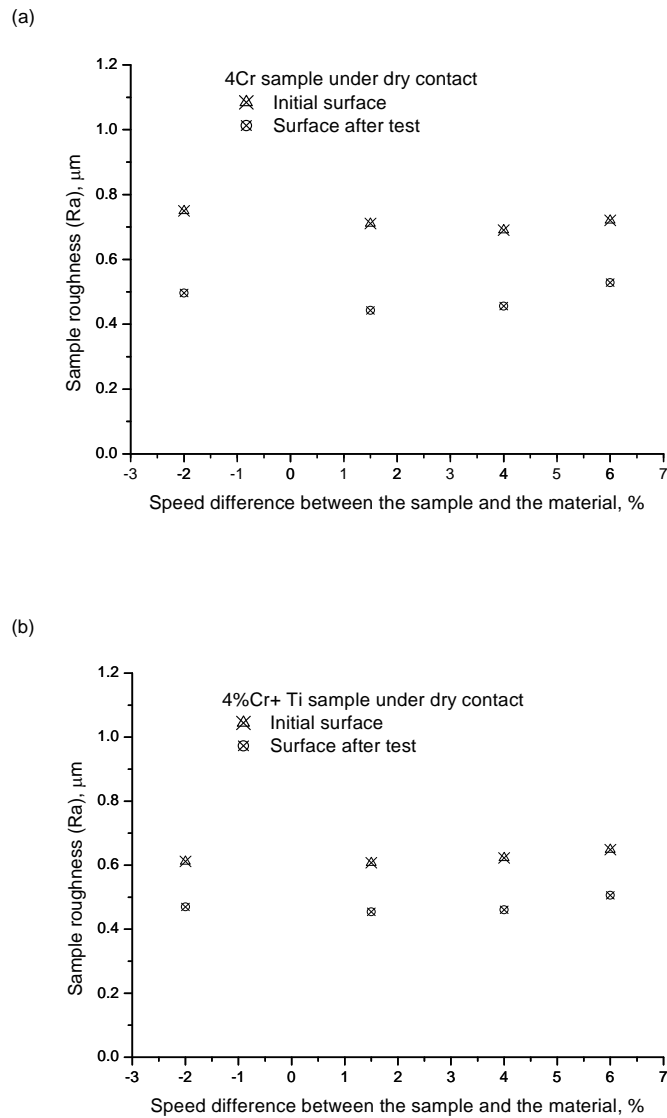


Figure 5.20 Surface roughness to speed under dry contact

5.6 Test conditions on the coefficient of friction and torque

The effect of wear on the coefficient of friction and torque (measured by the test system) are discussed here, the lubrication and surface roughness are the same as those discussed in previous sections.

5.6.1 Disc slip

The tests were carried out for 30 minutes at 597rpm with a load of 1000N under dry contact. The results are shown in Figure 5.21.

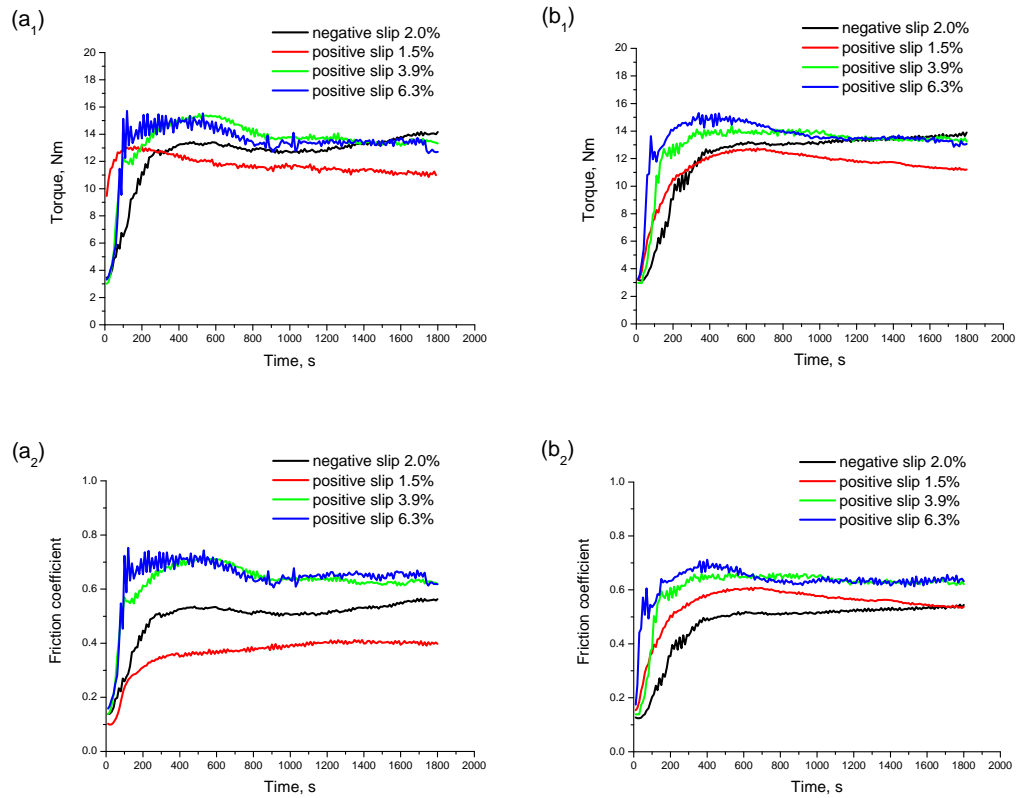


Figure 5.21 Result of disc slip on torque and the coefficient of friction at dry contact. (a₁) and (a₂): 4%Cr disc ; (b₁) and (b₂): 4%Cr+Ti disc

In Figure 5.21 the torque and coefficient of friction for each disc are consistent at each coordinating slip value. These results also indicate that neither the torque nor the coefficient of friction is dependent on positive slip between 3.9% and 6.3% for both discs.

Figure 5.22 is a set of SEM micrographs showing the surface after 30 minutes of

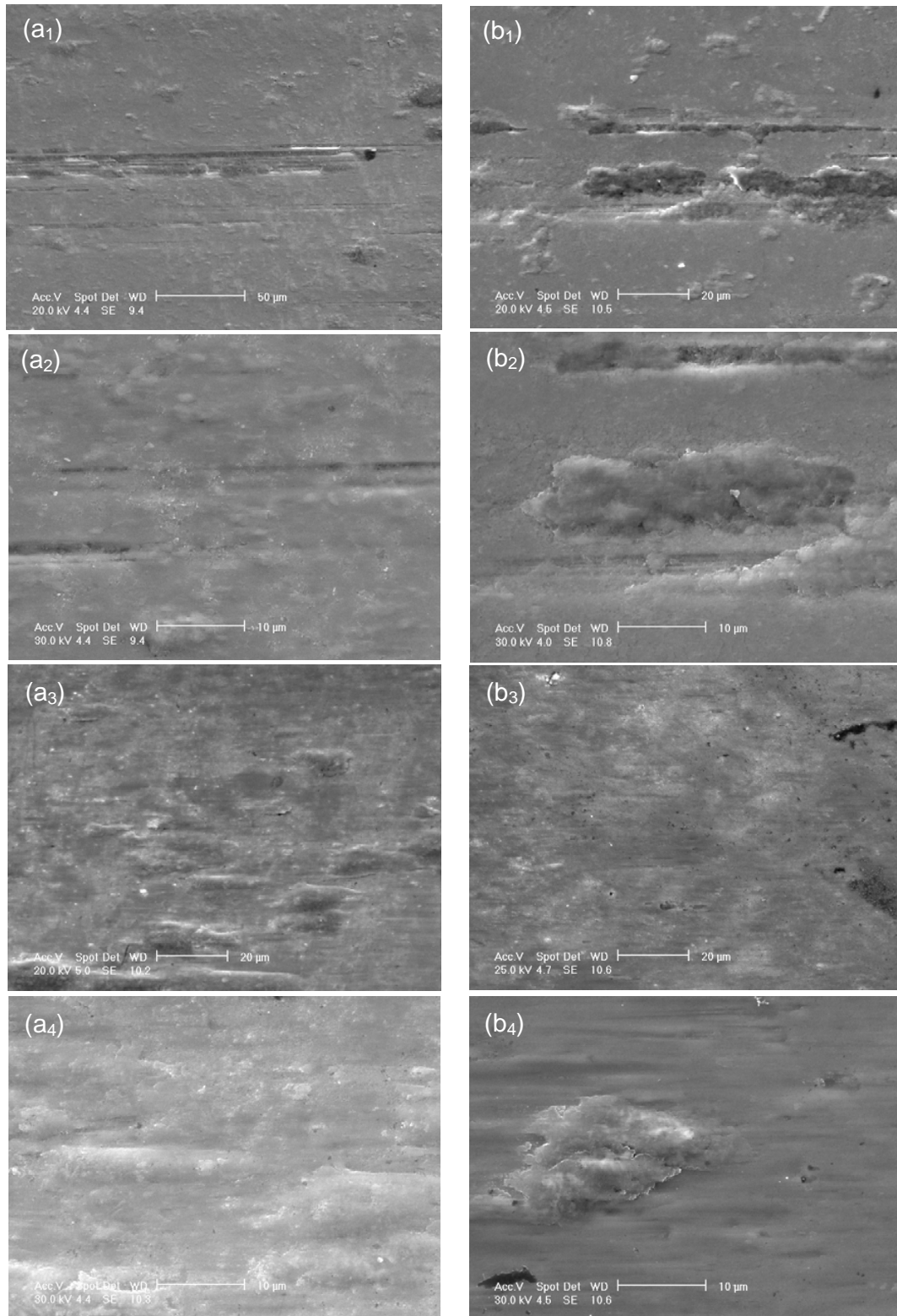


Figure 5.22 SEM photographs of the surface after 30 minutes wear at 1000N at dry contact. (a): 4% Cr disc, (b): 4%Cr+Ti disc; subscript '1' and '2' at 1.5%, subscript '3' and '4' at 6.9% slip

wear at 1000N under dry contact. It indicates that the surface morphology is different after wear at dissimilar rates of slip, although both materials show uneven wear after 30 minutes of friction under dry contact.

The surface discrepancies will inevitably bring about diverse contact situations and hence different resistance to movement that results in relatively different torque and friction. As found in Figure 5.21, even though the torques are close for both discs when the slip values are -2%, 3.9% and 6.3%, the coefficient of friction is lower at negative slip than the other slip conditions. But it is evident that the two discs exhibit different patterns of friction when the positive slip is 1.5%.

The disc with 4%Cr has a lower coefficient of friction than that with 4%Cr+Ti which implies there is difference between the friction mechanisms which will be discussed in Chapter 6.

5.6.2 Result of speed on torque and the coefficient of friction

Two lubricating conditions were applied to determine the effect of speed on torque and the coefficient of friction. The load was 1000N at a positive slip of 1.5% for 30 minutes. Figures 5.23 and 5.24 display the test results under dry contact and lubrication respectively. To facilitate comparison the torque and coefficient friction are labelled at the 1750th second in each figure.

It is evident that the effect of speed on the torque and coefficient of friction depends on the lubricating conditions.

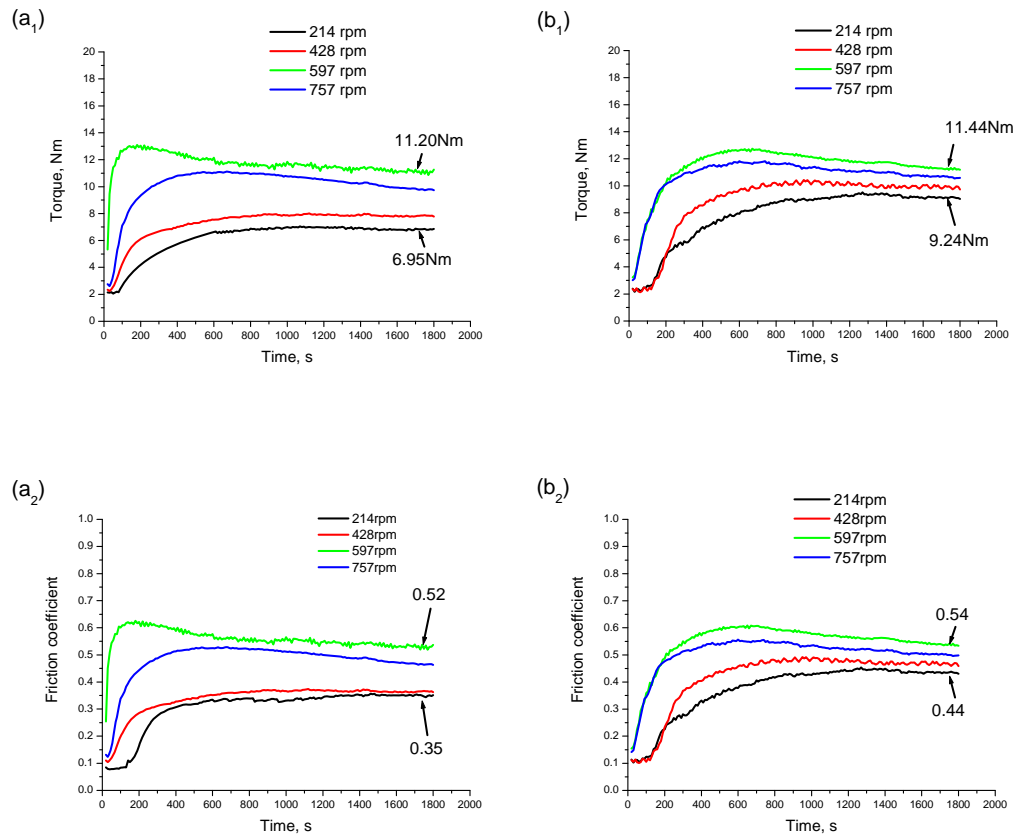


Figure 5.23 Result of disc speed on torque and friction under dry contact.

(a₁) and (a₂): 4%Cr disc ; (b₁) and (b₂): 4%Cr+Ti disc

For the disc with added Ti in dry contact the faster the speed the higher are the torque and friction, except at the highest speed of 757rpm when they decrease. This results in the same order of distribution for the coefficient of friction (Figure 5.23 b₁ and b₂). The results for the disc with 4%Cr are the same as that with 4%Cr+Ti, but the amplitudes of torque and coefficient of friction for the disc with 4%Cr are lower at each speed and they distribute in a wider range than the disc with 4%Cr+Ti.

With added lubrication, the speed affects torque and friction in the opposite way

which results in a smaller torque and lower coefficient of friction. The disc with 4% Cr does not show any significant difference when the speed is either 428rpm or 597rpm and it fluctuates significantly at each speed than the disc with added Ti.

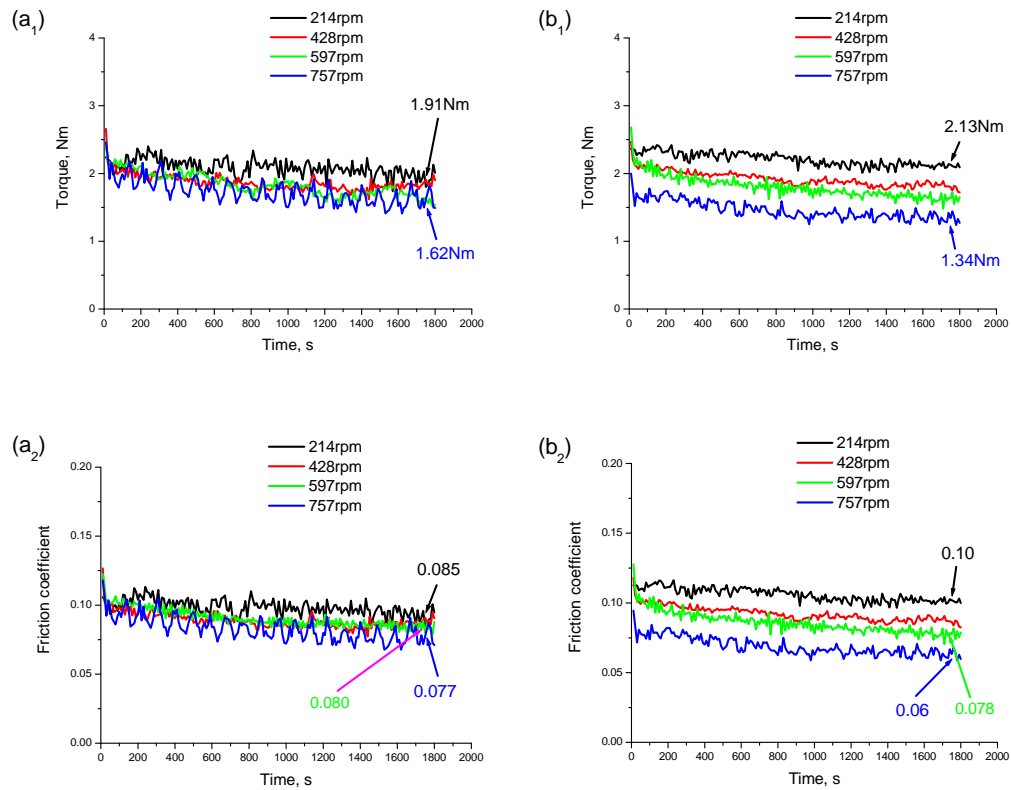


Figure 5.24 Result of speed on torque and friction under lubrication. (a₁) and (a₂): 4%Cr; (b₁) and (b₂): 4%Cr+Ti

The torque values and coefficients of friction are much smaller with lubrication than without but it should be noted that they are more sensitive to lubrication on the disc with added Ti than the disc with 4% Cr. The coefficient of friction for the disc with added Ti varies from 0.44 to 0.54 under dry contact when the speed increases from 214 to 597rpm and is 0.10 to 0.06 with lubrication when the speed increases from 214 to 757rpm. The experiments indicate that if lubrication is

applied to the disc with added Ti, the friction exhibits a reduction of 3.4 times at a slower speed of 214rpm and up to 5.9 times at 597rpm where the torque exhibits a peak value under dry contact. When the speed increases to 757rpm the torque begins to decline and the friction reduces by up to 10 times than dry contact. For the disc with 4%Cr the corresponding friction results in 3.1 and 5.5 times reduction at speeds of 214 and 597rpm respectively. A further increase in speed to 757rpm only produces a limited reduction in intensity of the coefficient of friction which is 5.7 times less than that under dry contact. The ratios of friction between lubrication and dry contact are summarised in Table 5.3.

Table 5.3 Ratios of friction between dry contact and lubrication

speed	214rpm	597rpm	757rpm
4%Cr	3.1	5.5	5.7
4%Cr+Ti	3.4	5.9	10

The above analysis also suggests that the application of lubrication at certain speed may reduce the torque and coefficient of friction, although it is not practical for limited test speeds considered here

5.6.3 Result of load on torque and coefficient of friction with lubrication

In these lubricated tests the speed was 597 rpm for 30 minutes at a positive slip of 1.5%. The results are illustrated in Figure 5.25.

For both materials the torque increases as the load increases but for the material

with 4% Cr the torque increases more than that with 4%Cr+Ti. However, little difference can be found as the load increases for the two discs except for at 2000N. The coefficient of friction for the disc with 4% Cr is almost the same when the loads are 500N and 1000N. It seems that coefficient of friction for the disc with 4%Cr is more sensitive to load than the disc with 4%Cr+Ti, in Figure 5.25 (a₂) and (b₂).

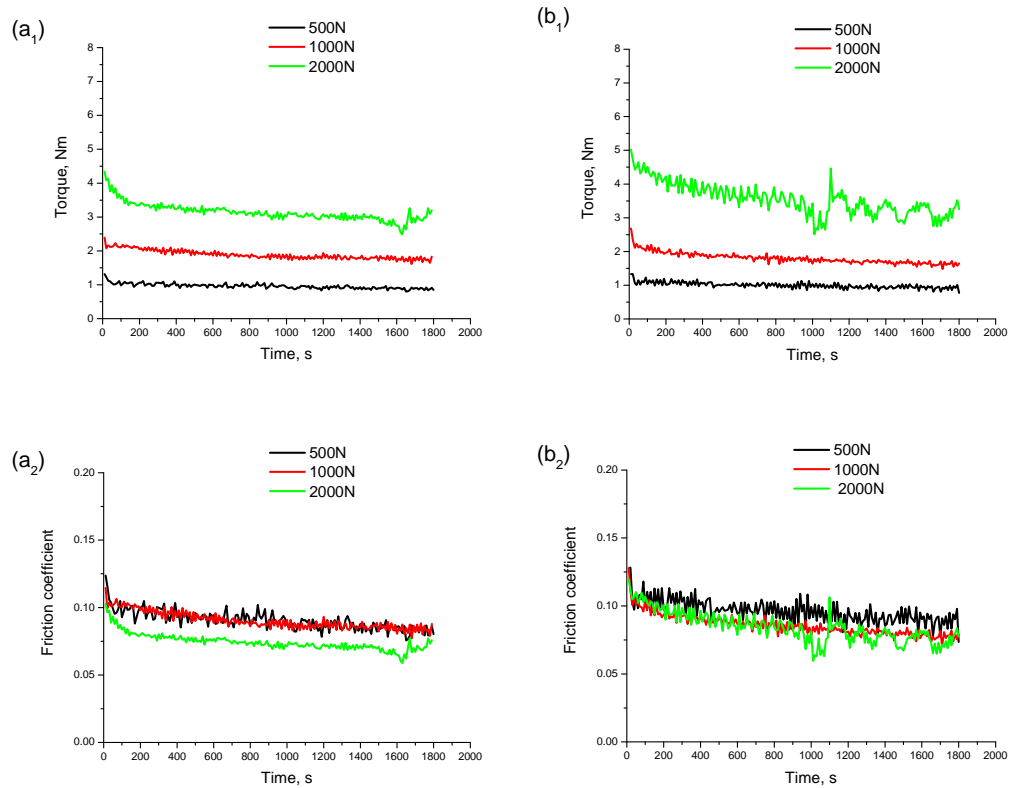


Figure 5.25 Result of disc load on torque and coefficient of friction with lubrication. (a₁) and (a₂): 4%Cr disc; (b₁) and (b₂): 4%Cr+Ti disc

Figure 5.26 presents the surface morphology of the two materials with lubrication under different loads. A comparison between Figures 5.11 and 5.26 indicate that the surfaces deteriorate in a different way when the friction tests were carried out under different lubricating conditions.

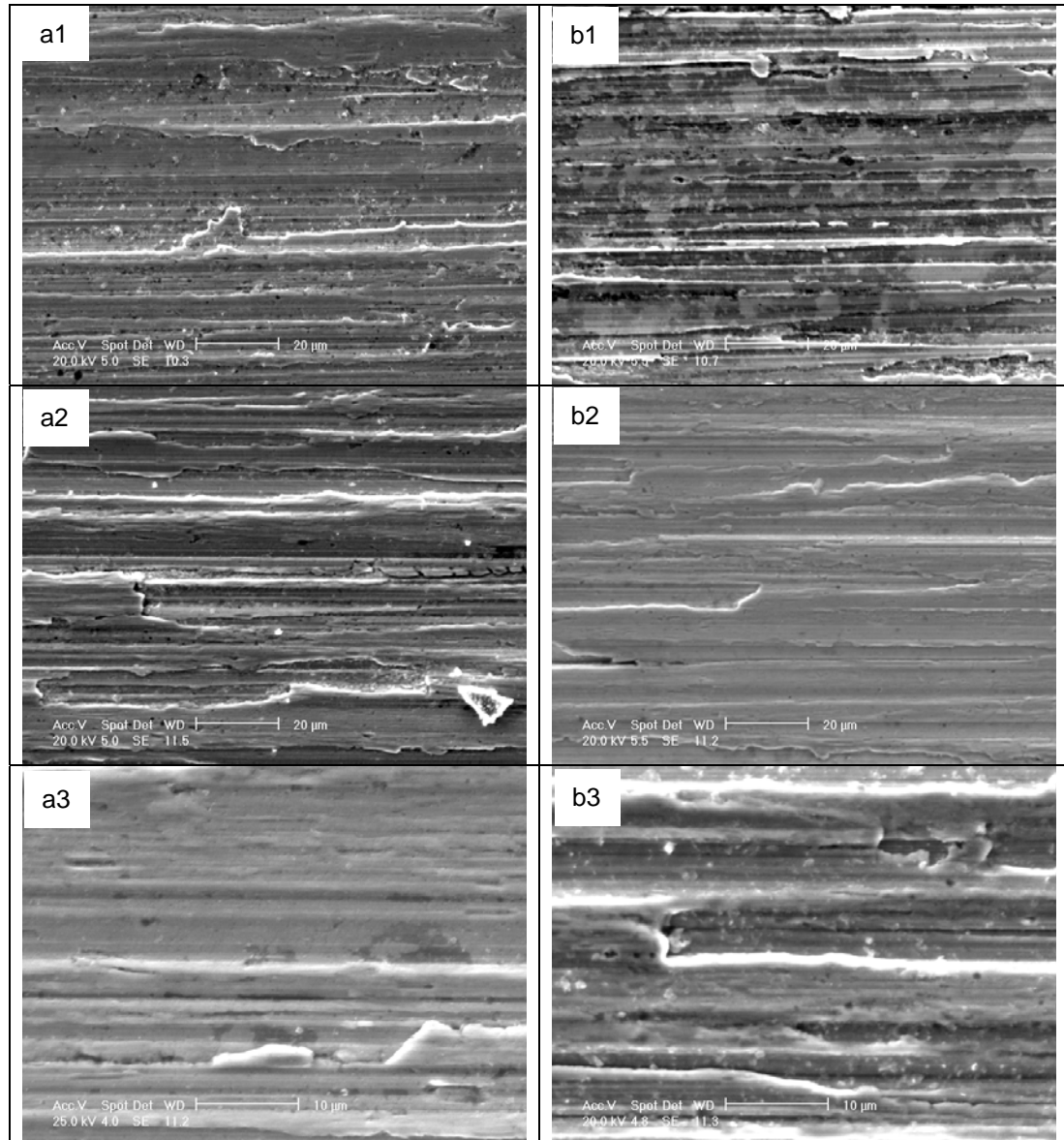


Figure 5.26 Surface comparisons between the two materials at lubricated contact under different loads. a: 4%Cr disc; b: Ti-additive disc; 1 to 3: 500, 1000 and 2000N respectively, positive slip is 1.5%.

In Figure 5.26 the disc with 4%Cr was found with voids and deformed asperities at 500N load after 30 minutes wear. But when the load increases up to 1000N the ranges and grooves on this surface become discontinuous with micro-debris. At 2000N the asperities were flattened and the peaks become smoother. This is consistent with the results in Figure 5.25 (b₂) where the disc with 4%Cr displayed a smaller coefficient of friction than when the loads were 500 to 1000N.

The disc with added Ti showed a slow surface deterioration and obvious surface ranges or asperities deformation at a heavier load than the disc with 4%Cr. However the surface appears to have more grooves when the load reaches 2000N.

5.7 Findings

In this chapter, it was found that at a certain testing condition the testing materials show different friction behaviour.

5.8 Summary

1. Without lubrication the weight loss increases with the duration of contact. More material was worn off the disc with 4%Cr+Ti roll material than the disc with 4%Cr up to 60 minutes, and subsequently the wear on the disc with added Ti slows down. Lubrication significantly reduces the material loss, in mass and

rate of wear.

2. It was observed that the material with 4%Cr+Ti has better anti-wear properties than the material with 4%Cr. When lubrication is applied the surface roughness of the material with added Ti deteriorates much slower than with 4%Cr.

3. The disc weight loss is significantly affected by load for the disc with 4%Cr under both contact conditions although lubrication may slow down surface roughness deterioration for both materials.

4. Speed affects the weight loss to a great extent under dry contact while lubrication has a different effect on both discs for the material worn off. Weight loss increases with speed under dry contact and lubrication conditions although the disc with added Ti lost the least amount in both cases.

5. Negative and positive slip affects the weight loss for both materials under dry contact but as the slip increases, so too does the weight loss. For all slip, lubrication reduces in weight loss and for both contact conditions the material with added Ti has less weight loss.

6. A negative slip of 2% and positive slip of 1.5% resulted in different coefficients of friction under dry contact even though the resulting torques are similar. The 4%Cr disc presents a smaller friction coefficient than the 4%Cr+Ti disc.

7. The torque and coefficient of friction are sensitive to speed under dry contact for the 4%Cr disc.

8. Lubrication alleviates friction for both materials. For the disc with 4%Cr+Ti the faster the speed, the smaller is the coefficient friction . The material with 4%Cr is affected less by speed but the coefficient of friction is sensitive to load.

9. In the present study the coefficient of friction ranges from 0.35 to 0.75 under dry contact and from 0.06 to 0.11 when lubrication is applied.

Chapter 6 Microstructure and Tribological Behaviour of Roll Material with Ti additive

6.1 Introduction

As mentioned in Chapter 1, mechanical contact will inevitably result in friction and wear at the interface between the work roll and the workpiece. Mechanical interactions such as “deformation, brittle fracture, thermal degradation, chemical reactions, solid state bonding and solution transfer.” [137-138], are significant causes for wear and friction. Besides the original surface finishing features, rolling parameters such as speed, reduction and lubrication are of prime importance in accounting for friction and wear. Many of the above parameters interact with each other to some degree but the microstructure and nano-scale precipitates also play a key role in tribological behaviour of roll materials. Many papers have been published relating microstructure to the wear of engineering materials [139-143] but few were found which related microstructure to the tribology of material used in the form of rolls [17].

The objective of the work presented in this chapter was to investigate the microstructure of the roll material (i.e. 4%Cr with and without Ti) with a view to understanding its wear resistance. It is expected that a comprehensive understanding of roll surface wear and the friction patterns described in Chapters 4 and 5 can be obtained. The material with 4%Cr is also analysed to compare

with the material with 4%Cr+Ti.

6.2 Microstructure and mechanical properties of roll material

6.2.1 Experiments

The phases present in the steel were identified using X-ray diffraction techniques. Rigaku D/max-rB (Japan) diffractometer using Cu-K α radiation at 60 kV and 40mA was used to obtain chart recordings in the 2θ range from 40 to 70°. The microstructure of the steel was investigated by optical microscopy, scanning electron microscopy (SEM) and transmission electron microscopy (TEM) equipped with an energy dispersive X-ray analysis (EDX). Both thin foils and extraction replicas were prepared for the TEM experiments. Thin foils were prepared by grinding to 20 μm and then by ion milling with argon ions under 4 kV accelerating voltage. Extraction replicas were prepared in a four stage procedure by etching the polished surface in 2% Nital, coating it with a thin film of C, and then cleaning them in distilled water and alcohol. The samples were examined using an H-800 transmission electron microscope. Selected area of diffraction and EDX were carried out to determine the crystal structure and chemical composition of the carbides.

6.2.2 Microstructure and phase characteristics

Figure 6.1 shows the optical micrographs of the test rolls whose manufacturing procedures were outlined in Chapter 3. Both materials had a hardness of HRC 58 to 62, their tensile strengths are 940~980MPa, and their torsion strengths are from

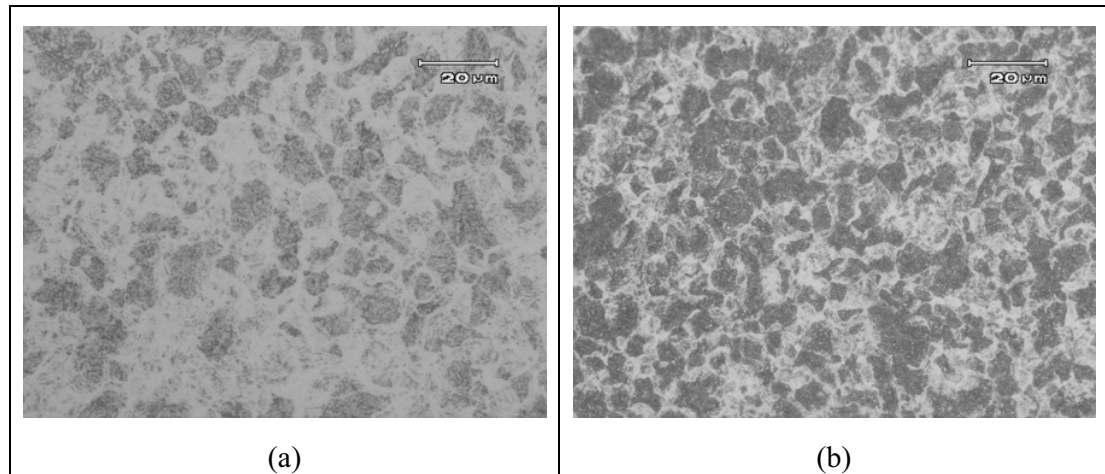


Figure 6.1 Optical micrographs of the test rolls. (a) 4%Cr; (b): 4%Cr with Ti

550 to 590 MPa. It is evident that the microstructure of the roll with 4%Cr+Ti is more homogenous and refined than the roll with 4%Cr. In the rolls with 4%Cr the coarse carbides formed along martensite boundaries (Figure 6.2). They can initiate fatigue cracks, and therefore can seriously degrade the wear resistance [37]. This problem can be alleviated by adding Ti to the 4%Cr rolls. Figure 6.3 shows the distribution of carbides in this roll. Near spherical shaped carbide particles are dispersed uniformly in the matrix which can be separated into two groups, relatively larger particles about 300nm and nano-particles of a size smaller than 20nm. Carbides improved the hardness and wear resistance of the roll with 4% Cr and 4%Cr+Ti while the tempered martensitic matrix containing fine carbides, is responsible for strength and toughness. Under this concept these rolls contain a strong carbide forming element, namely Ti, which helps to form very hard carbides that significantly improve hardness and wear resistance.

It is well known that the properties of rolls are determined by the carbide type,

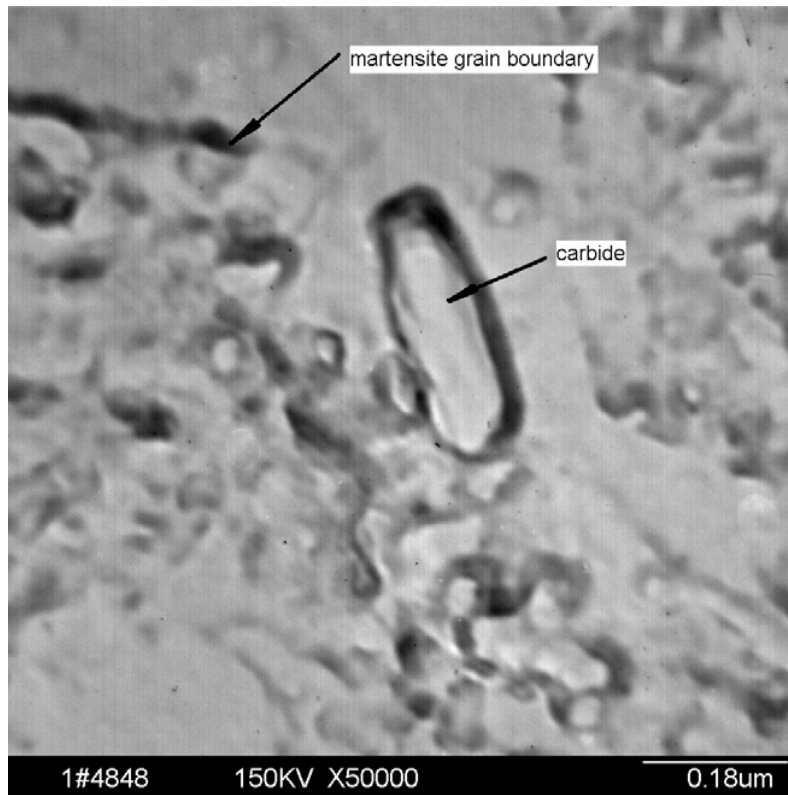


Figure 6.2 TEM image of replicas taken from 4%Cr roll

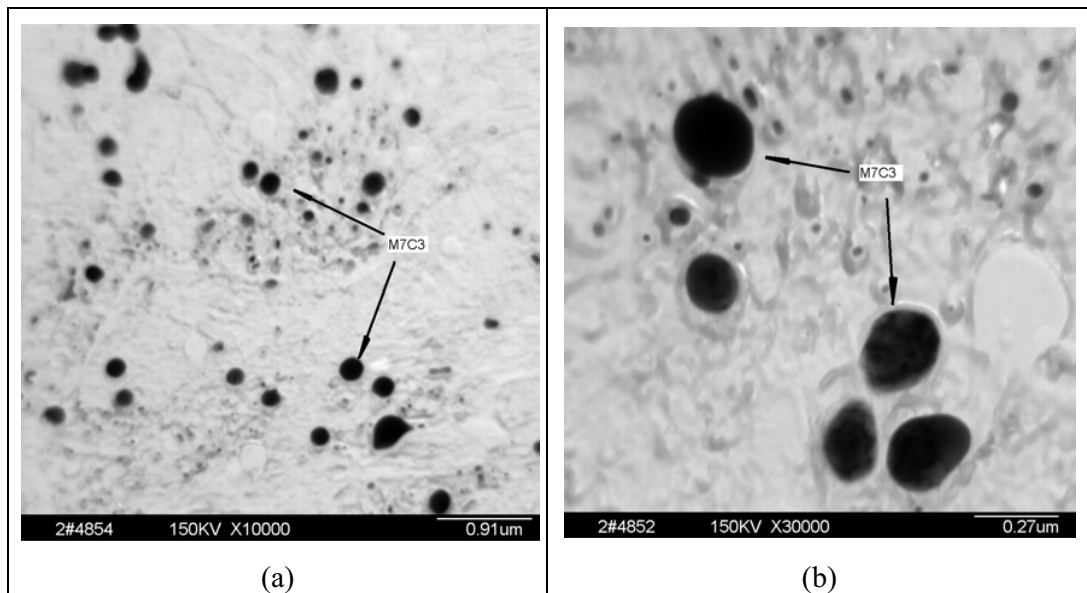


Figure 6. 3 TEM image of replicas taken from 4%Cr+Ti roll. (a) low magnification;(b) high magnification

morphology, volume fraction and their distribution [17, 37]. According to Shimizu et al [17], carbides in roll material varies from 1000 to 3200 Vickers Hardness and they directly influence the wear resistance of rolls and the surface quality of rolled strips. Thus it is necessary to determine the type of carbides precipitated. X-ray diffraction of the surface of the roll with 4%Cr + Ti revealed peaks of M_7C_3 in addition to the martensite matrix (see Figure 6.4). However, no diffraction peaks corresponding to titanium carbonitride, which is precipitated in steels at very low concentrations of titanium. This is probably because the particles were too small or even transparent to X-ray, or distributed unevenly. A TEM experiment on thin foil taken from a roll with 4%Cr+Ti also indicated distribution of M_7C_3 . EDAX suggested the presence of Fe and Cr in carbides so the large carbide particles can be determined as $(Fe,Cr)_7C_3$ (Figure 6.5). No orientation relationship between the martensite matrix and $(Fe,Cr)_7C_3$ was found.

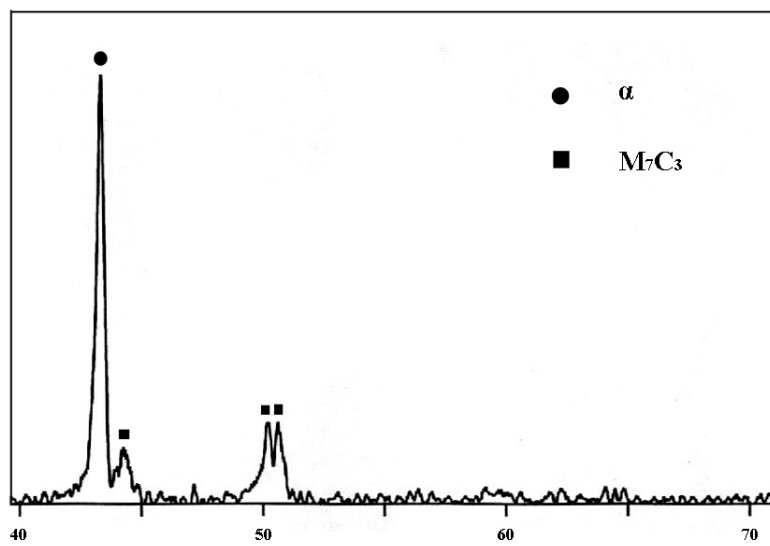


Figure 6.4 XRD pattern for the surface of 4%Cr +Ti roll

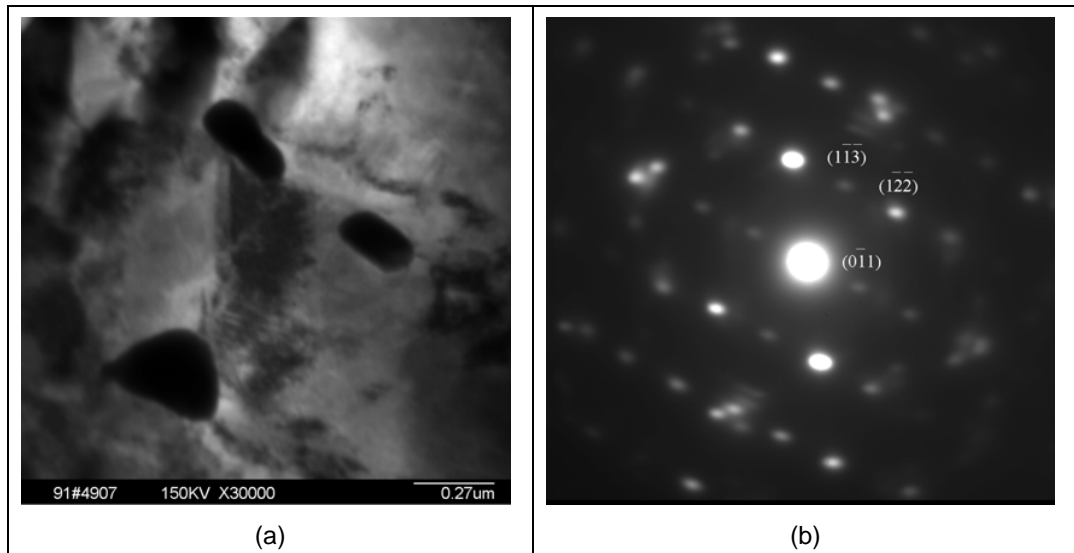


Figure 6.5 TEM image of thin foil taken from 4%Cr +Ti roll: (a) morphology of (Fe,Cr)₇C₃; (b) corresponding selected area diffraction (SAD) pattern

6.2.3 Carbonitrides in the material with 4%Cr+Ti

Titanium has a very strong affinity for carbon and nitrogen and can form stable titanium carbonitride, Ti(C,N). Figure 6.6 displays the qualitative analytical results for the precipitates determined with an Electro Probe Micro Analyser. It shows that the cubic morphology of titanium carbonitrides are from 4μm to 7μm. Meanwhile, a large quantity of fine Ti(C,N) nano-particles from 8-15nm were observed in roll with 4%Cr+Ti. Figure 6.7 further shows a typical morphology of a Ti(C,N) nano-particles. The corresponding selected area electron diffraction (SAED) pattern is shown in Figure 6.7 (b), from which the orientation relationship between the two phases can be directly identified as

$$(1\bar{1}0)_\alpha // (010)_{\text{Ti(C,N)}}$$

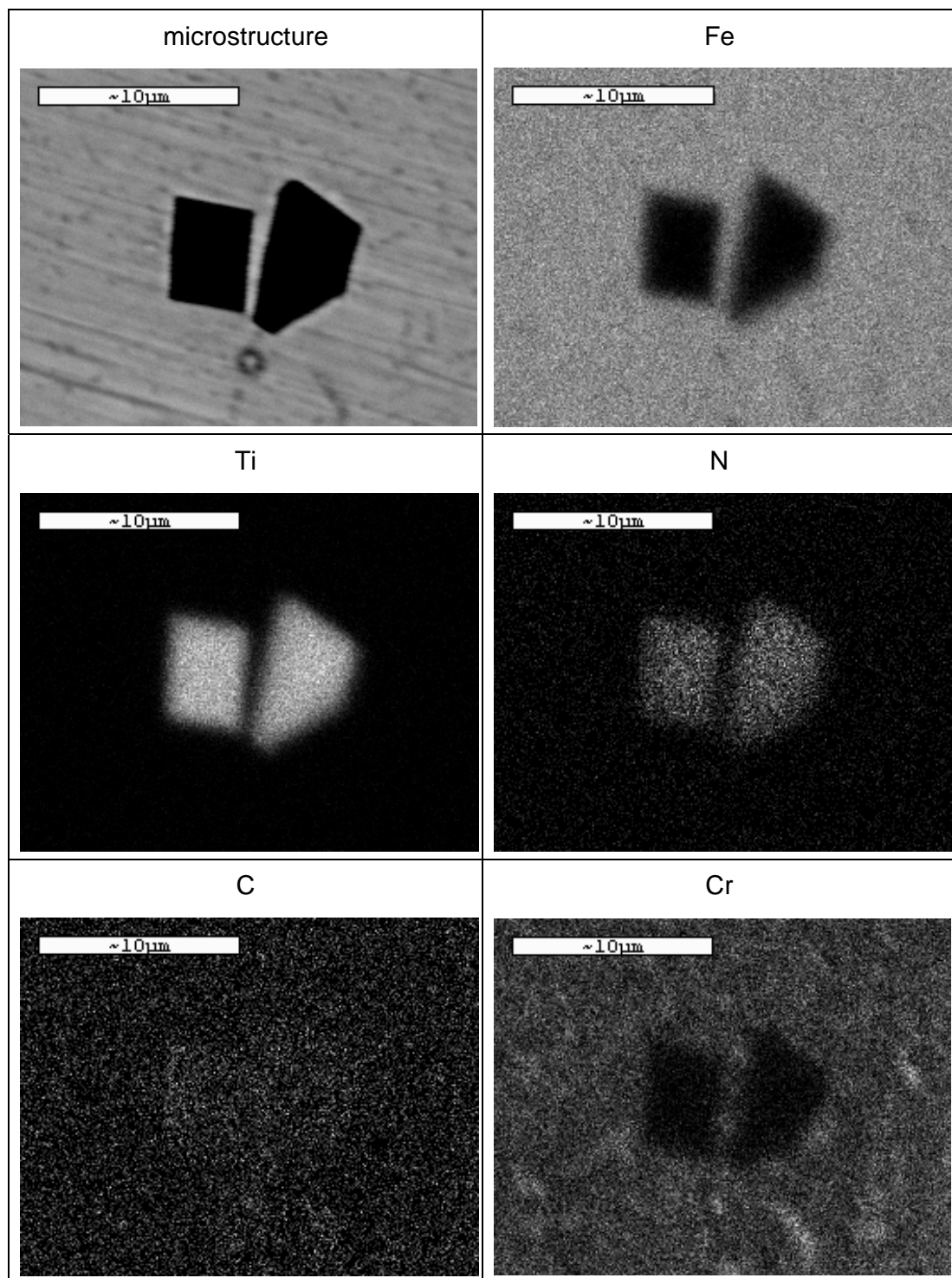


Figure 6.6 Chemical compositions of titanium carbonitride in the material with 4%Cr+Ti

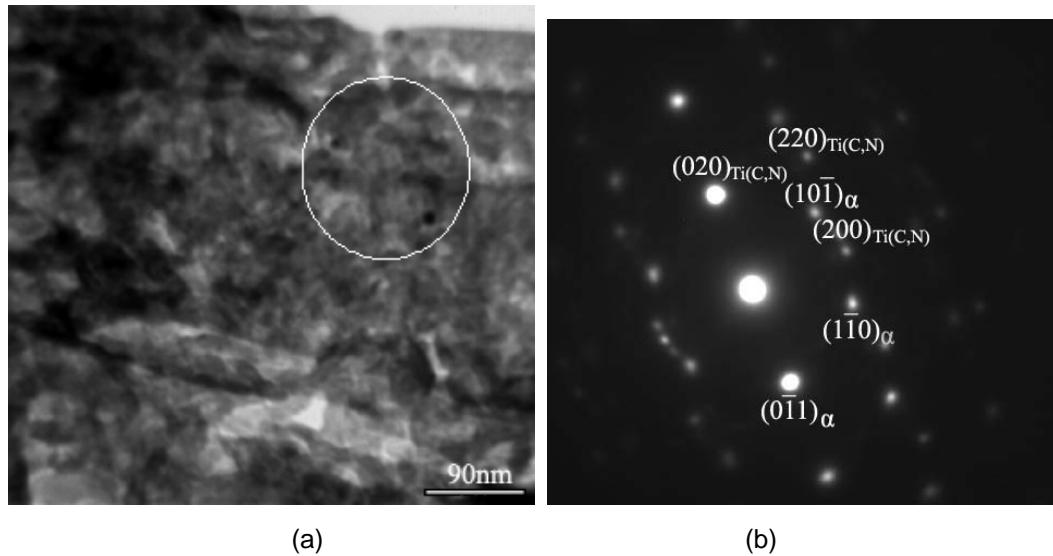


Figure 6.7 TEM image of thin foil taken from a roll with 4%Cr+Ti showing the presence of Ti(C, N): (a) morphology of Ti(C,N); (b) corresponding selected area diffraction pattern

From the above analysis it can be concluded that both types of roll materials are characterised by the presence of (M_7C_3) type eutectic carbides in a matrix of tempered martensite (M). The difference between them lies in the fact that the Ti added material has spherical shaped carbide particles, relatively larger particles about 300nm, and nano-particles smaller than 20nm uniformly dispersed in the matrix. In addition the material with 4%Cr+Ti also has cubic titanium carbo-nitrides in micro-scale and nano-scale respectively. The existence of titanium carbo-nitrides are expected to perform an enhanced anti-wear role.

6.3 Wear pattern of material with 4%Cr+Ti.

It was concluded in Chapters 4 and 5 that the material with 4%Cr+Ti displays its improved wear resistance in the following area better than the 4% Cr material:

- a) less abrasion under dry contact and with lubrication ;
- b) a lower drop in roughness under both contact conditions ;
- c) friction has less sensitivity to speed under dry contact friction and higher sensitivity with lubrication .

Roll surface wear involves a wide range of mechanisms. Because cold rolling operations always include lubrication, a discussion on wear and roll material property will principally focus on lubricating conditions. Figure 5.8 in Chapter 5, which is about the disc-to-disc tests at a forward slip of 1.5% at a load of 1000N and speed of 597rpm, describes the surface appearance after several test intervals. A detailed study in micro-scale on these samples in the later sections of the present chapter indicates ridges deformation, flattening, debris flaking off, and pitting of the roll surface. However, the roll with 4%Cr+Ti exhibits a different surface deterioration from the 4%Cr roll.

6.3.1 Heave deformation, flattening, and abrasive wear

Figure 6.8 illustrates the disc surface flattening up to 0.89×10^4 cycles (approximately 1.29 km) under lubrication. There were pores on the original surface of the disc with 4Cr% and 4%Cr+Ti. It is evident in Figure 6.8 that the 4%Cr material experiences deformation and flattening with grinding debris wiped away which resulted in a smoother surface than 4%Cr+Ti material. It seems that the peaks on the surface of the 4%Cr disc were flattened, leaving angular valleys. The 4%Cr+Ti disc kept its sharp penniform edges, which implies there is a lower drop in roughness, consistent with the results in Figure 5.4.

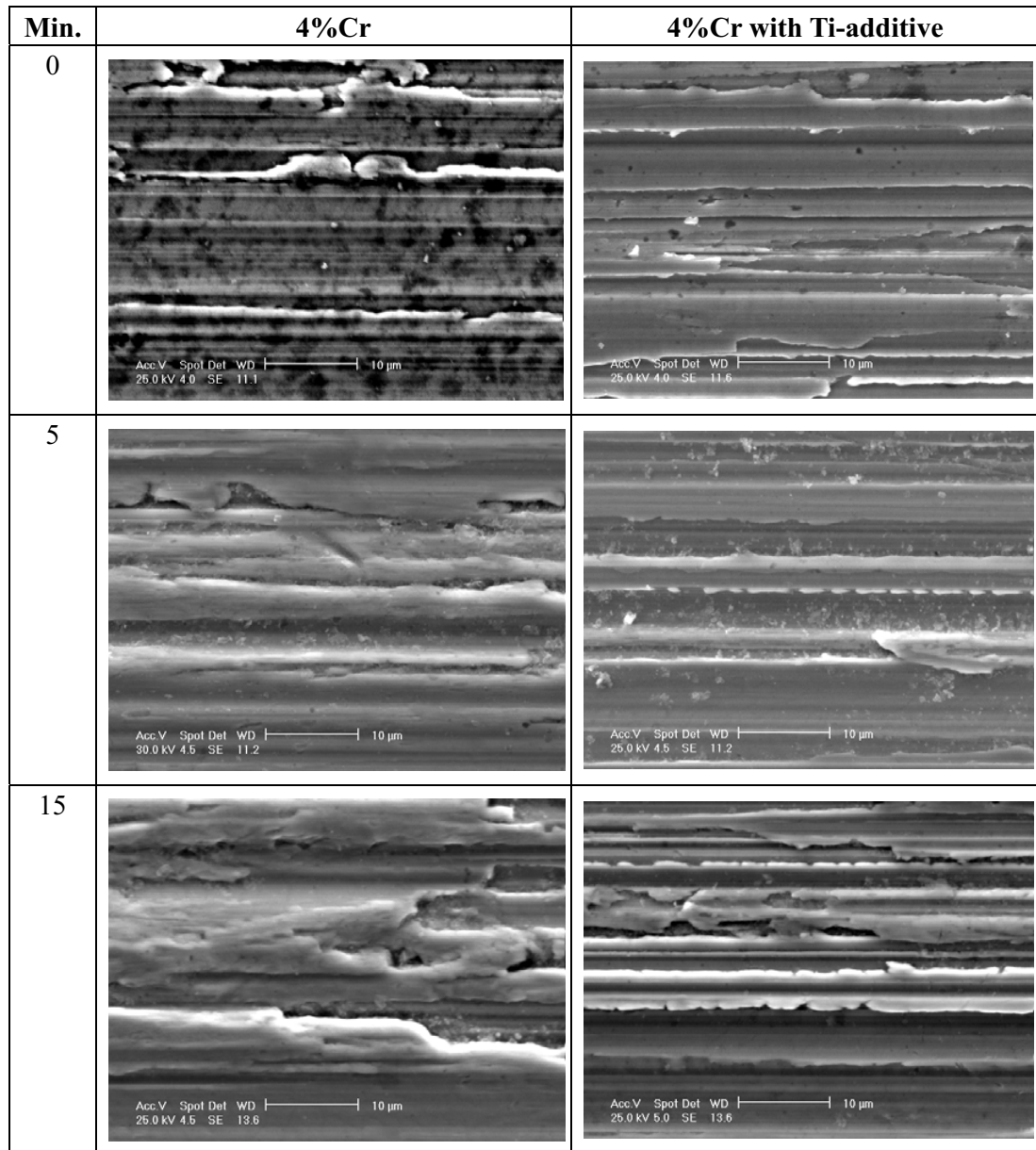


Figure 6.8 Disc surface flattening: up to 0.89×10^4 cycles (15 minutes) at lubricating contact at 1000N, 597rpm in disc-to-disc tests

Flakes were found accumulated in the grooves when the friction test progressed to 5 minutes (Figure 6.8) and 30 minutes (Figure 6.9) on the surfaces of both materials.

6.3.2 Ploughing and delamination wear

The discs experienced different wear patterns from 1.79×10^4 to 2.86×10^5 cycles of contact, as shown in Figures 6.9 and 6.10. The test condition was the same as in Figure 6.8 except for the duration of wear, in which both discs underwent intense deformation, ploughing and delamination wear as well.

Sharp edged angular ridges kept on breaking from the side of the disc with 4%Cr+Ti (30 minutes in Figure 6.9) which resulted in new abrasive particles. Repeated load on the surface of the rotating disc produces deformation on disc surface resulting in material particles up to 10 μm transferring and depressed on the disc surface (60 and 210 minutes in Figure 6.9). Apparent smoothing was found on asperities after 210 to 330 minutes of wear as shown in Figure 6.10. After 1.97×10^5 of cycling, the grinding marks on the surface of the discs regenerated (330 minutes in Figure 6.10). Micro-pits were found after 480 minutes (2.86×10^5 cycles) of wear. A major feature of any abrasive wear is the presence of longitudinal grooves in the direction of sliding. The discs already have grooves from grinding, it is difficult to discern changes from pre-existing grooves to wear generated grooves. If the latter is occurring, and it may well be the case, then it is suspected that the grooves result from ploughing at raised work hardened asperity junctions [169].

Smoothed asperities were repeatedly deformed elastically and plastically on the work-hardened surface of disc with 4% Cr after 0.89×10^4 cycles (15 minutes) of contact, which led to a concentration of residual stress causing breaking off of

the material from the surface peaks (30 minutes in Figure 6.9). The surface ridges were further smoothed progressively (60 to 120 minutes in Figure 6.9).

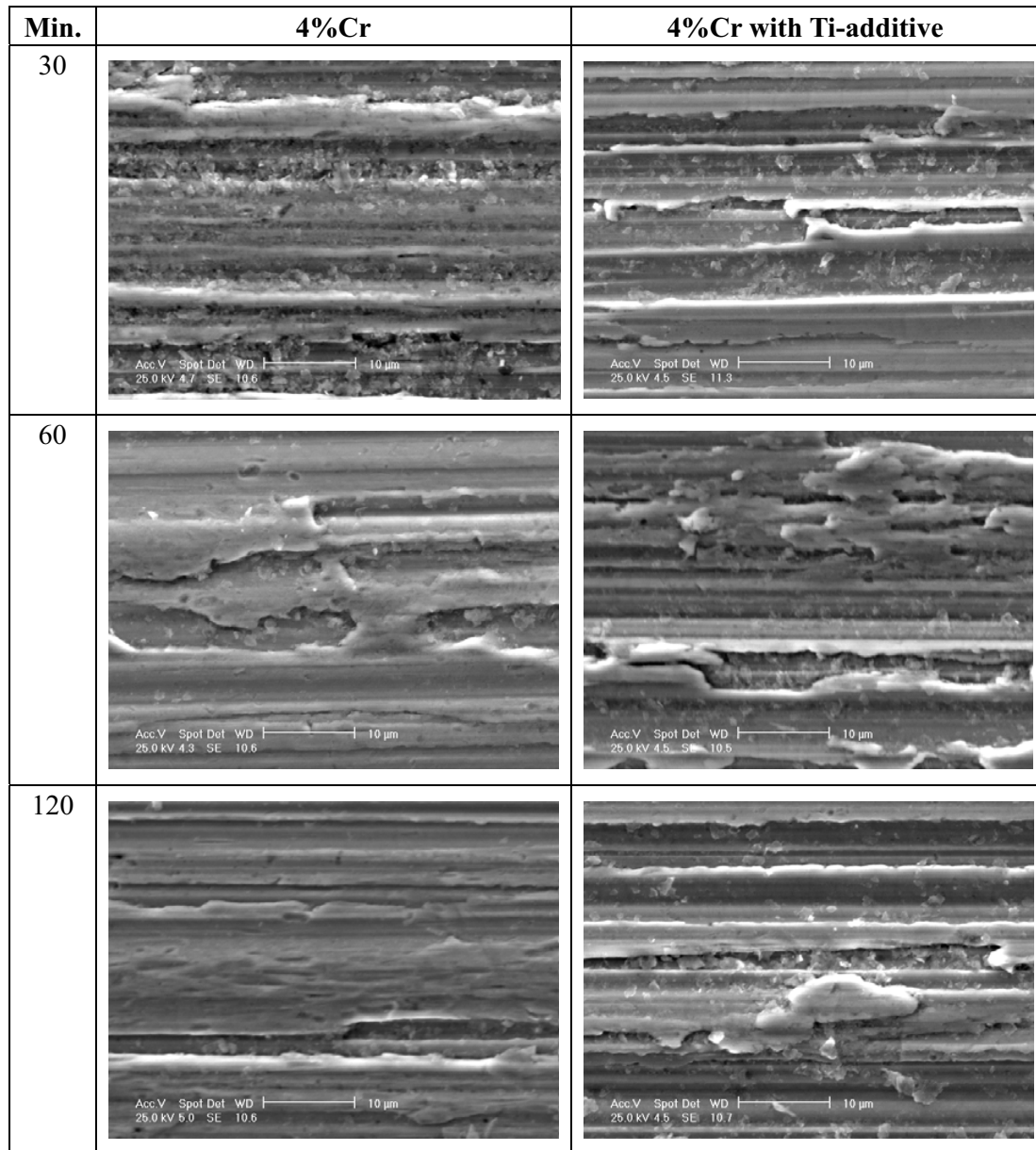


Figure 6.9 Disc surface flaking and further flatting: from 1.79×10^4 to 7.16×10^4 cycles at lubricating contact at 1000N, 597rpm in disc-to-disc tests

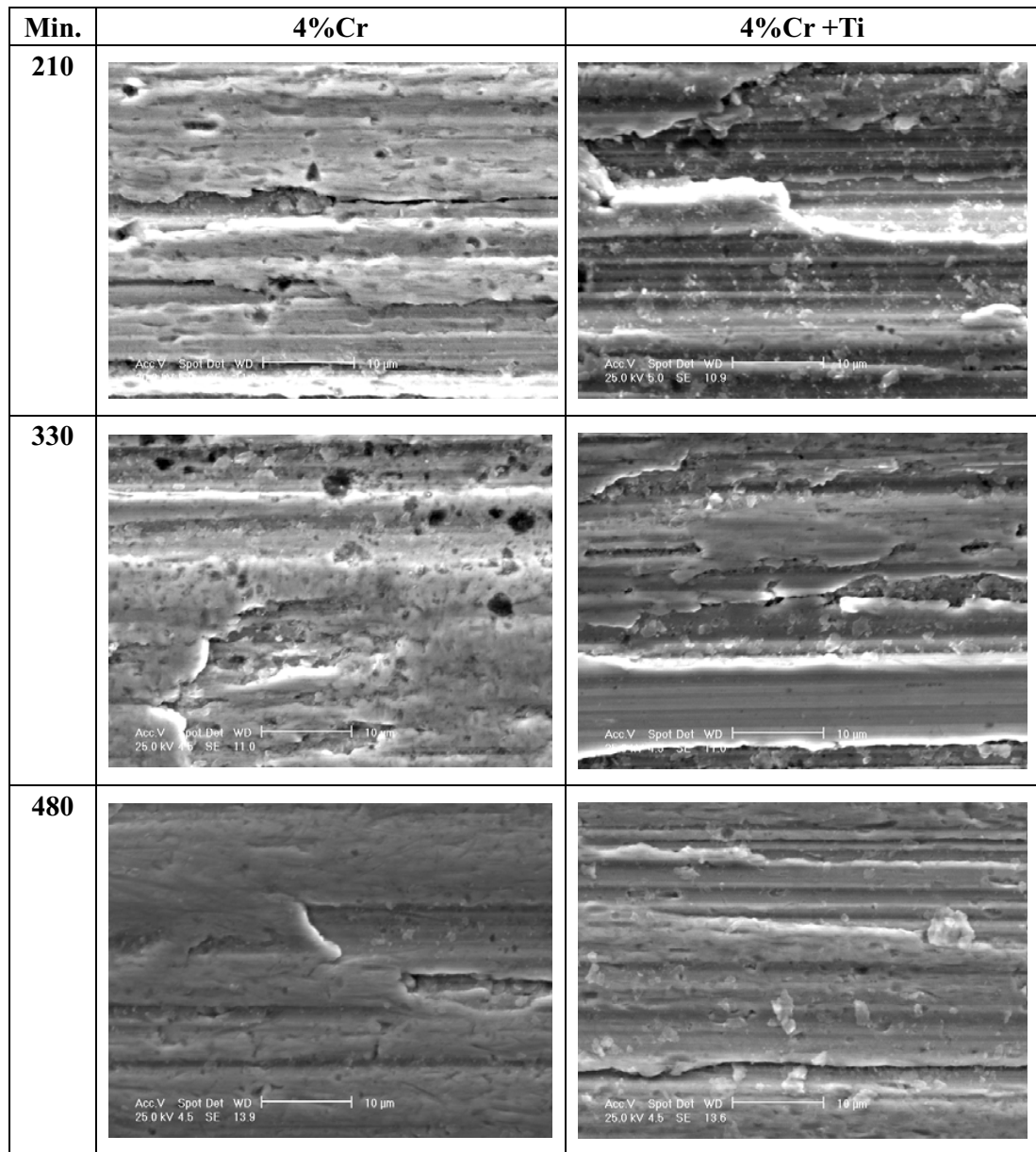


Figure 6.10 Disc surface flaking and further flattening: from 1.25×10^5 to 2.86×10^5 cycles at lubricating contact at 1000N, 597rpm in disc-to-disc tests

Micro-spalling and local pits were found during 210 to 330 minutes of wear (4%Cr material in Figure 6.9). Micro-pits also characterised the surface of the disc with 4%Cr in this period of wear.

Another subjective interpretation of Figures 6.9 and 6.10 according to Doyle [169] is asperity growth due to intense plastic deformation (effectively ‘smoothing’). If we accept that this mechanism is occurring then this will give rise to delamination [53, 167, 170-172]. The latter allows for material transfer and back-transfer. It also allows for the formation of ‘holes’ due to ductile dimple failure at the junction of the deformed layer and substrate [169].

6.3.3 Wear and microstructure

Wear is effectively influenced by the material microstructure which should be incorporated and optimised in order to produce roll material with excellent performance. The matrix is important to the overall hardness, strength, and fracture toughness and therefore it should be strengthened. It has been suggested that the chemical composition and manufacturing process, especially heat treatment, are of great importance to the microstructure and wear properties of the cold work roll material [144-147]. It is suggested that the processing technology is not the main task of the present study. However, heat treatment and material selection is critical, as is shown in this thesis.

Figure 6.11 illustrates the microstructure 0.1mm underneath the surface of both materials before the wear tests.

It is known that the addition of Cr improves resistance to cracking through solid-solution hardening. To further improve wear resistance, it is crucial to form a large amount of homogeneously distributed carbides in a martensitic matrix.

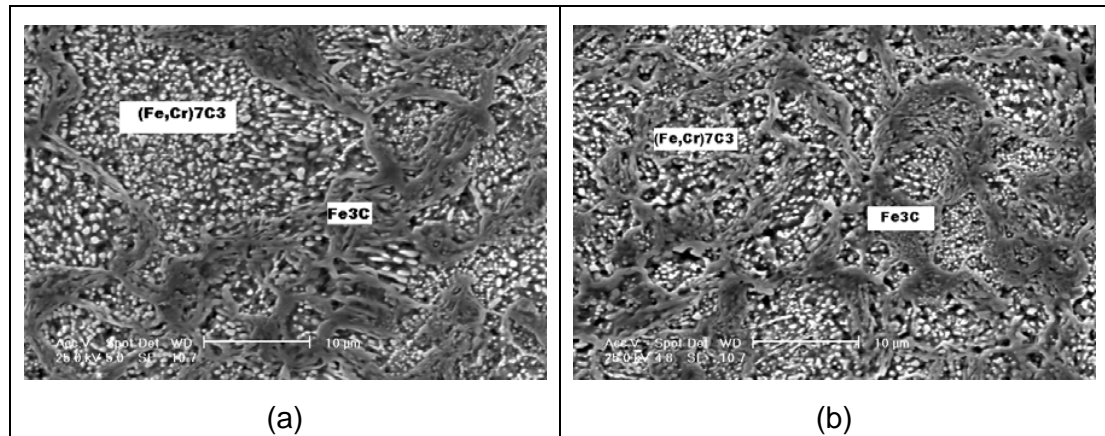


Figure 6.11 Microstructure 0.1mm underneath the surface of both materials before wearing. (a) 4% Cr; (b) 4%Cr+Ti

Figure 6.11 further demonstrated the results in Figure 6.1. In fact, the key factor of addition of Ti is the strong carbide/nitride forming tendency. This results in a finer grain size and a finer carbide precipitation. A key factor of any addition of Ti will be the strong carbide/nitride forming tendency. This results in a finer grain size and a finer carbide precipitation.

A comparison between the two materials shows that a disc with 4% Cr displayed gross plastic deformation leading to delamination earlier than the 4%Cr+Ti disc, as discussed in section 6.3.2. In fact both failures are caused by relatively large carbides and coarse cementite in the material which may be removed from the material matrix and cause pitting or spalling. Titanium carbonitride precipitates retarded re-crystallisation and grain growth during heat treatment on the disc with 4%Cr+Ti, which improved its transformation characteristics and lead to the superior mechanical properties of micro-alloyed steels.

Figure 6.12 shows a TEM micrograph from the worn surfaces of both discs where they both feature a heavily strained matrix. The images indicate substance of near spherical and elongated shape on the surface of the disc with 4%Cr+Ti but no such traces were found on the other disc. It has been recognised that the service life of work rolls in cold rolling could be prolonged through the regeneration of roughness by wear, making use of the hardness differential between carbide and matrix [17]. During cold rolling the hard titanium carbonitrides is supposed to be removed from the roll surface and become third-body abrasives, resulting in roughness regeneration.

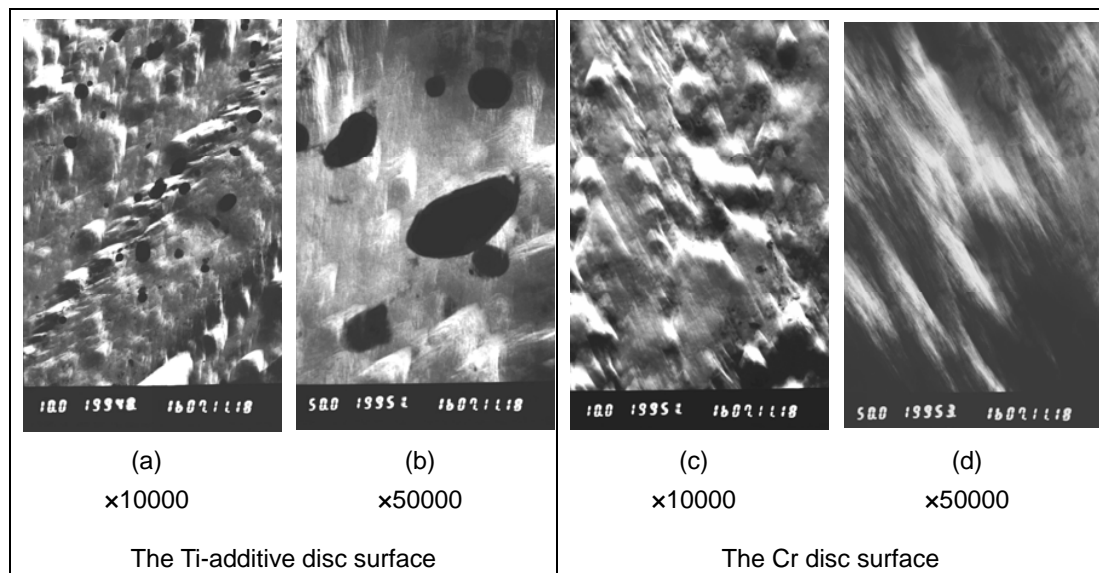


Figure 6.12 TEM micrograph of the worn disc surface after 480 minutes

Electro Probe tests confirm the existence of carbonitrides, as well as MnS, in the flakes which were collected after disc-to-disc wear (Figure 6.13). Table 6.1 summarises the Vickers of different carbides and demonstrate the extremely high

hardness of titanium carbide. It is realised that the carbon particles detach from honing mediums to generate the surface roughness of the disc with 4%Cr+Ti in the disc-to-disc wear tests.

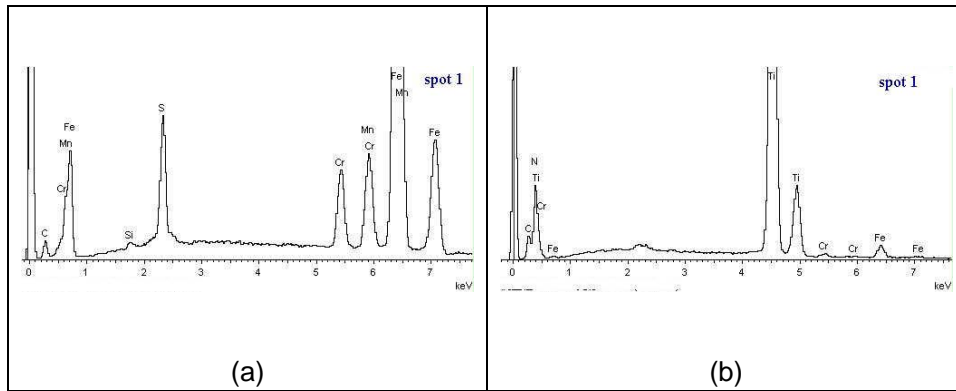


Figure 6.13 Electro Probe tests of the flakes collected after disc-to-disc wear.

(a) 4%Cr; (b) 4%Cr+Ti

Table 6.1 Vickers of different carbides

Carbides	Vickers hardness	Density, g/cm ³
TiC	3200	4.93
VC	2600	5.81
WC	2400	15.77
NbC	2400	7.76
(Fe, Cr) ₇ C ₃	1600~1800	6.92
Mo ₂ C	1500	9.20
Fe ₃ C	1340	7.40

The continuous roughness regeneration has a close relationship with the size and distribution of the titanium carbonitrides in the martensitic matrix. However, if much more titanium is added, the titanium carbonitrides are larger and precipitate

in a net like pattern which results in poor grinding. The optimal amount of titanium is determined by considering both the degree of generated roughness and grindability [17]. From Figures 6.6 and 6.12 the cylindrical and rectangular types of precipitates characterise the material with 4%Cr+Ti.

It should be pointed out that the apparent traces of sulphur were unfortunately identified in Figure 6.13. Sulphur is easy to form an MnS inclusion which is a detrimental substance to lamination. This may be another reason that the disc with 4%Cr experienced surface failure faster than the 4%Cr+Ti.

6.4 Friction

Figure 6.14 shows the coefficient of friction of the two materials during 480 minutes of wear at lubricated condition.

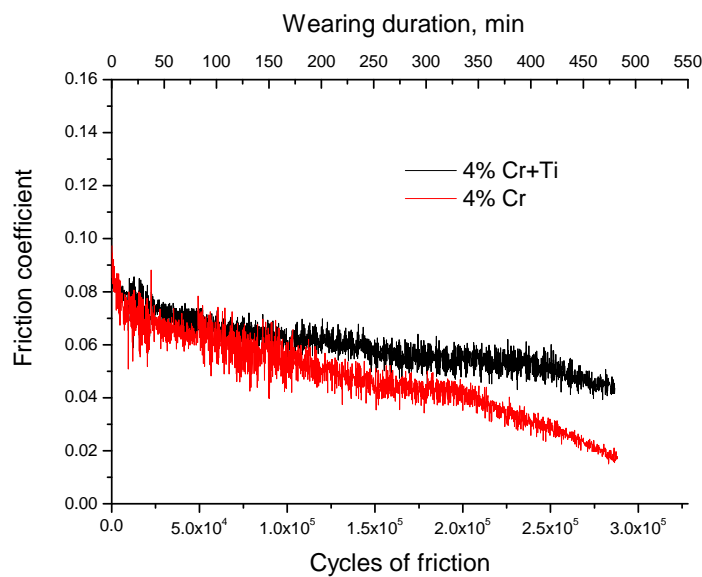


Figure 6.14 Change in coefficient of friction during 480 minutes of wear

According to Figure 6.14, the coefficient of friction of the disc with 4%Cr is lower than that of the disc with 4%Cr+Ti up to 175 minutes but after this time friction difference becomes larger. The coefficient of friction of the disc with 4%Cr reduces to lower than 0.02 after 480 minutes. The coefficient of friction of the disc with 4%Cr+Ti decreases slowly and remains at either 0.040 or above at the end of the test. This change in value is consistent with the discussions in section 6.3.1 and 6.3.2.

It can be concluded from Figure 6.14 that the addition of Ti alters the friction pattern significantly. This is contrary to the results in [142] where a tool steel was tested under dry contact. On one hand the surface has undergone abrasive and delamination wear during 480 minutes of friction where detached particles such as titanium carbonitrides play an important role, while on the other hand lubrication is also responsible for the difference in friction that resulted from different wear regimes during the whole process. Under dry contact adhesion is the principal wear mechanism (Figures 5.7 and 5.8). The grooved surfaces of both discs feature a work hardened surface (Figure 6.15 (a)) and oxidation (Figure 6.15 (b)) respectively. Elastic and plastic deformation, and abrasion brought about the friction pattern (at 120 minutes in Figure 6.9).

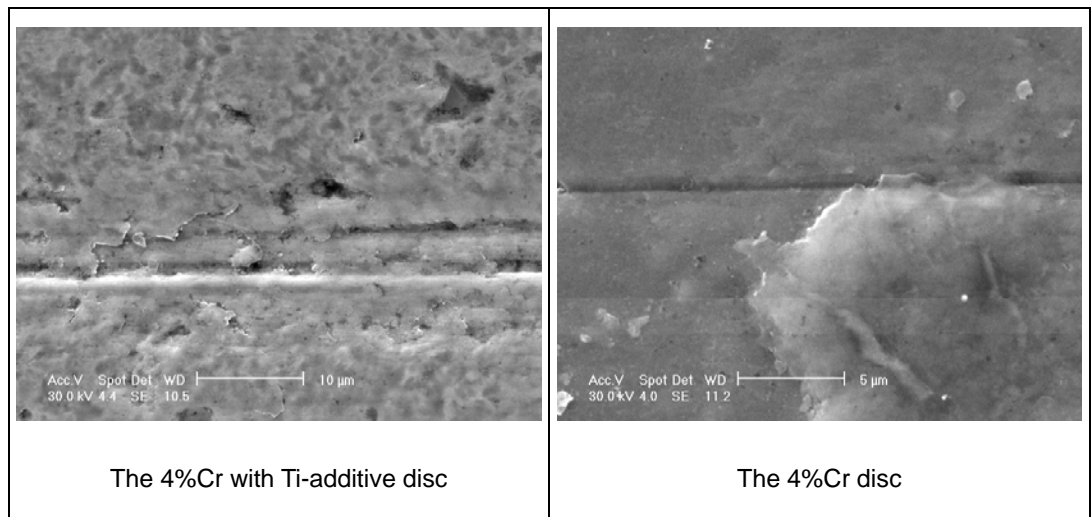


Figure 6.15 Grooved surface under dry contact after 120 minutes wear at 1000N, 597rpm in disc-to-disc tests

6.5 Findings

In this chapter it was found that designing the roll material and its manufacturing are important factors that control the wear properties of rolls.

6.6 Summary

In this chapter the wear and friction pattern were discussed by correlating disc surface morphologies and microstructures of both disc materials. SEM, TEM and X-ray diffraction technologies were used to study the tribological properties of these materials. The following points are conclusions stemming from an analysis of the whole wear process of both material discs under lubricating conditions.

1. The disc with 4%Cr+Ti is characterised as carbonitrides precipitated in a finer tempered martensite matrix. Coarse carbides (M_7C_3) are features of the materials with 4%Cr.

2. The material with 4%Cr+Ti wears differently to that with 4% Cr. In the first 15 minutes flakes from the grinding ridges were the dominant abrasive particles. Deformation and surface flattening characterise the disc with 4%Cr. Apparent ridge flattening occurred on the disc with 4%Cr+Ti after 210 minutes of friction.
3. Delamination became an important wear mechanism at an earlier stage for the disc with 4%Cr than that with 4%Cr+Ti. Micro-spalling and pitting occurred after 120 minutes of wear on the disc with 4%Cr but this did not occur on the disc with 4%Cr+Ti until after 330 minutes of wear.
4. Detached carbides are responsible for the abrasive wear on both discs at a later stage. Ti and lubrication alter the friction pattern due to surface regeneration that resulted from the abrasive effect of carbonitrides.

Chapter 7 Case Studies on Premature Failure of Work Rolls in a Cold Strip Plant [†]

7.1 Introduction

At present cold rolled strip is produced on a tandem or reversing cold strip mill where the work rolls are flattened [148] into an elliptical shape [149]. The control models applied to cold strip rolling resulted in strip with good shape, profile, and flatness [150, 151]. In cold rolling it is the work rolls that deform the strip into the desired shape and size.

These work rolls operate under extremely arduous conditions and as such are one of the most important items in the operating cost of a cold rolling mill [152]. The effects of the material, deformation, thermal crown, oxide scale and surface roughness, etc., on the wear of a work roll [153–160] have been investigated and a tribological model for mixed film lubrication was developed [161]. Roll wear affects the quality of the rolled strip and roll service life significantly. In cold strip rolling work rolls are subjected to high cyclic loading and high levels of abrasion. The resistance of rolled materials to deformation is extremely high in cold rolling compared to hot rolling. The roll in the roll bite is subjected to pressures higher than 10,000MPa, and the shear stress generated by friction [162]

[†] The present chapter was published in *Wear* 263 (2007), at pp 1442–1446.

at the roll/strip interface.

The premature failure of a work roll increases not only the cost of the rolling but also the down time of the mill. The reasons why forged alloy work rolls fail prematurely may be the combined effects of operating techniques and the metallurgical composition of the roll. Operating factors include the choice of rolling parameters such as rolling load, lubrication, rolling speed, and the experience of operators. Work roll quality includes the presence of non-metallic inclusions, casting defects, and phase transformations [162].

In this chapter the author reports on the premature failure of work rolls in a cold strip mill. The chemical composition, microstructure, and hardness of the roll materials were examined by conducting tensile tests on spalled samples. The stress states in the spalled area were also determined to find the causes of roll wear and spall damage. The surface images of the damaged work rolls have been studied and the characteristics of wear identified. It was found that metallurgical defects and operating parameters affected their service life. The experimental results from Chapters 5 and 6 are cited to explain some reasons of the failures.

7.2 Rolling process and parameters

Figure 7.1 schematically outlines a 2-stand compact cold strip rolling mill. Hot rolled strip was the initial feed stock for this 4-high cold mill. The hot rolled coil is about 1.5–5.0mm thick by 900–1680mm wide and weighs 35 tonnes. The

oxide scale was removed by pickling before rolling. The maximum pickling speed was 60 m/min and the temperature of acid bath was about 70–85⁰ C. An AGC hydraulic control, on-line thickness control, and automatic speed measurement were used in the rolling process. Quakerol N680-2-BPD with 47.8-51.8 mm²/s viscosity at 40°C was used as a lubricant. Emulsion properties is shown in Table 5.2.

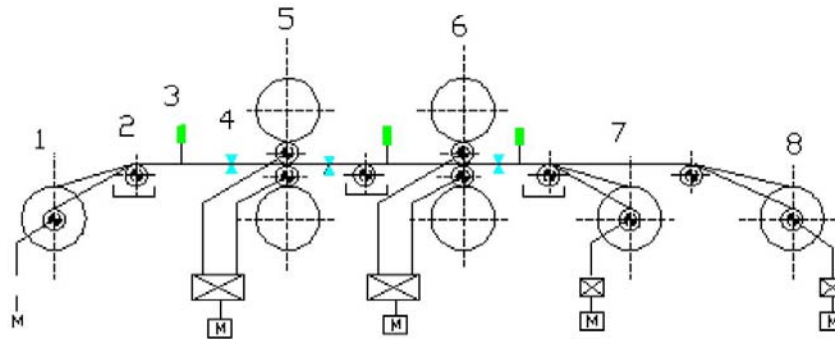


Figure 7.1 2-stand tandem cold strip mill: (1) Coiling #2, (2) tension meter, (3) laser velocimeter, (4) thickness gauge, (5) stand #2, (6) stand #1, (7) coiling machine #1 and (8) uncoiling machine.

The work rolls were made from forged alloy steel containing approximately 4%Cr with hardness from HS 83 to 85, 0.2% proof strength, tensile strengths and the torsion strengths are 460, 940MPa and 570MPa, and had a Continuous Variable Crown (CVC) profile.

Tables 7.1 and 7.2 show the parameters of the rolling and work rolls.

Table 7.1 Rolling parameters

Roll	Stand	Diameter mm	Rolled strip mm	Reduction (%)	Roll separating force (KN)	Rolling speed m/min	Rolled length km	Expected life km
A	1	449	1.35×1240	34	19890	867	4.515	120
B	2	448	0.85×1500	35	19932	960	13.64	
C	1	449	1.1×1240	28.5	17652	498	5.139	
D	2	449	0.61×1240	28.2	17528	679	11.304	

Table 7.2 Work roll parameters

Roll	Chemical composition (wt, %)						Roughness (μm)		Hardness (HSC)
	C	Mn	Ni	Si	Cr	Mo	Before working	After working	
A	0.81	0.36	0.27	0.40	3.97	0.51	0.8	0.729	83-85
B							0.82	0.323	
C							0.83	0.55	
D							0.87	0.47	

7.3 Results and discussion

7.3.1 Samples of Work Rolls

Samples from a spalled work roll were cut and prepared for observation using a scanning electron microscope and optical microscope.

Surface images of the defects taken from each of the four rolls were marked by metal welding, banding, and spalling. All the work rolls were used in different

stands. The surface roughness R_a was measured from the work roll before and after installation.

7.3.2 Spalling

Spalling is the most common failure. Indeed it is estimated that surface spalling accounts for more than 70% of work roll consumption. There are several causes, micro-cracks on the surface, insufficient hardness and/or tensile strength, improper microstructure and folding strip, etc. Fatigue cracks also lead to surface spalling. Figure 7.2 (a and b) shows the defective portion of work rolls A and D. In the case of roll D, the spall seems to be a curve which is about 18mm long but according to an ultrasonic test, has no depth. Nevertheless the damage on roll D is possibly at the first stage of that for roll A.



Figure 7.2 Spalling of work rolls: (a) roll D and (b) roll A.

The typical size of this damaged area was measured on roll A and found to be 1430mm long by 85mm deep by 353mm in circumference. This roll failed

prematurely after 4.515 km of service, which is less than the service life of roll D. Its microstructure was examined by an optical microscope, as shown in Figure 7.3.

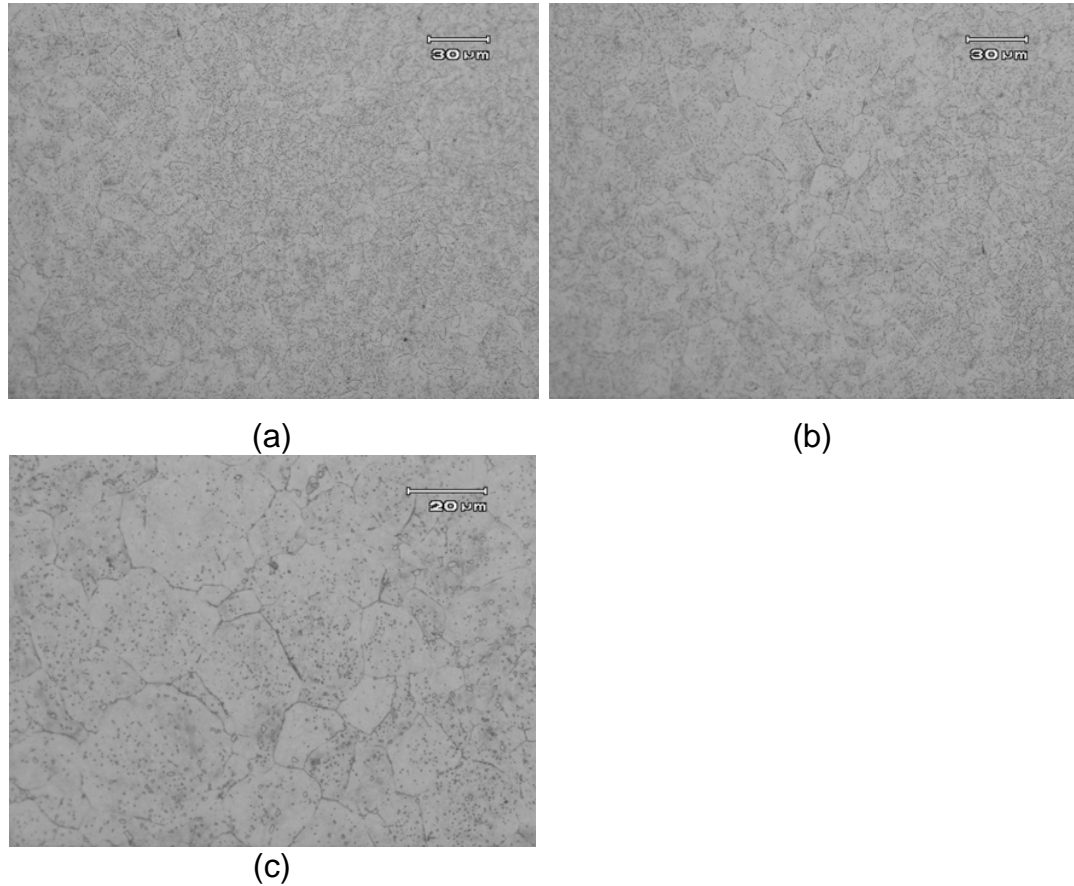


Figure 7.3 Microstructure of the material of work roll: (a) A region close to the surface; (b) Approximately 75 mm in depth from the surface; (c) About 85 mm in depth from the surface

It can be seen that there is a 75mm depth on hardening on the roll so the area from which the microstructure was examined was within a distance from the surface to the centre of roll A. Figure 7.3(a) is a region close to the surface, (b)

approximately 75mm deep, and (c) about 85mm deep. It can be seen that the grain size varies from 11.5 to 20 μ m and further, coarse grain was found 75mm beneath the surface (Figure 7.3b) which is less than the guaranteed minimum hardening depth of 85 mm.

Tensile tests on flat specimens were carried out with an Instron testing machine. Samples were cut from the large spalled pieces of roll A with the results indicating that the tensile and yield strengths are below the manufacturer's specifications. Figure 7.4 shows the crack on roll A. The normal stress and shear stress of work roll A were calculated by Hertzian analysis. The calculated normal stress and shear stress [163] developed as a result of contact with the steel strip are shown in Figures 7.5 and 7.6. It can be seen in Figure 7.5 that some of the components of stresses ($S_{xx} = \sigma_r$) and ($S_{zz} = \sigma_z$) reach a large value at the surface.

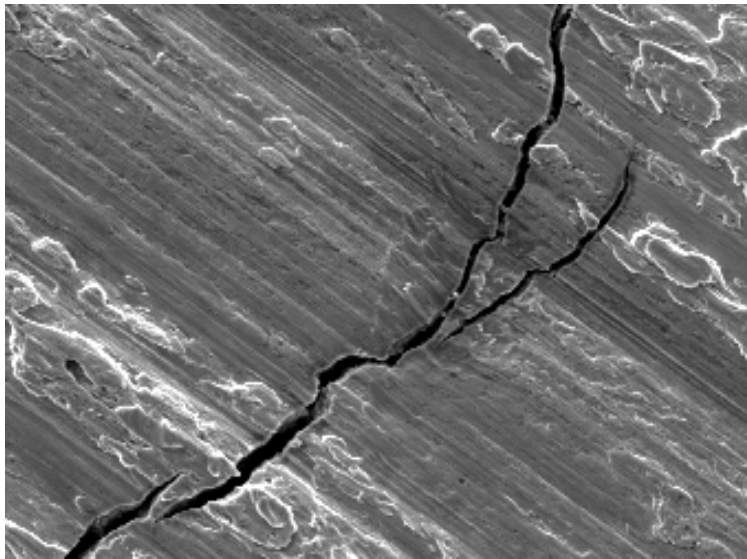


Figure 7.4 Crack on roll A

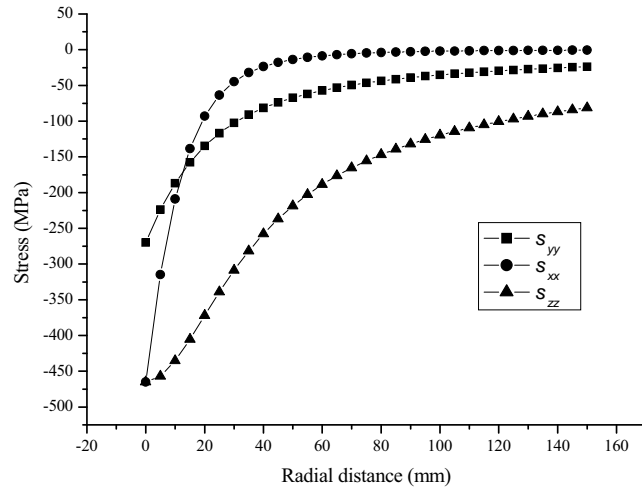


Figure 7.5 Normal stress gradients developed as result of contact with the rolled strip

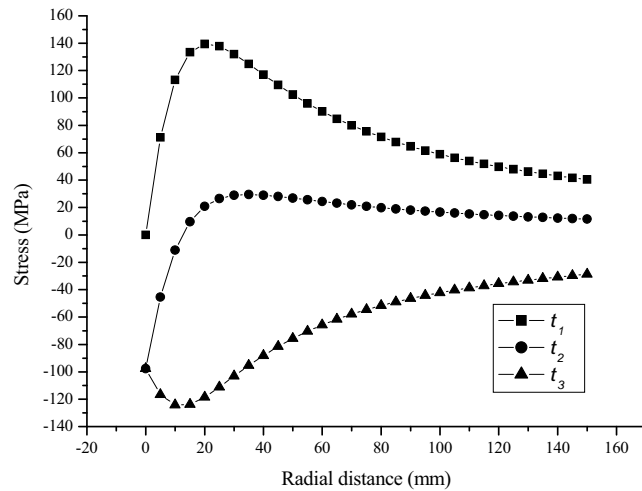


Figure 7.6 Shear stress gradients developed as result of contact with the rolled strip

Roll A and D are new rolls. The worn profile of either the work roll or back up roll may not be the factor that caused the damage but high local loads at the

leading edges or doubling of the rolled thickness due to folding strip may have exceeded the surface shear strength. It is likely that one or more pressure cracks were formed in an area of local overload near the surface. The cracks are parallel to the axis but propagate in a non-radial direction (Figure 7.2(b)). Due to the reversing rolling features of a rolling mill, cracks may propagate progressively (Figure 7.4). Due to improper microstructure (Figure 7.3(b)), cracks propagate inside the working surface which resulted in a large surface spall. This can reduce its service life considerably (see Figure 7.7, the rolling length of strip for roll A was short before it was removed from service).

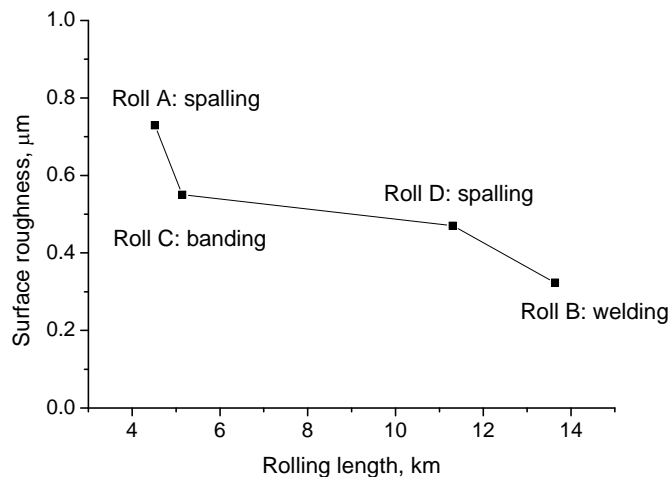


Figure 7.7 Relationship between the length of rolled strip and surface roughness

7.3.3 Strip welding

In the disc-to-disc dry contact tests the disc with low carbon fused with the 4%Cr

disc. Figure 7.8 illustrates two incidents which occurred at 597rpm under

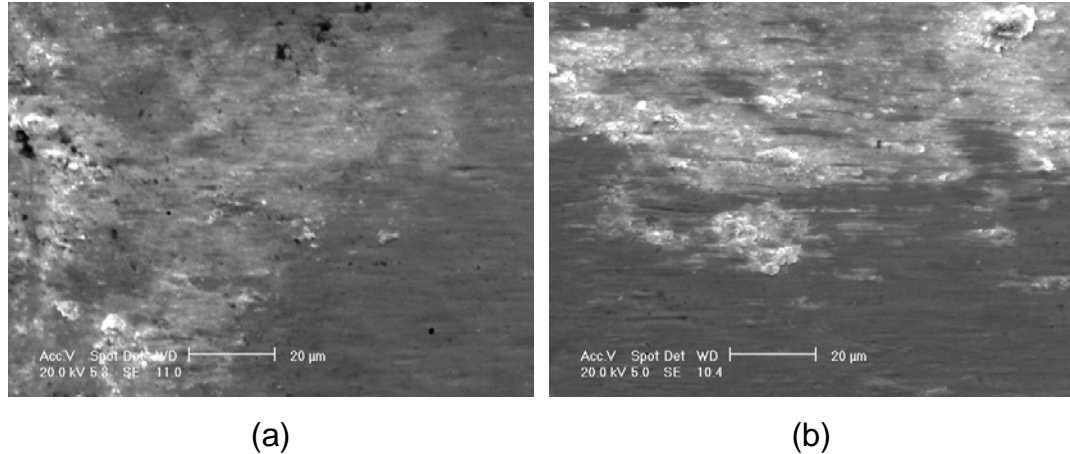


Figure 7.8 4%Cr disc surface welding in the disc-to-disc dry-contact wearing tests: (a) after 5 minutes at 1700N load, 597rpm and 3.5% forward slip; (b) after 30minutes at 1500N load, 597rpm and 6.5% forward slip

1700N and 1500N loads respectively and 3.5% and 6.5% forward slip. The fused surface formed after sliding 0.43km (Figure 7.8 (a)) and 2.59km (Figure 7.8 (b)) respectively. These incidents imply that material was transferred to the disc with 4%Cr disc under relatively heavy loads when the interface was not lubricated. Under dry contact and at heavy loads the heat and severe friction cause the discs to fuse together.

Figure 7.9 shows the metal fusing onto the surface of work roll B on the second stand of the mill after the third pass of rolling. The damage occurred at the edge of the rolled strip and was approximately 65mm wide and 707mm around the periphery.



Figure 7.9 Strip welding (roll B in Figure 7.7)

This incident happened when the intermediate strip exhibited a poor profile. An incorrect roll profile or poor strip shape can result in high specific rolling pressure which in turn leads to a high roll surface temperature at a local area. This increases plastic deformation of the surface in the form of indentations, or even high sub-surface shear causing spalling, where the severe heat adds fire cracks or bruises. This is consistent with the results in Figure 7.8.

A work roll may still be used but only after the strip welding area is cleaned up, however in this case the wear is significant, as shown in Figure 7.7, where the surface roughness was reduced dramatically (see roll B), compared to other cases. The service life of roll B was obviously not affected despite its continuous usage.

7.3.4 Mechanical marking and banding

The surface failure on roll C is rather interesting because of the mechanical

marks (area A and C in Figure 7.10) and banding (area B in Figure 7.10).

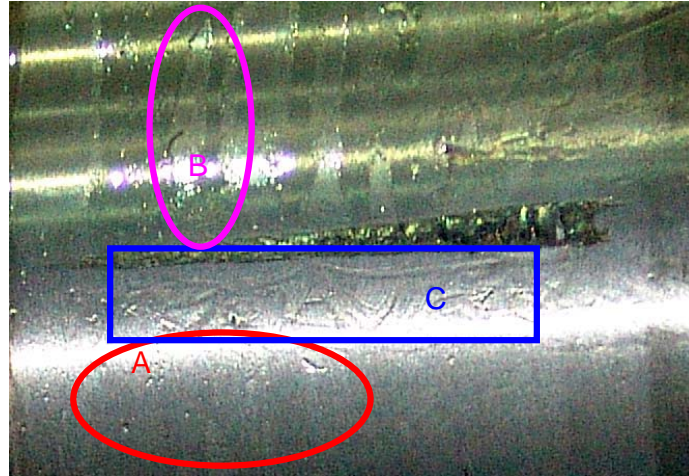


Figure 7.10 Mechanical marks and banding (Roll C in Figure 7.7)

a) Mechanical marking

Pits and various intended marks characterise the surface failure of roll C. Within area A in Figure 7.10, it seems that foreign objects or thicker particles of scale have passed through the roll gap or the contact line between the work and back up roll. Surface failure in area C is a typical example of where the folded ends of cold strip were pressed onto the roll surface. These incidents were found when the mill operation failed. These incidents occurred at high rolling speed and high pressure which generated heat and deformation.

b) Banding

Bright areas of heavy peeling around the periphery of work roll C appear in the

form of bands with a very rough surface, as shown in Figure 7.10. The layer that was removed was between 0.1 and 0.9 mm thick. It is accepted that banding is typical surface damage to high chrome work rolls when they are used after a longer run time in the same critical stands and positions. However in the case of roll C, this occurred at the first rolling pass after a short campaign.

Figure 7.11 shows the banding that occurred on the disc with 4%Cr during the disc-to-disc dry contact wear tests after 180 minutes (a) and after 210 minutes (b). The load was 1000N and the speed was 597rpm with a 6.5% forward slip. A micro-crack was found on the surface at the 180th minute surrounded by oxides. The crack appeared to be propagating and material opposite the direction of rotation was torn off the surface at 210 minutes (Figure 7.11 (b)).

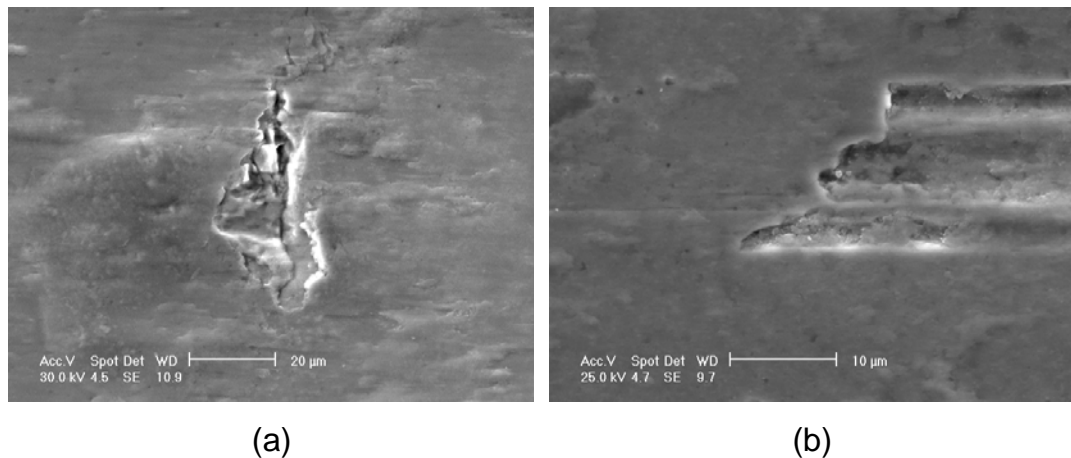


Figure 7.11 Surface crack and banding on the disc with 4% Cr in the dry contact wear tests: (a) after 180 minutes; (b) after 210 minutes

In fact the origin of banding occurs when alternating friction forces in

combination with alternating thermal loads exceed the fatigue shear strength of the surface material. It is assumed that the surface cracks within the depth of primary fire cracks develop and propagate until this area shears away from the roll. When the roll surface deteriorates locally the peak shearing forces are induced, which lead to a very fast development of peeled bands around the roll barrel that cause wear. Another cause of banding could be due to non-uniform lubricant across the roll length, resulting in different polishing contact patterns.

The case exhibited in Figure 7.10 has a significant influence on the service life and wear of the roll because it demonstrated that the surface roughness decreases dramatically in a short kilometer length of rolled strip (see Figure 7.7, roll C). Therefore this defect significantly increase roll wear.

7.4 Conclusions

Four types of surface defects were investigated in this chapter. Early failure of work rolls in cold rolling may have resulted from operating factors and microstructure defects in the material, rather than wear. It was found that single case or multiple cases of roll failure may occur during operations. The following conclusion may be reached:

1. Some components of stresses reach a large value at the surface which can cause cracks and reduce their service life.
2. Metallurgical defects such as the improperly prepared microstructure, increase

the risk of surface spalling.

3. Strip welding is caused by incorrect mill operations or lubrication break down.

Such incidents may be avoided by improving control of the work roll temperature and of shape of the feeding strip and proper emulsion.

4. Banding was the third surface damage encountered in this study. It is believed that better cooling and uniform lubrication across the roll length may reduce the risk of damage and improve the service life of work rolls.

5. Mechanical marks are suspected impressions of folded strips during operation.

6. In all cases, extreme load and/or local friction is responsible for the types of surface failures mentioned.

Chapter 8 Conclusions and Future Work

8.1 Introduction

The present study has concentrated on the deterioration of cold work roll surfaces. To accomplish these investigations, an innovative facility called the Lateral-setting test (LST) was designed and manufactured. This is the first time the evolution of surface roughness by single pass and multi-pass stalled rolling tests which include several rolling parameters on two high chrome steel roll materials, has been investigated. Experiments on disc-to-disc wear were also undertaken to investigate the tribological properties of these roll materials. Cases where forged alloy work rolls in a two-stand compact cold mill failed prematurely were studied whilst simultaneously considering the tribological properties of similar roll materials.

8.2 General conclusions

8.2.1 Innovation of the LST facility

The LST-mill has been incorporated on the Gleeble machine and can be used for hot and cold rolling. Experimented data are available and may be acquired by the inherent functions of the machine.

It has been demonstrated that this LST-mill can successfully accomplish single

pass and multi-pass stalled rolling experiments. Its application has successfully fulfilled the scheduled experiments which investigate the evolution of the roller surface roughness.

8.2.2 Roll surface features after single pass and multi-pass stalled rolling

This LST system has been used for single pass and multi-pass rolling experiments in a Gleeble 3500 Thermal-Mechanical simulator. This is a new method for understanding how roll surfaces change after single and multi-pass cold rolling. Two materials, 4%Cr and 4%Cr with Ti-additive, were tested under dry contact and with lubrication. The effect of reduction, rolling speed and the surface roughness of both the roll and strip were considered in the stalled rolling experiments.

It has been found that there was less waviness on the roll surface after large reductions in all single pass rolling tests. Dominant waviness still existed after each pass of rolling. A 30.5% reduction proved to be a critical parameter of the power spectrum density, especially in the axial direction of the roll.

A rougher work piece brings about a higher power spectrum of the surface profile of the roll in the whole frequency range. It is new to find that the PSD amplitude of the surface in the roll axial direction is affected so significantly by a rougher work piece. The amplitude of the PSD in the circumferential direction of the roll surface is more sensitive to its original surface roughness after one pass of rolling. Lubrication affects the 4%Cr and the 4%Cr+Ti surfaces differently; it reduces surface roughness on the 4%Cr roller but not to the same extent as

4%Cr+Ti roller.

As the number of rolling passes increase, the PSD amplitude of the roller with 4%Cr has been 'shifted' to the longer wavelength range than the roller with added Ti. It has been found that roller with 4%Cr+Ti can retain shorter wavelengths better than the 4%Cr roller in dry contact rolling and it exhibits an ability to regenerate roughness in the rolling direction. The dominant and effective wavelength of the roller surface with added Ti deteriorates at a lesser rate than that with 4%Cr roller.

8.2.3 Tribological properties of 4%Cr and 4Cr+Ti materials

Disc-to-disc experiments have been carried out to investigate the effect of duration, load, disk speed and slip on the 4%Cr and 4Cr+Ti roll wear, friction and torque. It has been found that the Ti additive disc is characterised as carbonitrides precipitated in a finer tempered martensite matrix. Coarse carbides are features of the disc material with 4%Cr.

More material was worn off the disc with 4%Cr+Ti than the disc with 4% Cr in the first 60 minutes at dry contact, but afterwards the wear on the disc with Ti slowed down. When lubrication is used the surface roughness of the roll with 4%Cr+Ti deteriorates much slower than that with 4%Cr.

Speed affects weight loss significantly in dry contact while lubrication reduces the material worn from both discs. As the speed increases so too does the weight loss, for both dry and with lubrication contact, although the disc with 4%Cr+Ti loses less weight under both conditions. With dry contact the roll slippage affects

the weight loss of both materials but as the slip rate increases, so too does the weight loss. Lubrication reduces the weight loss at any forward slip but under both conditions the disc with 4%Cr+Ti loses less weight.

Generally, lubrication reduces the friction of both materials. As the speed of the disc with 4%Cr+Ti increases the coefficient of friction is reduced but the effect of load is in an opposite direction. The disc with 4%Cr was not affected so much by speed. The coefficient of friction of the disc with 4% Cr is more sensitive to load at a higher speed than the disc with 4%Cr+Ti at slower speeds.

A backward slip of 2% and a forward slip 1.5% results in a different coefficient of friction when dry, even when the resulting torques are similar. Torque and the coefficient of friction are sensitive to speed with dry contact.

It has been found that deformation and surface flattening characterises the disc with 4%Cr. Apparent peak flattening occurred on the disc with Ti after 210 minutes of friction. Detached carbides are responsible for the abrasive wear that occurred on both discs at a later stage. Carbonitrades play a significant role in the abrasion of the disc with Ti. Delamination for the disc with 4%Cr appeared earlier than that with 4%Cr+Ti. Micro-spalling and pitting occurred in the disc with 4% Cr after 120 minutes of wear and 330 minutes with 4%Cr+Ti material.

In the present study, adding Ti alters the friction characteristics under lubrication conditions due to surface regeneration that results from the abrasive effect of Carbonitrades. Wear on the disc under dry conditions is characterised by ploughing.

8.2.4 Case studies of the premature failure of a cold work roll

In the present work, four kinds of surface defects were investigated and it was found that early failure may have been resulted from operational factors and microstructure defects in the material rather than wear, such as one of the following:

- over load condition causes high stresses at the surface leading to development of cracks.
- Metallurgical defects such as improperly prepared microstructure may increase the risk of surface spalling.
- Strip welding caused by incorrect mill operations.
- Banding is the third surface damage which can be remedied by better cooling and non effective lubrication.
- Roll marks could be due to foreign bodies or folded strip impressions from mill operations.
- Extreme loads and/or localised heat from friction due to inadequate lubrication is responsible for the types of surface failures mentioned.

8.3 Suggestions for future work

In this present work the experimental LST innovation and tests have started a new method to investigate detailed changes in surface roughness after a single pass or multiple passes. In the meantime two kinds of cold work roll materials

were used in the LST and disc-to-disc experiments, however the author suggests that more work is needed in the future.

8.3.1 LST Equipment

- In this study the surface profile of the deformed strip or work-piece has not been investigated. It is therefore suggested that further studies be carried out on the surface features of rolled product that correlate with the roll surface features. Further, more computer simulation of changes in surface roughness by FEM will further our understanding of its evolution.
- It is feasible to use the LST with rollers made from different materials but it is strongly recommended that roll materials such as High Speed Steel (HSS), Semi-HSS (SHSS), and Ti-additive HSS, etc., be tested.
- More cycles of rolling to one pass to evaluate the evolution of roll wear.
- A wider range of test strip surface roughness needs to be studied simultaneously with roller surface. Moreover, medium and higher carbon steels as well as high strength steels are recommended to be investigated to simulate more hardened materials in a tandem cold mill in the future.

8.3.2 Disc-to-disc wear tests

The tribological property of roll material is affected by its microstructure and mechanical properties. Smelting, forging, and heat treating roll materials are important factors in controlling their wear properties and therefore, it is suggested that their manufacturing technology be considered in the future.

Different materials with different hardness should be carried out to simulate more hardened materials through tandem mills.

References

- [1] D. F. Chang and W.R.D. Wilson, Tribol. Trans., Vol. 39 (1996), pp. 407–415.
- [2] P. B. Kosasih and A. K. Tieu, Tribology International, Vol. 40 (2007), pp.709–716.
- [3] V. B. Ginzburg, Steel Rolling Technology, Marcel Dekker, New York, 1989.
- [4] A. Ohmuk, T. Kikuchi, T. Kawanami and T. Asamura, Journal of Japan Society of Plastic Technology, Vol. 23 (1982), p. 990.
- [5] A. Yanagishima, T. Jimba, S. Fujiwara, H. Kuguminato, K. Kitamura and K. Yasuda, Testu to Hagane, Vol. 68 (1982), S1024.
- [6] H. Kuwamoto, T. Jimba, S. Iwadoh and Y. Okami, Journal of Japan Society of Lubrication Engineering, Vol. 8 (1982), p. 17.
- [7] S. Iwadoh, H. Kuwamoto and S. Sonoda, Testu to Hagane, Vol. 75 (1989), pp. 2059-2066.
- [8] J. Jase-Bnrr and K. G. Marhew, Wear, Vol. 14 (1969), pp 199-205.
- [9] P. Clayton, Wear, Vol. 60 (1980), pp 75-93.
- [10] D. N. Hanlon, W. M. Rainforth and C. M. Sellars, Wear, Vol. 203-204 (1997), pp. 220-229.
- [11] M. M. Kbwcbv. Proc. Conf. on Lubrication and Weaar. Inst. of

- Mechanical Engineer. London. 1957. p. 655.
- [12] E.S. Skolionos. T.Z. Katiamis. M. Chin and B.V. Chambers. *Marer. Sci. Eng.*, Vol. A183 (1994), p. 195.
- [13] A. Kasak and T.A. Neumeyer, *Wear*, Vol. 14 (1969), pp 445-454.
- [14] A.M. El-Rakayby and B. Mills, *Wear*, Vol. 112 (1986), pp 327-340.
- [15] G. Wang, X. Liu and J. Wang, *Steel Rolling*, Vol. 20 (2003), p. 42-47.
- [16] T. Inoue, O. Katoh, S. Yamamoto and M. Ataka, *ISIJ*, Vol. 4 (1991), p.447-455.
- [17] S. Shimizu, K. Aoki, M. Kobayashi, T. Saito, Y. Yamada and F. Kosumi, *ISIJ International*, Vol. 32 (1992), pp. 1238-1243.
- [18] S. Kondo, *ASME J. Lub. Technol.* Vol.97 (1975), pp. 37–43.
- [19] K. Matsui, T. Matsushita, K. Takatsuka and Y. Yamaguchi, *Adv.Tech. Plast.*, Vol. 1 (1984), pp. 247–252.
- [20] J. Kihara, *Adv. Techn. Plast.*, Vol. 4 (1990), pp. 1693–1702.
- [21] P.C. Nautiyal and J.A. Schey, *ASME J. Tribol.*, Vol.112 (1990), pp. 282–287.
- [22] J.A. Williams, *Engineering Tribology*, Oxford University Press, Oxford, 1994.
- [23] A. Azarkhin and O. Richmond, *ASME, Journal of Tribology*, Vol. 113, (1991), pp. 789-794.
- [24] J.G. Lenard and S. Zhang, *J. Mater. Proc. Technol.*, Vol.72 (1997), pp. 293–301.

- [25] T.P. Adams and D.B. Collins, *Iron Steelmaker*, Vol. 26, (1999), pp. 29–33.
- [26] M.P.F. Sutcliffe, H.R. Le and D. Farrugia, *Wear*, Vol.254 (2003), pp 523-531.
- [27] B. Ma, A.K. Tieu, C. Lu and Z. Jiang, *Journal of Materials Processing Technology*, Vol.125–126 (2002), pp. 657–663
- [28] T. Ohkubo, J., Shibata, K. Sato, K. Seki and Y. Odaka, in: *First International Conference on Tribology in Manufacturing Processes*, Gifu, Japan, 1997, pp. 59–64.
- [29] W. Sun, PhD Thesis, University of Wollongong, 2005.
- [30] S. Beretta and S. Matteazzi, *Int J Fatigue* Vol.18 (1996), pp.451–456.
- [31] D. Oswald, *Iron & Steel Engineer*. Vol. 74 (1997), pp. 35-40.
- [32] O. Deutscher, *Stahl und Eisen*, Vol. 7(1995), pp. 39-45.
- [33] A. F. Bastawros, H. Ortiz, L. J. Deistler, L. B. Donkle, L. L. Fierst and M. O. Mauck, in: *Mechanical Working and Steel Processing Conference Proceedings*. Publ. by Iron & Steel Soc. of AIME, Warrendale, PA, USA. Vol. 30(1992), pp. 485-489.
- [34] D. L. Owen, H. P. Evans and T. E. de la Rue, *Ironmaking and Steelmaking*, Vol. 24(1997), pp. 95-98.
- [35] C. Vergne, C. Boher, C. Levailant and R. Gras, *Wear*, Vol. 250 (2001), pp. 322–333.
- [36] S. Spuzic, K. N. Strafford, C. Subramanian and G. Savage, *Wear*, Vol.176 (1994), pp. 261-271.

- [37] T. Kimura, M. Ishii, K. Amano, S. Ueda, Y. Oka and S. Nakano, *ISIJ International*, Vol. 32 (1992), pp.1224-1231.
- [38] G. Xinjian and H. Yiyun, *Wear*, Vol. 137 (1990), pp.275–285.
- [39] Y.Z. Hu and K. Tonder, *Int. J. Mach. Tools Manufact.* Vol.32 (1992), pp. 83–90.
- [40] K. Yanagi and S. Hara, *J. JSPE*, Vol. 69 (2003), pp.1057–1060 (in Japanese).
- [41] B. Ma, A.K. Tieu, C. Lu and Z. Jiang, *Journal of Materials Processing Technology*, Vol.125–126 (2002), pp.657–663
- [42] W.R.D. Wilson and J.A. Walowit, *Tribology convention*, Vol.71-86 (1971), pp.164–172.
- [43] P.M. Lugt, A.W. Wemekamp, W.E. ten Napel, *Wear*, Vol.166 (1993) pp.203–214.
- [44] P.M. Lugt, W.E. ten Napel, *ASME J. Tribol.*, Vol.117 (1995), pp.475–488.
- [45] B. Ma, A.K. Tieu, C. Lu and Z. Jiang, *J. Mater. Process. Technol.*, Vol.131–132 (2002), pp.450–455.
- [46] M. D. Griffioen and J. G. Lenard , 44 th MWSP Conference Proceedings, Vol. XL, 2002
- [47] J.G. Lenard and S. Zhang , *Journal of materials Processing Technology* , Vol.72 (1997), pp. 293-301
- [48] C. McConnell and J.G. Lenard *Journal of Materials Processing Technology*,

- Vol.99 (2000), pp. 86-93
- [49] R. J. Wakelin, *Annu. Rev. Mater. Sci.*, Vol. 4(1974), pp. 221-253.
- [50] S.B. Petersen , P.A.F. Martins and N. Bay, *Journal of Materials Processing Technology*, Vol.66 (1997), pp.186- 194
- [51] M.P.F. Sutcliffe, R. Combarieu and P. Montmitonnet, *Wear*, Vol.257 (2004), pp.1071–1080
- [52] I. S. Yun, W.R.D.Wilson and K.F.Ehmann, *International Journal of Manufacture*, Vol.38 (1998), pp.1499-1530
- [53] A. W. Batchelor and G. W. Stachowiak, *Journal of Materials Processing Technology*, Vol.48 (1995), pp.503--515
- [54] H. Pawelski, *Journal of Materials Processing Technology*, Vol.125-126 (2002), pp.392-397
- [55] Y. Jimbo and A. Azushima, *Wear*, Vol. 249 (2001), pp. 415–421
- [56] S. Saxena, P.M. Dixit and G.K. Lal, *Journal of Materials Processing Technology*, Vol.58 (1996), pp.256 -266
- [57] A. Azushima and Y. Morita, *ISIJ International*, Vol. 32 (1 992), pp. 1232-1237
- [58] J.G. Lenard, *Journal of Materials Processing Technology*, Vol.80–81 (1998), pp. 232–238
- [59] H.R. Le, M.P.F. Sutcliffe, P. Wang and G.T. Burstein, *Wear*, Vol.258 (2005), pp.1567–1576
- [60] C. W. Wu, G. J. Ma and H. S. Sun, *Journal of Tribology*, Vol. 127(2005),

- pp. 605-610.
- [61] K. Dick and J. G. Lenard, *Journal of Materials Processing Technology*, Vol. 168 (2005), pp 16–24.
- [62] Y.Z. Lee and B.J. Kim, *Wear*, Vol. 232 (1999). pp 116–121.
- [63] J. G. Lenard, *Journal of Materials Processing Technology*, Vol. 152 (2004), pp 144–153
- [64] T. Hisakado, K. Miyazaki, A. Kameta and S. Negishi, *Wear*, Vol.239(2000), pp.69–76
- [65] M. Angelo de Carvalho , R. R. Xavier , C. H. Silva , E. Cannizza and A. Sinatora, in: *Proceddings of 44 th MWSP Conference Proceedings*, Vol. XL, 2002, pp. 534-444.
- [66] S. Iwadoh and T. Mori, *J. ISIJ*, vol. 32(1992), pp.1131-1140
- [67] T. Kimura, M. Ishll, K. Amano, S. Ueda, Y. Oka and S. Nakano, *ISIJ*, Vol. 32(1992), pp.1224-1231
- [68] C.R.F. Azevedo and J. B. Neto, *Engineering Failure Analysis*, Vol.11 (2004), pp.951–966
- [69] A. K. Raya, K.K. Mishra, G. Das and P.N. Chaudhary, *Engineering Failure Analysis*, Vol. 7 (2000), pp. 55-67.
- [70] R. Ahmed and M. P. F. Sutcliffe, *Journal of Tribology*, Vol. 123(2001), pp. 1-7.
- [71] H.R. Le and M.P.F. Sutcliffe, *Journal of Tribology*, Vol. 124 (2002), pp 129-137.

- [72] H.R. Le , M.P.F. Sutcliffe, P.Z. Wang and G.T. Burstein, *Acta Materialia*, Vol. 52 (2004), pp .911–920.
- [73] P. Montmitonnet, F. Delamare and B. Rizoulières, *Wear*, Vol.245 (2000), pp.125–135
- [74] M. P. F. Sutcliffe , H.R. Le and D. Farrugi, *Wear*, Vol.254 (2003), pp.523–531
- [75] H.R. Le and M.P.F. Sutcliffe, *Tribology International*, Vol.35 (2002) pp.123–128
- [76] M.F. Frolich, D.I. Fletcher and J.H. Beynon, Blackwell Science Ltd, Vol.25(2002), pp.1073-1086
- [77] D.F. Cannon and H. Pradier, *Wear*, Vol.191 (1996), pp.1-13
- [78] S. Beretta and M. Boniardi, *International Journal of Fatigue*, Vol.21 (1999), pp.329–335
- [79] R.C. Dommarco, K.J. Kozaczek, P.C. Bastias, G.T. Hahn and C.A. Rubin, *Wear*, Vol.257 (2004), pp.1081–1088
- [80] A. B. Jacuinde and W.M. Rainforth, *Wear*, Vol.250 (2001), pp.449–461
- [81] D.N. Hanlon, W.M. Rainforth and C.M. Sellars, *Wear*, Vol.203-204(1997), pp. 220-229
- [82] G. V. Tsybanev and O. N. Belas, *Strength of Materials*, Vol. 37, No. 1, (2005),
- [83] T. Donaldson, R. G. Christier and P. H. Hewitt, in: *Proc. 21st Century Steel Industry of Russia and CIS*, Vol.4.(1994), pp.88-90.

- [84] G.S. Wang , Eng. Fract. Mech., Vol. 51 (1995), pp.787 803
- [85] M. Hashimoto, T. Tanaka, T. Inoue, M. Yamashita, R.Kurahashi and R. Terakado ISIJ ,, Vol. 42(2002), pp.982-989
- [86] D. Du, Y.F. He, B. Sui, L.J. Xiong and H. Zhang, Journal of Materials Processing Technology, Vol.161 (2005), pp.456–461
- [87] S. Shimizu, K. Aoki, M.Kobayashi, T. Saito, Y. Yamada and F.Kosumi ISIJ International, Voi. 32 (1 992), pp. 1238-1 243
- [88] L. Barbulovic-Nad and J. G. Lenard, Journal of Materials Processing Technology, Vol.142 (2003), pp.65–71
- [89] M. D. Griffioen and J. G. Lenard, 44 th MWSP Conference Proceedings, Vol. XL, 2002
- [90] M. Ikeda, T. Umeda, C. P. Tong, T. Suzuki, N. Niwa and O. Kato ISIJ International, Vol. 32 (1992), pp. 1157-1 162
- [91] A. B. C. Larbi, A. Cherif and M.A. Tarres, Wear, Vol.258 (2005), pp.712–718
- [92] D.N. Hanlon¹ and W.M. Rainforth, Wear, Vol.255 (2003), pp.956–966
- [93] A.J. Leonard and W.M. Rainforth, Wear, Vol.255 (2003), pp.517–526
- [94] H. Ike, K. Tsuji and M. Takase, Wear, Vol. 252 (2002), pp 48–62.
- [95] H.R. Le and M.P.F. Sutcliffe, Wear, Vol.244 (2000), pp.71–78
- [96] M .P .F.Sutcliffe and R .Ahmed, Wear, Vol. 244(2000), pp. 60-70
- [97] M. P. F. Sutcliffe and F. Georgiades, Wear, Vol.253 (2002), pp.963–974
- [98] M. P. Cavatorta and C. Cusano, Wear, Vol.242(2000), pp. 133-139.

- [99] M. P. Cavatorta and C. Cusano, *Wear*, Vol. 242(2000), pp .123-132.
- [100] H.R. Le, M.P.F. Sutcliffe and J.A. Williams, *Tribology Letters*, Vol. 18, No. 1, January 2005, pp. 99-104.
- [101] A. Shirizly and J. G. Lenard, *Journal of Tribology*, Vol. 122(2000),pp 550-557
- [102] S. Huart, M. Dubar, R. Deltombe, A. Dubois and L. Dubar, *Wear*, Vol. 257 (2004), pp. 471–480.
- [103] R. Deltombe, M. Dubar, A. Dubois and L. Dubar, *Wear*, Vol.254 (2003), pp. 211–221
- [104] M. Uchidate, T. Shimizu, A. Iwabuchi and K. Yanagi, *Wear*, Vol. 257 (2004), pp. 1288–1295.
- [105] L. Gjønnes, *Wear*, Vol. 192 (1996), pp. 216-227.
- [106] S. Bogdański, M. Olzak and J. Stupnicki, *Wear*, Vol. 191 (1996), pp 14-24.
- [107] C.H. Luo, *Journal of Materials Processing Technology*, Vol. 59 (1995), pp 373-380.
- [108] Cheng Lu, A. Kiet Tieu and Zhengyi Jiang, *Journal of Materials Processing Technology*, Vol .140 (2003), pp.569–575
- [109] D. Kumar and U.S. Dixit, *Journal of Materials Processing Technology*, Vol.171 (2006), pp 331–340.
- [110] S. Hao, B.E. Klamecki and S. Ramalingam, *Wear*, Vol. 224 (1999) pp.1–7.

- [111] H. R. Le and M. P. F. Sutcliffe, Journal of Tribology, APRIL 2003, Vol. 125, pp. 384-390.
- [112] M. P. F. Sutcliffe, H. R. Le and R. Ahmed, Journal of Tribology, Vol. 123 (2001), pp.791-798.
- [113] Z. Mrz and S. Stupkiewicz, Int. J. Mech. Sci., Vol. 40 (1998), pp. 281-303.
- [114] X. Tan, Tribology International, Vol. 35 (2002), pp.385–393.
- [115] X. Lu, J. Cotter and D.T. Eadie, Wear, Vol. 259 (2005), pp.1262–1269.
- [116] B. Ma, A.K. Tieu, C. Lu and Z.Y. Jiang, Journal of Materials Processing Technology, Vol .140 (2003), pp.635–640
- [117] Y. A. Karpenko and A. Akay, Tribology International, Vol.34 (2001), pp.531–545
- [118] H.C. Xie , D.R. Chen and X.M. Kong, Tribology International, Vol.32 (1999), pp.83–87
- [119] A. Stephany, J.P. Ponthot, C. Collette and J. Schelings, Journal of Materials Processing Technology, Vol .153–154 (2004), pp.307–313
- [120] H. Lin, N. Marsault and W. R D Wilson, Tribology Transactions, Vol . 41(1998), pp.317-327
- [121] H. R. Le and M. P. F. Sutcliffe, Journal of Tribology, JULY 2003, Vol. 125, pp. 670-677.
- [122] R. Bünten, K. Steinhoff, W. Rasp, R. Kopp and O. Pawelski, Journal of Materials Processing Technology, Vol.60 (1996),pp.369-376
- [123] B. Ma, A.K. Tieu, C. Lu and Z. Jiang, Journal of Materials Processing

- Technology, Vol .125–126 (2002),pp.657–663
- [124] H.R. Le and M.P.F. Sutcliffe, Tribology International, Vol.35 (2002), pp. 123–128
- [125] Designing Institute of Ma-an Shan, in: Design and Poof Calculation of Medium Rolling Mill. Metallurgical Publication, Beijing, 1979.12.
- [126] Cheng, Daxian, in: Design Manual for Machinery. Beijing, Chemical Industrial Publication, 1986.9.
- [127] Zou, Jianxiang, in: Steel Rolling Machinery. Metallurgical Publication, Beijing, 1989.6.
- [128] D.N. Hanlon, W.M. Rainforth and C.M. Sellars, Wear, Vol. 203-204 (1997). pp 220-229
- [129] W. Sun, A. K. Tieu, Z. Jiang, C. Lu and B.de Jong, in: Proceedings of the 6th Engineering Mathematics and Applications Conference, Ed. By R. L. May and W. F. Blyth, Jul, 2003, Sydney, Australia, pp. 277-281.
- [130] MultiMode SPM Instruction Manual, version 3.0, Digital Instruments, Veeco Metrology Group (2000).
- [131] J. A.Schey, Tribology in metalworking: friction, lubrication and wear. ASM, Metals Park, Ohio 44073, USA, 1983.
- [132] Lundberg, S-E and Gustafsson, T, J. Mater. Proc. Technol., Vol. 42 (1994), pp. 239–291.
- [133] A. Magnee, C. Gaspard, and M. Gabriel, CRM Metallurgical Reports, Vol. 57(1980), pp.25–39.

- [134] H. Noguchi, H. Hiraoka, Y. Watanabe, and Y. Sayama, *Trans.ISIJ*, Vol. 28(1988), pp.478–485.
- [135] S. Spuzic, K. Strafford, C. Subramanian, and G. Savage, *Wear*, Vol. 176(1994), pp.261–271
- [136] J. Goodchild and J. Beynon, Laboratory simulation of work roll wear in hot mills. Paper presented at: First World Tribology Congress, London, 8–12 September 1997.
- [137] L. H. Mair, T. A. Stolarski, R. W. Vowles and C. H. Lloyd, *Journal of Dentistry*, Vol. 24 (1996), pp. 141-148.
- [138] G. W. Stachowiak and A. W. Batchelor in: *Engineering tribology* (Third Version). Elsevier, on-line, 2005. pp 39-62, pp461-494, pp573-589.
- [139] Yong Choi, N. I. Baik, J. S. Lee, S. I. Hong and Y. D. Hahn, *Composited Science and Technology*, Vol. 61 (2001), pp.981-986.
- [140] S.V. Fortuna, Y.P. Sharkeev, A. J. Perryc, J. N. Matossian and I.A. Shulepov, *Thin Solid Films* , Vol. 377-378 (2000), pp.512-517.
- [141] Y. Chen and H. M. Wang, *Surface and Coatings Technology*, Vol. 168 (2003), pp.30–36.
- [142] A.J. Leonard and W. M. Rainforth, *Wear*, Vol. 255 (2003), pp.517–526.
- [143] A. B. Jacuinde and W. M. Rainforth, *Wear*, Vol. 250 (2001), pp.449–461.
- [144] D.N. Hanlon, W.M. Rainforth and C.M. Sellars, *Wear*, Vol. 203-204 (1997), pp.220-229.
- [145] M., Ikeda, T. Umeda, C. Tong, T. Suzuki, N. Niwa and O. Kato, *ISIJ*

- International, Vol. 32 (1992), pp. 1157-1 162.
- [146] D. Liu, Z. Yin, D. Xu, F. Gao, Z. Li and H. Zhao, Iron and Steel, Vol. 40 (2005), pp.69-82. (in Chinese)
- [147] Q. Wang, D., Yang, S. Wei and R. Long, Lubrication Engineering, Vol. 10 (2006), pp 104-108.
- [148] P. Montmitonnet, E. Massoni, M. Vacance, G. Sola and P. Gratacos, Ironmaking Steelmaking, Vol.20 (1993), pp.254–260.
- [149] J. Shi, D.L.S. McElwainand and T.A.M. Langlands, Int. J. Mech. Sci., Vol.43 (2001), pp.611–630.
- [150] E.N. Dvorkin, M.A. Cavaliere and M.B. Goldschmit, Comput Struct, Vol.81 (2003), pp.559–573.
- [151] Z.Y. Jiang, A.K. Tieu, X.M. Zhang, C. Lu and W.H. Sun, J. Mater. Proc. Technol, Vol.140 (2003), pp.542–547.
- [152] R. Colas, J. Ram'irez, I. Sandoval, J.C. Morales and L.A. Leduc, Wear, Vol. 230 (1999),pp.56–60.
- [153] S. Iwadoh, H. Kuwamoto and S. Sonoda, J. Iron Steel Inst. Jpn., Vol.75 (1989), pp.2059–2066 (in Japanese).
- [154] N. Koshizuka, T. Kimura, M. Ohori, S. Ueda and H. Wanaka, J. Iron Steel Inst. Jpn., Vol.75 (1989), pp.509–516 (in Japanese).
- [155] J.J. Robinson, G. van Steden and F. ter Lingen, Iron Steel Eng., Vol.73 (1996),pp.15–19.
- [156] X.M. Zhang, Z.Y. Jiang, A.K. Tieu, X.H. Liu and G.D.Wang, J. Mater.

- Process. Technol., Vol.130–131 (2002), pp.219–223.
- [157] D.-F. Chang, Thermal stresses in work rolls during the rolling of metal strip, J. Mater. Process. Technol., Vol. 94 (1999), pp. 45–51.
- [158] C.R.F. Azevedo and J. B. Neto, Eng. Fail. Anal. Vol.11 (2004), pp.951–966.
- [159] G. Zhang, H. Xiso and C.Wang, J. Iron Steel Res. Int., Vol.13 (2006), pp.23–26.
- [160] C. Vergne, C. Boher, R. Gras and C. Levailant, Wear, Vol.260 (2006), pp.957–975.
- [161] H.R. Le and M.P.F. Sutcliffe, ASME Tribol. Div. Trib., Vol 43 (2001), pp.1–8.
- [162] A. K. Ray, K.K. Mishra, G. Das and P.N. Chaudhary, Eng. Fail. Anal. Vol. 7 (2000), pp.55–67.
- [163] A. Borezi and O.M. Sidebottom, Advanced Mechanics of Materials, Wiley, 1985.
- [164] S.-E. Lundberg, Evaluation of deterioration mechanisms and roll life of different roll materials, Steel Res., Vol. 64 (1993), pp. 597–603.
- [165] R. D. Armell, P. B. Davies, J. Halling and T. L. Whomes, Tribology-Principles and Design Applications, Macmillan, 1991, p. 72.
- [166] A. Maksumov, R. Vidu, A. Palazoglu and P. Stroeve, Journal of Colloid and Interface Science, Vol. 272 (2004), pp 365–377.
- [167] P.J. Blau, Tribology International, Vol. 30(1997), pp. 321-331.

- [168] C. R. Gagg, P. R. Lewis, *Engineering Failure Analysis*, Vol. 14 (2007), pp. 1618–1640.
- [169] D. Doyle, *Private Communication* (2008).
- [170] N. P. Suh, M. Moleh, J. Arinez, *Wear*, Vol. 214 (1998), pp 231-236.
- [171] Y. Wong, E. D. Doyle, *Wear*, Vol. 233-235 (1999), pp 395-401.
- [172] S. G. Harris, E. D. Doyle, A. C. Vlasveld, J. Audy, J. M. Long, D. Quick, *Wear*, Vol. 254 (2003), pp 185-194.

APPENDIX I Details of design of the mini mill

The LST-mill designed for the Gleeble system must have strong structural parts so that numerous experiments can be carried out. The design and manufacture of the principle parts will now be explained but due to the length limitations of this thesis only the housing, cover, base, coupling mount, work roll, shafts, bearings, method of adjusting the roll gap, etc, will be described in detail. Figure A.1 illustrates its assembly.

a) Work roll

The shaft and work roll unit should facilitate assembly and reduces the size of the window in the housing so that a simple work roll structure and convenient work roll disassembly can be achieved. The work roll system is composed of a shaft and a roller ring type working segment. When assembling the roller ring is placed onto the shaft but when disassembling, the roll material can be removed and changed to the next one. The shaft and the roller ring were manufactured from dissimilar materials. According to the rolling force pre-calculation, the shaft must be strong enough to cope with a large rolling force so it was manufactured from a 0.4%C-1.05%Cr steel. Material for the roller-ring was selected according to the requirements of each experiment.

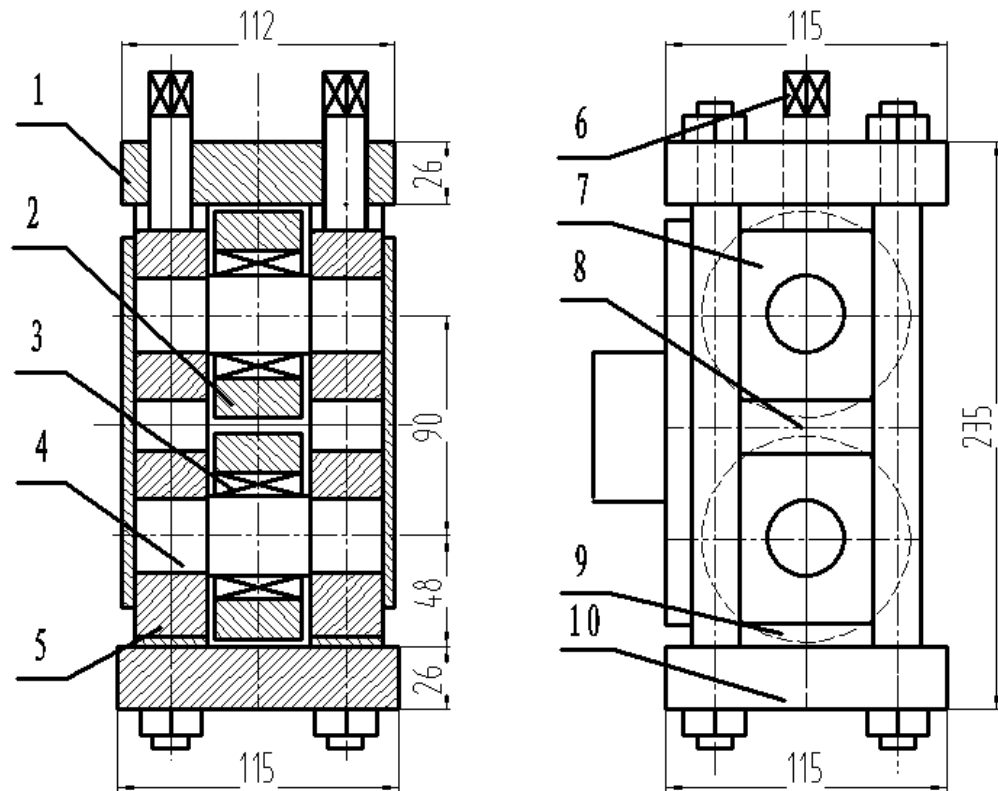


Figure A.1 Assembly of the mill (dimensions in mm)

1: Top cover; 2: Work roll; 3: Roller bearing; 4: Shaft; 5: Mill housing; 6: The pressing down bolt; 7: Shaft bushings; 8 and 9: Blocks for roll gap adjustment; 10: lower cover

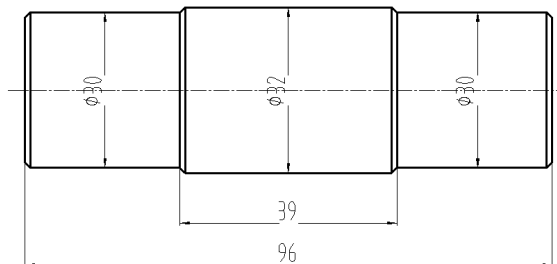


Figure A.2 Roller shaft (a 0.4%C-1.05%Cr steel and dimensions in mm)

The Gleeble System will drive the material into the roll gap through the friction between the material and roll surface. The barrel will hold the roller ring to carry out scheduled experiments so the shear strength of the shaft is more important than its bending strength. A schematic drawing is shown in Figure A.2.

The length of the roller ring must satisfy either the width of the mill housing or length of the bearing length. It is illustrated in Figure A.3 below.

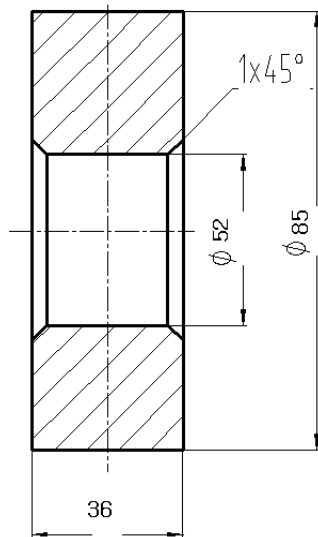


Figure A.3 Roller-ring (dimensions in mm)

The shaft sits on the roll gap adjustment blocks and is supported by the bushings. To obtain proper orientation and ensure that the adjustment blocks remain stationary, pins are located in each end. Both the upper and lower bushings are illustrated in Figure A.4.

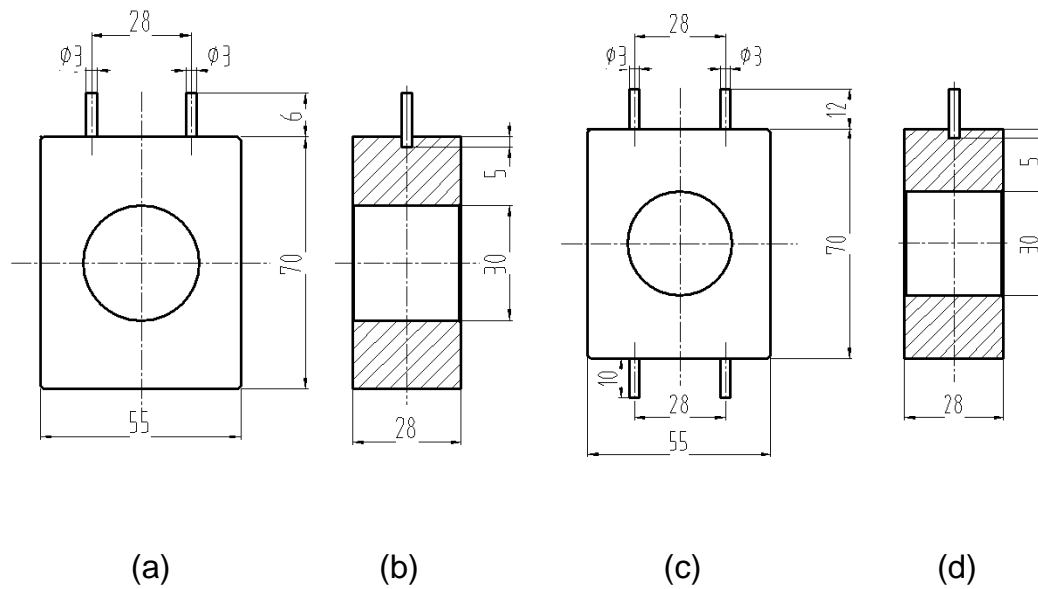


Figure A.4 Bushings: (a) upper bushings; (b) cross-section of (a); (c) lower bushing; (d) cross-section of (c). (dimensions in mm)

b) Bearings

The bearings are the smallest available to accommodate the size of the shaft, bearings, and roller ring. This compact assembly makes use of the limited space available in the mill while enabling the roller ring to be changed quickly. During the selection process it was assumed that the roll system withstands maximum radial force while the axial force is neglected during rolling. A couple of NA-type roller bearings are installed on the end of each shaft. The correct tolerance between the inside diameter of the roller ring and the outside diameter of the bearing means the radial load can be sustained when rolling and the roller ring can still be changed quickly.

c) Housing

The housing has a rectangular section that fits the Gleeble chamber. It comprises of an upper and lower cover and two vertical plates connected by four rods. The top cover is a single plate while the bottom one is integrated into the base of the rolling mill and held by four rods. The housing is pre-stressed with the nuts which enables the gap between the roll adjustable by blocks. It was manufactured from quenched and tempered 0.4%C-1.05%Cr steel.

Connecting rods. Figure A.5 illustrates the connecting rods [126].

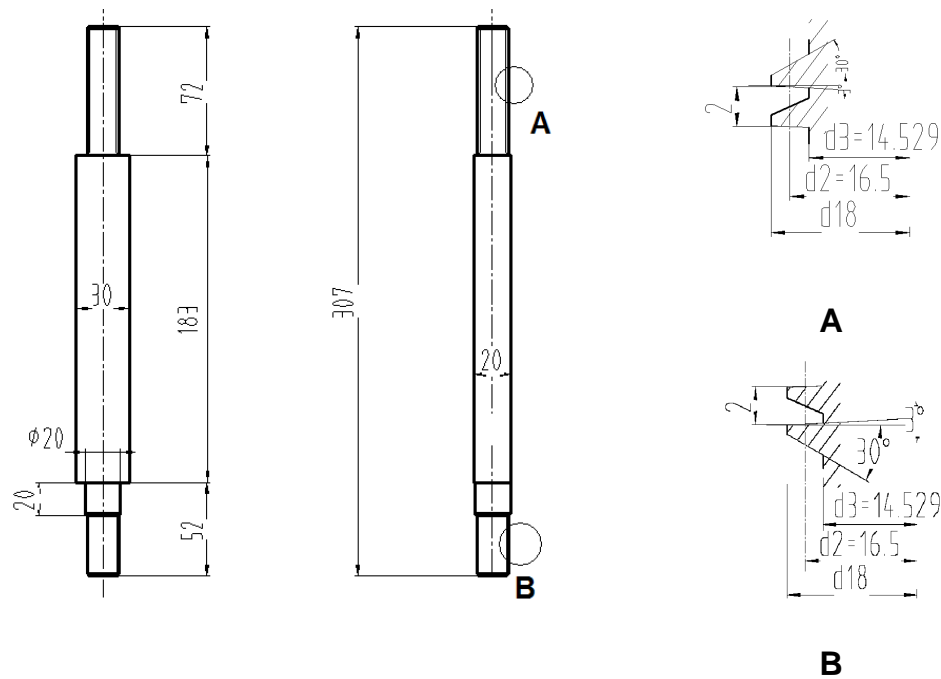


Figure A.5 Rods (dimensions in mm)

Upper and bottom covers. In a traditional rolling mill the mill housing principally bears heavy vertical forces but only 3-4% of this load laterally [2]. The mill described here is driven by the Gleeble moving a stroke which transfers

APPENDIX

rolling force laterally to the mill housing. The mill is connected into the Gleeble System so the top and bottom covers bear the same load when rolling. The top cover is a single plate while the bottom plate is connected by the rods. Figure A.6 illustrates the design schematically.

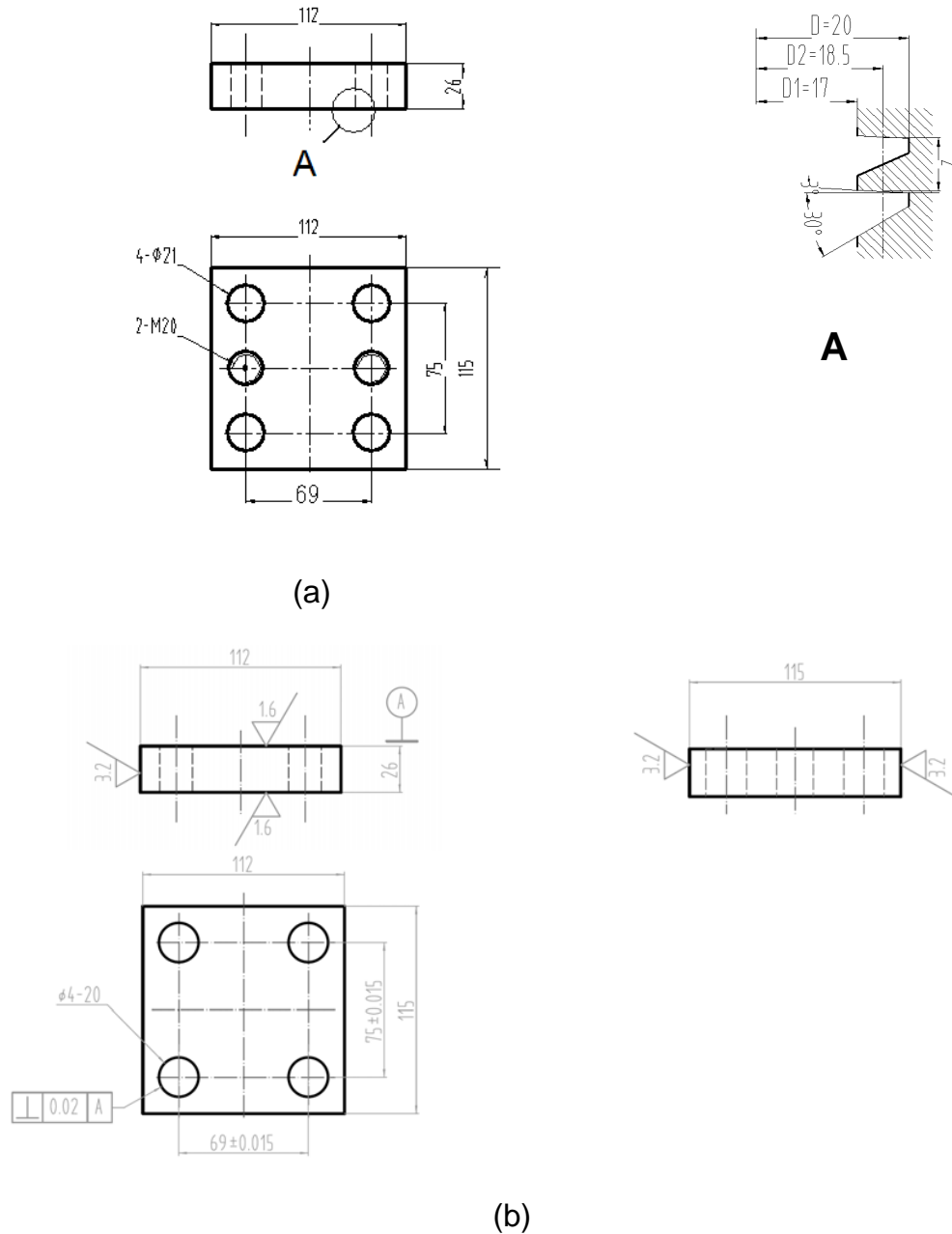


Figure A.6 Covers. (a) top cover and (b) lower cover (all dimensions in mm)

Coupling mount. The coupling mount bears the load when rolling and is the only part which holds the mill and connects to the jig of the Gleeble system. The surface in contact with the Gleeble jig consists of a trapezoidal block and plate [127]. The two parts are welded around their circumference and fillet welded in the middle, as illustrated in Figure A.7.

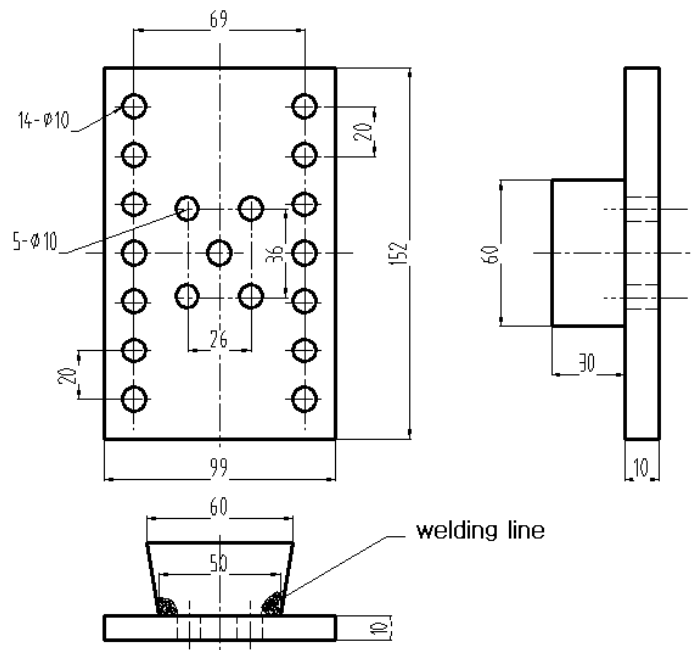


Figure A.7 Coupling mount (all dimensions in mm)

d) Roll gap adjustment

In the Gleeble chamber the mill is attached to the coupling mount where its stability is controlled by the Roll system balance and roll gap adjustment. A combination of blocks of varying thicknesses is used to adjust the roll gap and keep the system in balance. For the experiments, 4 series of block combinations have been selected to satisfy the scheduled reductions. Figure A.8 illustrates a 13 mm thick block.

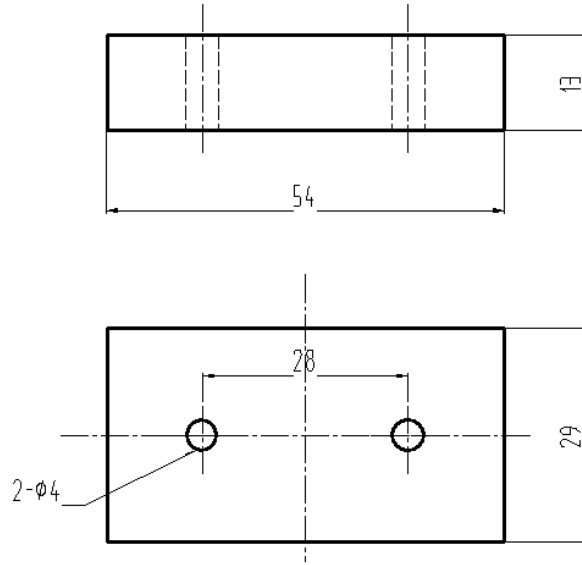


Figure A.8 Block for roll gap adjustment (all dimensions in mm)

APPENDIX II Power Spectrum Density

It is assumed that stationary surface profile data can be viewed as signals [129].

A Fourier transform (FT) is known to separate individual frequency components from stationary surface profiles and transform them from the amplitude-space domain to the amplitude–frequency domain. The Fourier transformation of a continuous stationary signal $z(x)$ for a given frequency f is defined as

$$L(f) = \frac{1}{N} \int_{-\infty}^{+\infty} z(x) \exp(2\pi ifx) dx \quad (1)$$

where N is the number of data points. In practice a discrete form of Fourier

transformation is called the fast Fourier transform (FFT) and is usually used for transforming the signal.

$$L(f) = \frac{1}{N} \sum_{k=1}^N z_i \exp(2\pi i \Delta N / k) (\Delta N) \quad (2)$$

The FFT is used to obtain the frequency of a given profile distributed over the whole frequency range. The resulting function is known as the power spectral density (PSD) function that is defined as a plot of power as a function of the spatial wavelength, or frequency. The Power Spectral Density (PSD) function represents the amplitude of surface roughness as a function of the spatial frequency of roughness, which is the inverse of the in-plane spatial wavelength of the roughness features. As for the AFM applications, some definitions of PSD are defined as following:

Total power spectrum - Power is the roughness amplitude squared, so power is in units of length squared for a topographic image. The power spectrum is a plot of power as a function of spatial wavelength or frequency.

1D PSD is called a one dimensional power spectral density. Power spectral density is a plot of the density, in spatial frequency space, of the power spectrum. The units are length squared divided by a one dimensional frequency, or 1 over length, which is its length cubed. A 1D PSD can be calculated in either the X direction of the data or in the Y direction.

1D isotropic PSD is a different version of a one dimensional power spectrum.

2D isotropic PSD is a two dimensional power spectral density. Its units are

length squared divided by a two dimensional frequency, or 1 over length squared, which is length to the fourth power. This is isotropic in the sense that it is an average taken over all directions in the data.

For a digitised profile of length L, consisting of N points sampled at intervals of d_0 , the frequency distribution is approximated by [130]:

$$PSD(f) = \frac{2d_0}{N} \left| \sum_{m,n=1}^{m,n=N} e^{\frac{i2\pi}{N}(n-1)(m-1)} z(n) \right|^2 \quad \text{for } f = \frac{m-1}{Nd_0} \quad (3)$$

where $i = -1$, and frequencies, f , range from $1/L$ to $N/(2L)$. After the power P has been obtained, the values of PSD for one-dimensional and two dimensional power spectral density may be written as:

$$1D \quad isotropic \quad PSD = \frac{P}{2\pi f} \quad (4)$$

$$2D \quad isotropic \quad PSD = \frac{P}{2\pi f(\Delta f)} \quad (5)$$

Section Analysis in AFM technology is a very useful approach for obtaining consistently accurate results of cross sectional profiles and fast Fourier transformation (FFT) of the data along the reference line by ascertaining the surface topology and orientation of the sample. In this case the results of Section analysis may vary tremendously depending upon the topology and orientation of the sample.

APPENDIX III Skewness, Root Mean Square and Kurtosis of Surface Roughness

The amplitude distribution function (ADF) indicates the probability that a profile of the surface has a certain height at any position. The root mean square roughness, skewness, and kurtosis, are the three statistical ADF parameters. Skewness (R_{sk}) is a simple measure of the asymmetry of the ADF, ie, it measures any variation in symmetry of a profile about its mean line. It is a non-dimensional parameter and is defined as:

$$R_{sk} = \frac{1}{NR_q^3} \sum_{j=1}^N Z_j^3 \quad (6)$$

where Z_j is amplitude distribution, N the number of data points and R_q the root mean square roughness, which is a statistical parameter that is used to measure the width of the ADF and is defined as $R_q = \sqrt{\sum_{j=1}^N (Z_j)^2 / N}$. Surfaces with positive skewness, such as raised surfaces, have fairly high spikes that protrude above a flatter average. Surfaces with negative skewness, such as porous surfaces, have fairly deep valleys in a smoother plateau. More random (e.g. ground) surfaces have a skewness near zero. A value of R_{sk} greater than 1.5 indicates that the surface does not have a simple shape.

Kurtosis relates to the uniformity of the ADF or, equivalently, to the spikiness of the profile. It is also a non-dimensional parameter defined as:

$$R_{ku} = \frac{1}{NR_q^4} \sum_{j=1}^N Z_j^4 \quad (7)$$

A Gaussian distribution has a kurtosis of 3. If $R_{ku} < 3$, the distribution has few high peaks and low valleys, which means a relatively flat surface. If $R_{ku} > 3$, the distribution has many high peaks and low valleys, which means a relatively sharp surface [29].